

University of New Hampshire

University of New Hampshire Scholars' Repository

Doctoral Dissertations

Student Scholarship

Spring 2009

"Chasing a ghost": Addressing the opalescence/aggregation relationship of an IgG 1 antibody

John C. Champagne

University of New Hampshire, Durham

Follow this and additional works at: <https://scholars.unh.edu/dissertation>

Recommended Citation

Champagne, John C., "Chasing a ghost": Addressing the opalescence/aggregation relationship of an IgG 1 antibody" (2009). *Doctoral Dissertations*. 469.

<https://scholars.unh.edu/dissertation/469>

This Dissertation is brought to you for free and open access by the Student Scholarship at University of New Hampshire Scholars' Repository. It has been accepted for inclusion in Doctoral Dissertations by an authorized administrator of University of New Hampshire Scholars' Repository. For more information, please contact Scholarly.Communication@unh.edu.

“CHASING A GHOST”

**ADDRESSING THE OPALESCENCE/AGGREGATION
RELATIONSHIP OF AN IgG 1 ANTIBODY**

BY

JOHN C. CHAMPAGNE

**Bachelor of Science, Plymouth State University, 1996
Master of Science, University of New Hampshire, 2000**

DISSERTATION

Submitted to the University of New Hampshire

in Partial Fulfillment of

the Requirements for the Degree of

Doctor of Philosophy

in

Biochemistry and Molecular Biology

May 2009

UMI Number: 3363713

INFORMATION TO USERS

The quality of this reproduction is dependent upon the quality of the copy submitted. Broken or indistinct print, colored or poor quality illustrations and photographs, print bleed-through, substandard margins, and improper alignment can adversely affect reproduction.

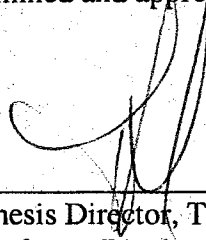
In the unlikely event that the author did not send a complete manuscript and there are missing pages, these will be noted. Also, if unauthorized copyright material had to be removed, a note will indicate the deletion.

UMI[®]

UMI Microform 3363713
Copyright 2009 by ProQuest LLC
All rights reserved. This microform edition is protected against
unauthorized copying under Title 17, United States Code.

ProQuest LLC
789 East Eisenhower Parkway
P.O. Box 1346
Ann Arbor, MI 48106-1346

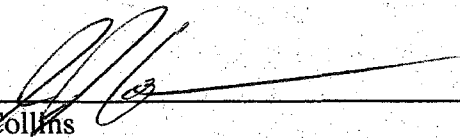
This thesis has been examined and approved.



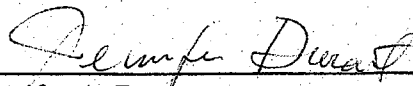
Thesis Director, Thomas M. Laue
Professor Biochemistry and Molecular Biology



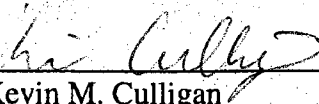
Philip J. Wyatt
CEO Wyatt Technology Corporation



John Collins
Associate Professor



Jennifer A. Durant
Research Assistant Professor



Kevin M. Culligan
Research Assistant Professor

April 10th, 2009

Date

DEDICATION

This work is dedicated to my family and friends, whose love and support has enabled me to be where I am today. It is also especially dedicated to the two loves of my life, my wife Donna and my son Ethan.

ACKNOWLEDGMENTS

It is nearly impossible to thank everyone who contributed to this work but I am going to give it my best shot. First and foremost I want to thank my teacher, mentor and friend Tom Laue. Tom has always been an inspiration to me and his enthusiasm, patience and incredible knowledge has allowed me to become the scientist that I am today, and for that, I am eternally grateful. I also want to thank all of the members of the Laue lab (past and present) and in particular, Sue Chase and Sue Lucius who have kept me both organized and on track since I started on this project. I also wanted to thank my colleagues at Wyeth Biopharma and in particular Steve Raso, John Steckert, Pilarin Nichols. They have been a never ending source of support and encouragement. This work would also not have been possible without the patience and support of everyone at Wyatt Technology Corp. Especially Philip Wyatt, Geoffrey Wyatt and Clifford Wyatt who allowed me to pursue this project while continuing to be gainfully employed! Lastly, I want to thank my wonderful family. From my wife Donna who should share in this honor as she completed about ½ of the project, my son Ethan and my mother-in-law and father-in-law, Lorraine and Vincent aka "Charlie". You have all inspired me to be my best and achieve this goal despite all of life's challenges along the way. I love you very much.

TABLE OF CONTENTS

Dedication.....	iii
Acknowledgments.....	iv
Table of Contents.....	v
List of Tables.....	ix
List of Figures.....	x
Abstract.....	xiii
Chapter I - Introduction.....	1
Antibody Structure and Function.....	1
Antibody Structure.....	1
Antibody Structure/Function.....	6
Issues with Protein Aggregation.....	7
Pharmaceutical Importance.....	7
Immunological Issues with Aggregation.....	9
The Antibody Opalescence Phenomenon.....	10
Description of the Opalescence Phenomenon.....	10
Proposed Model of Assembly.....	11
Techniques Proposed for Opalescence Characterization.....	12
Objectives of This Study.....	17
Chapter II - Material and Methods.....	18

Antibody Preparation.....	18
Protein Expression and Purification	19
Assessment of Protein Purity	36
Opalescence Characterization	23
Preparation of Sample.....	23
Visual Appearance and Description	24
Static Multi-Angle Light Scattering (MALS) Studies.....	27
Sedimentation Velocity Studies	29
Electro-Separation	30
Salt Induced Opalescence	32
Dynamic Light Scattering Studies.....	32
Digestion / Fragmentation.....	34
Differential Scanning Calorimetry (DSC) Studies.....	39
Non-Ideality Analysis	40
Viscosity Measurement.....	42
Circular Dichroism Analysis.....	43
Congo Red Studies	43
Urea Analysis	44
FTIR Structural Analysis	44
Capillary Electrophoresis Studies.....	45
Chapter III - Results	48
Antibody Purification	50
Characterization of Protein Purity.....	50

Opalescence Characterization	55
Visual Appearance and Description	55
Static Multi-Angle Light Scattering (MALS) Studies.....	63
Sedimentation Velocity Studies	68
Electro-Separation	72
Salt Induced Opalescence	74
Dynamic Light Scattering Studies.....	83
Digestion / Fragmentation.....	89
Differential Scanning Calorimetry (DSC) Study	89
Non-Ideality Analysis	98
Viscosity Measurement.....	100
Circular Dichroism and Fluorescence Structural Analysis	103
Congo Red.....	103
Urea Analysis	106
FTIR Structural Analysis	108
Capillary Electrophoresis Studies.....	111
Chapter IV - Discussion	116
Electrostatic Forces Driving Protein Aggregation	116
Comparability of Mab 1, 2 and 3	123
Mab 1 Self-Association is Electrostatically Driven	129
Opalescence as a HMW Phase Separation	142
Mechanism of HMW Phase Separation.....	151
Predicting Behavior of Antibodies to Phase Separate.....	161

Conclusion	165
Appendix A - CE Data Spreadsheet.....	169
Appendix B - Defense Presentation “Chasing a Ghost”	171
References.....	190

LIST OF TABLES

Characteristics of the Human Immunoglobulin Isotypes	2
Conductivity of NaCl Induced Opalescence of Mab 1.....	80
The Effects of Urea on Mab 1 with NaCl as Measured by DLS	107
Capillary Electrophoresis Results of the Intact IgG Antibody and F(ab') ₂ Fragments...	114

LIST OF FIGURES

The Four Sub-Classes of IgG Immunoglobulins	3
The Structure of IgG 1 Fab and F(ab') ₂ Fragments	5
The Electroseparation Device Designed to Induce Opalescence.....	31
The Parallel Detector Configuration of the Calypso with MALS and Concentration Detector.....	41
The A Typical CE Method Used for Valence Determination	48
Reducing and Non-Reducing SDS-PAGE Results of Mab 1	51
Overlay Details of the SEC-HPLC Profiles of Mab 1	53
CEX-HPLC Profile of Mab 1	54
Peptide Mapping Chromatograms of Mab 1	56
HPAEC-PED Chromatograms of Mab 1.....	57
Visual Appearance of EP Reference Suspensions	58
Initial Antibody Opalescence Assignment Using EP Standards.....	59
Characterizing the Effect of NaCl and Tween 80 on Mab 1 Opalescence Using EP Reference Suspensions.....	61
Characterizing the Effect of NaCl and pH on Opalescence of Mab 1 Using EP Reference Standards	62
SEC-MALS Chromatogram of Mab 1 at 100 mM NaCl	64
Batch Multi-Angle Light Scattering Analysis of Mab 1 (No NaCl).....	66

Batch Multi-Angle Light Scattering Analysis of Mab 1 (150 mM NaCl)	67
Field Flow Fractionation with Multi-Angle Light Scattering	
Analysis of Mab 1	69
Sedimentation Velocity Study of Mab 1 Without NaCl.....	70
Sedimentation Velocity Study of Mab 1 With 150 mM NaCl	71
Electroseparation Induced Opalescence of Mab 1	73
Salt Induced Opalescence of Mab 1	75
Measuring the Opalescence of Mab 1 as a Function of Salt Concentration.....	77
Comparison of NaCl Induced Opalescence of Mab 1 and Mab 2	78
Measuring the Dilution Effect of Mab 1, Mab 2 and Mab 3	82
Dynamic Light Scattering Characterization of the Mab 1 Association State as a Function of NaCl Concentration.....	84
Dynamic Light Scattering Characterization of the Mab 2 Association State as a Function of NaCl Concentration.....	85
Dynamic Light Scattering Characterization of the Mab 3 Association State as a Function of NaCl Concentration.....	86
Plate Reader DLS Characterization of the Temperature Dependence of Mab 1 as a Function of NaCl Concentration.....	88
SEC Chromatograms of the Pepsin Digestion Purification.....	90
Dynamic Light Scattering Characterization of F(ab') ₂ Fragments.....	91
Thermal Profiles of IgG 1 Antibodies Using Differential Scanning Calorimetry	92
Thermal Profiles of Mab 1 and Mab 2 Using Differential Scanning Calorimetry as a Function of NaCl Concentration.....	94

Thermal Stability of Mab 1 and Mab 2 Fragments as a Function of NaCl Concentration.....	95
pH Dependent Domain Shifts in Mab 1	97
Non-Ideality (A_2) Measured as a Function of NaCl Concentration.....	99
Viscosity of Mab 1 as a Function of Protein Concentration.....	101
Viscosity of Mab as a Function of NaCl Concentration	102
Structural Differences of Mab 1 as Measured by Circular Dichroism and Fluorescence	104
Congo Red Analysis of Mab 1.....	105
The Effects of Urea and Arginine on Mab 1 in NaCl as Measured by Viscosity and Dynamic Light Scattering.....	109
FTIR Structural Analysis of Mab 1, Mab 2 and Mab 3	110
Capillary Electrophoresis Analysis of the IgG Antibody F(ab') ₂ Fragments.....	113
Weak Forces Between Molecules	118
Noncovalent Interaction Energy Between two Approaching Molecules	121
The Activation Energy of Approach for Mab 1	164
Proposed Mechanism of the Mab 1 Opalescence Phenomenon	168

ABSTRACT

"Chasing a Ghost" **Addressing the Aggregation/Opalescence Relationship in an IgG 1 Antibody**

by

John Champagne

University of New Hampshire, May, 2009

This study was conducted to address the aggregation/opalescence relationship of an IgG 1 therapeutic antibody under a variety of conditions. The opalescence characteristics of three antibodies, Mab 1, 2 and 3, were examined as a function of salt dependence, protein concentration and temperature, using a variety of biophysical techniques. The high molecular weight species were initially identified using batch static and dynamic light scattering and separated by asymmetric flow field flow fractionation. When the salt dependence was examined, any structural changes were characterized using differential scanning calorimetry, circular dichroism and fluorescence, while the association state and temperature dependence was measured by viscometry. The resulting non-ideality was determined using multi-angle light scattering over a range of NaCl and protein concentration, and then used to assess the nature of the noncovalent association. In addition, the valence of the antibody therapeutics was directly measured using capillary electrophoresis and assessed as a predictive tool of non-ideal behavior.

The antibody that exhibited the highest degree of opalescence, and therefore was the main focus of the study, was Mab 1, with Mab 3 exhibiting a lower degree of opalescence and Mab 2 acting as a control. The results suggest that the opalescence phenomenon of Mab 1 was due to a salt induced non-mass-action driven self-association which is mainly entropic in origin and is driven predominantly by NaCl. The intermolecular interactions appear to be facilitated by enhanced flexibility of Fc region and the independent Fab folding domain on Mab 1. The opalescence phenomenon also appears to be a relatively small fraction of discrete HMW material which is freely reversible and results in a liquid-liquid or liquid-solid phase transition which is either clear or cloudy depending on A_2 . Finally, it was determined that there is a discrepancy between the measured and calculated valence of the IgG1 antibodies in the study and this may be used as a predictive tool of non-ideal behavior. Together, this information was used to propose a model of the opalescence phenomenon of Mab 1 based on an electrostatic interaction involving mainly the CDR region on the Fab.

CHAPTER I

INTRODUCTION

Antibody Structure and Function

Antibody Structure

In humans, antibodies may be classified as members of five families or isotypes, which have been named immune globulin alpha (IgA), delta (IgD), epsilon (IgE), gamma (IgG) and mu (IgM) (Frazer, 1999). The structural differences between the isotypes are summarized in **Table 1.1**, and include differences in molecular weight, stoichiometry, carbohydrate content, serum concentration and half life. The most prevalent antibody isotype in the human body is IgG, which comprises approximately 85% of the immunoglobulin in serum. As the majority of the therapeutic antibodies are of the IgG isotype, this work was a study on the issues pertinent to this family of immunoglobulins.

The basic structure of an intact IgG immunoglobulin is a Y-shaped molecule which comprises four polypeptide chains, including two identical light chains and two identical heavy chains where the chains are held together with a series of disulphide bonds. The IgG heavy chains may be categorized into four sub-classes: 1, 2, 3 and 4, each with a molecular weight of approximately 55 kDa, with the intact IgG molecule having a total molecular weight of ~150 kDa (**Figure 1.1**). Each of the heavy and light

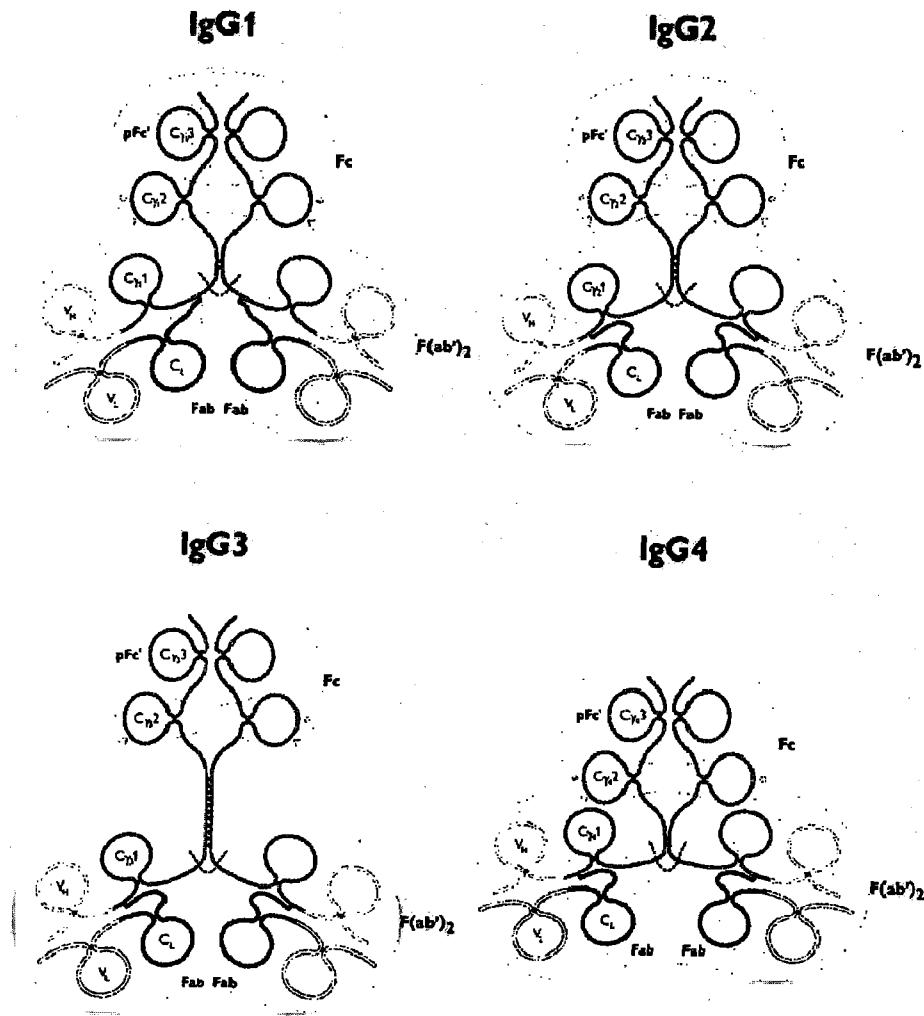
Table 1.1: Characteristics of the Human Immunoglobulin Isotypes

	IgA	IgD	IgE	IgG	IgM
Molecular Weight	160 kDa-400 kDa	175 kDa	190 kDa	150 kDa	950 kDa-1150 kDa
Stoichiometry	Monomer, Dimer	Monomer	Monomer	Monomer	Pentamer, Hexamer
Carbohydrate Content (%)	7-11%	9-14%	12%	2-3%	12%
Serum Conc. (mg/mL)	1.5-2.6	0.04	0.0003	9.5-12.5	0.7-1.7
Serum Half Life (Days)	6	3	2.5	23	5

From Frazer and Capra: Immunoglobulins: Structure and Function 4th Ed. © Lippincott-Raven Publishing Company, Inc.

Table 1.1: The characteristics of the five families or isotypes of human antibodies are listed. The data refers to human immunoglobulins in normal human subjects.

Figure 1.1: The Four Sub-Classes of IgG Immunoglobulins



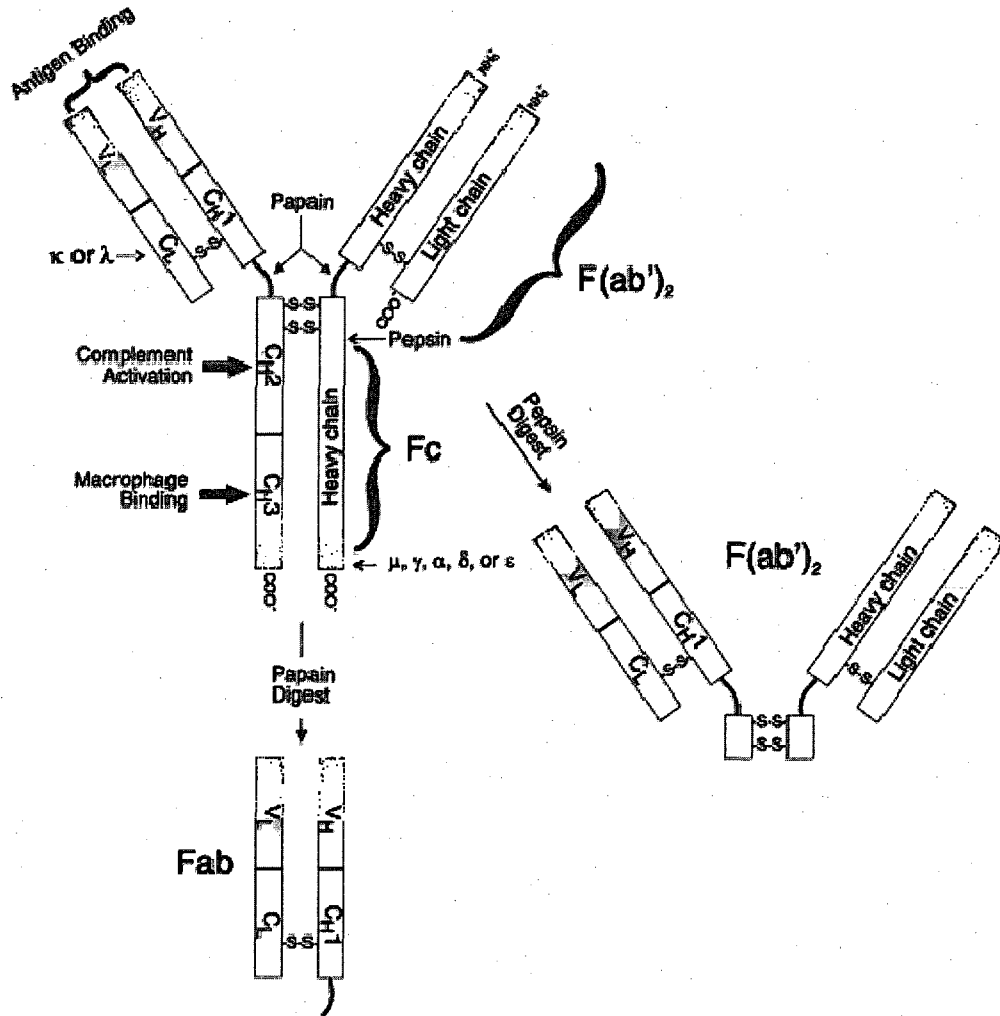
From: www.sanquin.nl

Figure 1.1: The characteristics of the four sub-classes of IgG immunoglobulins are depicted. Although their biological roles are vastly different, they are structurally similar with an average molecular weight of 150 kDa. The most prominent structural differences are the number of disulfide bonds at the hinge region. Gamma 1 and Gamma 4 isotypes have two disulfide bonds while Gamma 2 has four and Gamma 3 has 13. Also depicted is the site of attachment by carbohydrate side chains (+) and the major cleavage points for Pepsin (-----) and Papain (.....).

chain segments contains a variable region (also known as the complementarity determining region or CDR) and a constant region which are considered responsible for the diversity of antigen binding and the consistency in antibody structure (Lobo E. D., 2004). The light chains consist of V_L and C_L domains, and the heavy chain consists of V_H , C_{H1} , C_{H2} and C_{H3} domains. Furthermore, in humans, there are two light chain variants (κ or λ) which both have a molecular weight of ~ 25 kDa. Each of the domains on the light chain consists of about 100 residues, are similar in their primary structure, and are independent stable structural units (Creighton, 1993). All immunoglobulin domains (on the light and heavy chains) have essentially the same conformation, designated the immunoglobulin fold, consisting of two layers of anti-parallel β -sheets linked by a disulfide bond (Harris, 1998). The polypeptide chains between the domains are susceptible to proteases with the most susceptible being the hinge region linking the two Fab arms to the Fc base. After cleavage by Pepsin, the $F(ab')_2$ fragment contains two copies each of the V_L , C_L , V_H and C_{H1} domains, held together by the hinge region, while the Fc fragment has two copies each of the C_{H2} and C_{H3} domains. After cleavage by Papain, the Fab fragment contains only one copy of the V_L , C_L , V_H and C_{H1} domains (Figure 1.2).

The domains in an IgG immunoglobulin interact with each other in a variety of ways. The two C_{H2} domains and C_{H3} domains interact with each other in the Fc region and with each arm of the Fab region, there is interaction between the C_{H1} and C_L domains and the V_H and V_L domains. All pairs of the C domains associate in a similar manner in which the members of one of their pairs of β -sheets associate isologously, while in

Figure 1.2: The Structure of IgG 1, Fab and F(ab')₂ Fragments



From www.invitrogen.com

Figure 1.2: The structure of an IgG 1 and the Fab and F(ab')₂ fragments are depicted. The intact IgG is composed of two heavy chains and two light chains. Each of the heavy and light chain monomers has a constant region (V_H) and a variable region (V_L). The intact IgG antibody has a molecular weight of ~150 kDa which consists of ~50 kDa for the Fab fragment, and ~110 kDa for the F(ab')₂ fragment. Also highlighted are the results of the Pepsin and Papain digests.

contrast, the V domains associate by means of the other β -sheet (Creighton, 1993). There are also less stable interactions that occur between domains that are present in the primary structure, with the segments linking the polypeptide chains having varying degrees of flexibility. Especially flexible is the hinge region which links the Fc and F(ab')₂ portion of the molecule and this flexibility also makes the two Fab arms particularly mobile. It is also thought that hinge-dependent Fab-Fab and Fab-Fc flexibility may be important in triggering further effector functions such as complement activation and Fc receptor binding (Campbell, 2003). Exploring the flexibility of the IgG 1 immunoglobulin isotype in more detail reveals that of the four IgG subclasses, IgG 1 has the shortest hinge region (six amino acids shorter than IgG 2) and has been shown to be the most rigid (Harris, 1998) (Vermeer, 2000).

Antibody Structure/Function

The function of an IgG immunoglobulin is to recognize antigens which are not normally present in the host organism. This is achieved through the antigen-binding sites that are located at the end of the two Fab arms and are situated between the V_L and V_H domains. Different binding sites are generated by the amino acid side chains located on the three irregular loops between the β -strands of both the light and heavy chains. These variable regions, or CDR regions, depend on the conserved structure of the rest of the immunoglobulin fold to act as a scaffold in which to stabilize their conformation. Through these residues on the three loops of the CDR region, there are genetic variations that can be generated on the order of 10^8 - 10^{10} antibody molecules with different

specificities (Creighton, 1993). Accordingly, the CDR region is also known as the hyper-variable region, and may represent the only variation between different IgG antibodies of the same isotype.

In the process of producing an IgG antibody to recognize a specific antigen, progeny cells can adapt to changes in the immunological response. Initially, the antibodies that are produced are of low affinity ($K_d = 10^{-5}$ - 10^{-7}), but with time, antibodies of increasing affinity are produced. As antibodies of high affinity and specificity are produced, individual cells can be isolated and cloned to produce additional homogeneous antibodies. This protein engineering makes it possible to produce the antibody therapeutics that allow for the desired selectivity required for a specific antigen. These homogeneous antibodies are known as monoclonal antibodies and have become an important class of drugs for treating numerous human diseases.

Issues with Protein Aggregation

Pharmaceutical Importance

Over the past 15 years, the development of monoclonal antibodies has resulted in their evolution as an important class of therapeutic treatments for a range of human diseases including cancer, allergic diseases, asthma, and organ transplantation (Campbell, 2003) (Gelfand, 2001) (Loertscher, 2002). Currently it is estimated that over 30% of all protein therapeutics presently under development are full length, fragmented, or conjugated versions of monoclonal antibodies (<http://www.phrma.org>). As monoclonal antibodies are generated as a result of a normal immune response against an antigen, with

high affinity and specificity, they are ideal candidates for targeted therapy. As of 2007, there were more than 20 monoclonal, and Fc fusion products approved and licensed by the US Food and Drug Administration (FDA) with more than 100 additional therapies in development (<http://www.phrma.org>). It is estimated that by the year 2010, sales relating to antibody therapeutics will account for more than \$30 billion dollars (IMS Midas, Data Monitor Apr 2007).

Due to the size and relative instability of monoclonal antibodies, only limited routes of patient administration have been developed successfully. The majority of approved monoclonal antibody therapeutics, especially for oncology indications, are administered by the intravenous route (Grillo-Lopez, 2003). The intravenous route has been preferred because this form of administration allows complete systematic availability, rapid delivery of antibodies to the systemic circulation, and achievement of high concentrations (Lobo E. H., 2004). Additionally, relative to other parenteral routes of administration, the intravenous route allows the administration of larger volumes. However, this route is not convenient for patients, often requiring hospitalization and thereby greatly increasing the cost of therapy. Consequently, as monoclonal antibody therapy is targeting diseases that require several mg/kg dosing, often on a regular basis, it has become necessary to develop an alternate delivery route that can be administered in an outpatient environment. Subcutaneous administration has proven to be the preferred route used by physicians, and by patients who are able to self-administer at home. This form of administration is generally limited to small injection volumes, and for many of the antibody therapeutics that require high dosing, it is often necessary to develop high

protein concentration formulations (Liu, 2005). As many of the antibody therapeutics require an average weekly dosing rate of ~2 mg/kg, a patient weighing 65 kg (the average body weight for patients), would require a weekly dose of 130 mg. Unfortunately, it has been shown that for subcutaneous administration, an injection volume of more than 1.5 mL is not well tolerated (Gelfand, 2001). This would then necessitate a protein concentration for a weekly dose to be in excess of 100 mg/mL or 130 mg of protein in less than 1.5 mL volume.

Immunological Issues with Aggregation

As antibody molecules are large and complex, the development of therapeutic formulations at the high concentrations required can lead to a variety of complex, protein stability issues. These issues include not only maintaining the physical and chemical stability of the therapeutic throughout its proposed shelf life, but also having physical properties that are compatible with the manufacturing, storage, delivery and efficacy (Shire, 2004). In response to these high protein therapeutic formulations, the FDA has become keenly interested in the effects on antibody stability and the resulting immunogenic consequence in patients (Rosenberg, 2006) (Carpenter, 2008). In a recent FDA report regarding protein therapeutics, it was stated that “among the qualitative factors critical in inducing antibody responses are molecular weight and solubility”. The review goes on to report that although low molecular weight aggregates such as dimers and trimers appear inefficient in inducing immune responses, large multimers whose molecular weight exceeds 100 kDa are efficient inducers of an immune response.

However, it should be noted that multimerization is the key to immunogenicity, as protein monomers with a high molecular weight (such as an antibody monomer of 150 kDa) are not necessarily more immunogenic than monomeric proteins with a lower molecular weight (Rosenberg, 2006). Moreover, it has been long known that any protein therapeutic that develops a non-dissociable aggregate which is insoluble, will be rapidly endocytosed by antigen-presenting cells which initiate immune responses (Frei, 1965). Consequently, it was concluded that “protein product aggregates are potential inducers of immune responses to therapeutic protein products” and that manufacturers of therapeutic products should ensure that their products contain minimal product aggregates. Furthermore, the FDA report goes on to state that manufacturers must employ several orthogonal methods for assessment of protein aggregates, or changes in levels of product aggregates (Rosenberg, 2006).

The Antibody Opalescence Phenomenon

Description of the Opalescence Phenomenon

The visual appearance of a liquid protein therapeutic is an important criterion of quality for both physicians and patients. The appearance is usually evaluated in terms of two properties; color and clarity. While color can be objectively quantified with regard to the intensity and wavelength position of relevant chromophores associated with the protein, clarity is a far more complex property to describe. A protein solution containing no appreciable particulate matter will appear to the eye as clear. However, the presence or formation of large aggregates (either soluble or insoluble), as is often encountered with

antibody therapeutics, will introduce a definite element of subjectivity to the description of the solutions clarity. In the more commonly seen case where the protein aggregates are small enough to be uniformly suspended, there will be a significant increase in the light scattered at all wavelengths by the solution. During a visual inspection of a liquid protein therapeutic, this phenomenon is typically (and subjectively) reported as having varying degrees of turbidity, cloudiness or “opalescence”.

When formulating IgG 1 antibody therapeutics at high concentrations (10-100 mg/mL), they will often have a visually opalescent appearance. The apparent similarity of these opalescent solutions to the appearance of solutions containing large aggregated proteins raises concerns about the quality and efficacy of the antibody therapeutic, the potential to cause immunogenicity or injection site reactions, and the long term stability when formulated at high concentrations.

Proposed Model of Assembly

Although the IgG 1 antibody opalescence phenomenon is believed to be quite widespread throughout the biopharmaceutical industry, there have been few published reports that have examined the possible causes. Of the few reports that do exist, most focus on the techniques used to characterize the resulting opalescence phenomenon (Carpenter, 2008) rather than attempting to understand the underlying physical causes. It has even been suggested that the opalescent appearance is entirely unrelated to noncovalent association of the IgG 1 antibody, but rather “is a simple consequence of Rayleigh scatter” (Sukumar, 2004).

Based on previous analysis of protein turbidity (Champagne, 2000), it was proposed that the observed antibody opalescence phenomenon was due entirely to the formation of large asymmetric or symmetric structures as a result of specific (non-random) protein-protein interactions. These protein-protein interactions are believed to be concentration and NaCl dependent and consist of weak noncovalent associations. In addition, these interactions are thought to be fully reversible, and as such, do not alter the overall structure or stability of the antibody. The interactions appear to follow two routes of assembly and form either randomly associated agglomerates which have a cloudy appearance or highly ordered associations which can ultimately result in a clear gel state. In either case, the protein-protein assembly appears to undergo a NaCl induced separation into two metastable liquid phases of widely different concentration. This liquid-liquid phase separation also results in increased solution viscosities further strengthening the theory of higher-order protein-protein interactions.

Techniques Proposed for Opalescence Characterization

During this study, a range of first principle techniques were employed in the characterization of the antibody opalescence phenomenon. It was crucial to use first principle techniques as they directly measure the fundamental properties of molecules such as mass, charge, shape and size, optical properties and functional properties. In addition, fundamental laws govern these properties, conservation principles apply, the linkages to energetics are well defined and most importantly, the data stand on their own.

Through the visual observation of the opalescence of Mab 1, it was evident that several techniques would be necessary to adequately characterize this phenomenon. The techniques deemed essential for this analysis included, but were not limited to, Rayleigh light scattering (also used to measure non-ideality), analytical ultracentrifugation, differential scanning calorimetry, and the use of capillary electrophoresis to directly measure the valence on the antibody. A brief description of each aforementioned technique was provided to highlight the importance of each as it related to this study.

RAYLEIGH LIGHT SCATTERING: The light scattered from dilute solutions containing macromolecules or colloidal particles can be used to determine the molecular weight, size, and any interactions that occur between the species (Doty, 1950). Many factors influence these measurements including the destructive interference of the scattered light, the refractive index increment of the solute, and the refractive index of the solvent (Camerini-Otero, 1978). In 1871, Lord Rayleigh derived an equation that described the relationship between the intensity of the incident beam of polarized light and the intensity of the scattered radiation by a small particle in a vacuum at specified angles (Wyatt, 1993). This equation features a fourth-power dependence on the wavelength of the incident light, the intensity of which is usually several orders of magnitude higher than that of the scattered radiation intensity. Subsequently referred to as “Rayleigh scattering” this theory was applied by Debye and Zimm as a first principle method to determine the weight average molecular weight (M_w), the corresponding z-average square radii (r_g^2) and a measure of the thermodynamic non-ideality (A_2) for macromolecules in solution (Debye, 1944) (Zimm, 1945). This first principle use of

Rayleigh scattering is referred to as static or “classical” light scattering and is typically measured utilizing a multi-angle light scattering instrument. Alternatively, if the light scattering intensity is measured over time, the resulting intensity fluctuations can be used to directly determine the translational diffusion coefficient (D_T) for a macromolecule in solution. Referred to as dynamic light scattering, this technique can be used to then convert the measured D_T to a hydrodynamic radius (r_h) through the Stokes-Einstein equation (Tanford, 1961).

Recently, there has been considerable interest in the potential use of the thermodynamic non-ideality or second virial coefficient as a diagnostic of solution conditions commensurate with protein solubility. A measure of a positive second virial coefficient implies a dominance of intermolecular repulsive forces between protein molecules while a measure of a negative second virial coefficient implies a dominance of intermolecular attractive forces (Tanford, 1961). A more complete review of thermodynamic non-ideality is available through many sources including, Edsall and Wyman (1958) and Tanford (1961). Static light scattering was used in this study to measure the second virial coefficient, although it has been identified that these measurements may not be a direct determination of the actual osmotic virial coefficient as constraints of constant temperature and pressure were not imposed (Deszczynski, 2006).

ANALYTICAL ULTRACENTRIFUGATION: Analytical ultracentrifugation is a method of analysis that relies on the principle property of mass and the fundamental laws

of gravitation (Laue T.M., 1999). Because of this, it requires no standards for comparison. Sedimentation can be used to explore the behavior of molecules in solution over a broad range of solute concentration and in a variety of solvent conditions. Low concentrations of solute can be used to characterize tight associations, while high concentrations can be used to characterize the thermodynamic behavior of molecules. A more complete review of analytical ultracentrifugation is available through many sources including, Cassasa and Eisenberg (1964), Laue and Stafford (1999), Laue (1992), Shuster and Laue (1994), Tanford (1961), Yphantis (1964), Yphantis and Roark (1972), Yphantis and Waugh (1956), Williams, J.W., Van Holde, K.E., Baldwin, R.L. and Fujita, H. (1958). Through the use of sedimentation velocity, the hydrodynamic properties of a molecule moving in a gravitational field are described by its sedimentation coefficient (S) and the rate at which the concentration boundary spreads to provide a measure of the translational diffusion coefficient (D_T) (Laue, 2001). The ratio of S/D_T provides a direct measure of the buoyant molecular weight (M_b), from which the molar mass (M_Z) of a macromolecule in solution can be calculated (Svedberg, 1940).

DIFFERENTIAL SCANNING CALORIMETRY: In recent years the development of differential scanning calorimetry has evolved into a technique that can be used to assess the thermal and conformational stability of a protein under different buffer conditions (Wen, 2007). The melting temperature of a protein, or of individual domains can be obtained from the DSC profile, and if the reaction is reversible the thermodynamic parameters of the unfolding can also be determined. In addition to this information,

unfolding is often accompanied by an exotherm that corresponds to the aggregation and precipitation of the unfolded protein (Vermeer, 2000).

CAPILLARY ELECTROPHORESIS: Capillary electrophoresis was used as a method to determine the protein valence in a variety of buffer conditions. The measurement of the valence (Z) was determined based on the electrophoretic mobility (u) of a protein in an electric field. Although there are two definitions for the electrophoretic mobility, experimental and hydrodynamic, the CE determines a measure of the hydrodynamic definition. It is this definition of electrophoretic mobility that is equal to the effective charge (Q^*) divided by the frictional coefficient (f), where Q^* is equal to the corresponding apparent valence (Z^*) multiplied by the proton elemental charge (e), and the frictional coefficient is determined by analytical ultracentrifugation or dynamic light scattering (Chase, 2008). Finally, there is a conversion from Z^* to Z due to counter-ion shielding, the coupling of ionic flows and the deformation of the electric field in the vicinity of the protein (Chase, 2008). For a complete review of this technique there are several sources available including, Durant (2003), Moody (2005) and Chase (2008).

Objectives of This Study

The objective of this study was to address the aggregation/opalescence relationship of an IgG 1 antibody therapeutic. In order to understand the origin of the opalescence appearance and its relationship to noncovalent association, three IgG 1 antibodies (Mab 1, Mab 2 and Mab 3) were investigated as a function of concentration and NaCl dependence. Mab 1 was used as the model for the aggregation/opalescence relationship with Mab 2 exhibiting no opalescence phenomenon and serving as a control. Mab 3 also served as a control and although it exhibited the opalescence phenomenon, it was to a much lesser extent than Mab 1. Furthermore, due to the correlation between the antibody opalescence phenomenon, protein aggregation and the possible immunogenic consequences, it was also a goal of this study to assess various techniques to help predict this behavior in future antibody therapeutic candidates.

CHAPTER II

MATERIAL AND METHODS

Antibody Preparation

Protein Expression and Purification

Three recombinant humanized monoclonal antibodies with different complimentary determining regions (CDRs) were obtained for this study. The antibodies were all expressed in Chinese Hamster Ovary (CHO) cell lines and were constructed from the same IgG 1 human framework with κ light chains. Labeled as Mab 1, Mab 2 and Mab 3, the proteins were purified from the whole cell isolate by a series of chromatography methods including affinity chromatography using Protein A, hydroxyapatite chromatography (cHA), ion exchange chromatography (CEX-HPLC) and size exclusion chromatography (SEC-HPLC). The antibodies were initially concentrated in the column buffer, dialyzed into the final buffer and subsequently brought to the final concentration of ~75 mg/mL using a process of ultrafiltration/diafiltration. The resulting antibody solution was then stored in one liter Teflon containers at -80 °C. All the chemical reagents used in this research were analytical grade or higher and deionized reverse osmosis water was used throughout this study.

Assessment of Protein Purity

Analyses were conducted on all the antibody samples used in this study to determine the extent of protein purity. Methods performed on all of the antibody samples included SDS-PAGE, CEX-HPLC and SEC-HPLC. Peptide mapping and *N*-linked oligosaccharide analysis were also performed on each of the samples. The results of each method were then compared to assess sample to sample homogeneity across each of the antibodies used throughout the study. The composition of the protein solution after the purification steps is presented in the Results section for Mab 1 only, due to the aim of this study.

SDS-PAGE: Invitrogen Novex gels were used, 4-20% Tris-Glycine catalog #EC6025. All samples were diluted to 1 mg/mL in water. In the case of non-reducing samples, a 10 μ L aliquot of each diluted sample was mixed with an equal volume of 2X non-reducing buffer, heated for five minutes at 100 °C, and loaded on the gel. For reduced samples, an equal volume of 2X reducing buffer (100 mM DTT) was added to each diluted sample (final concentration: 50 mM DTT), mixed, heated for two minutes at 100 °C, and loaded on the gel. Gels were run at 150 V for 1 ½ hours. Coomassie staining was performed by placing gels in 0.05% Coomassie blue solution for 1 ½ hours and then de-stained for three hours with periodic shaking until clear. BioRad broad range SDS-PAGE markers were used (catalog #161-0317). A standard solution of Bovine Serum Albumin (1 mg/mL) was also prepared using protein purchased from Sigma Chemical Co. Lot 041K7613. Each of the protein samples was compared to assess purity and to determine the degree of non-dissociable aggregates present.

SIZE EXCLUSION CHROMATOGRAPHY (SEC-HPLC): Size exclusion chromatography experiments were conducted using a TosohHaas G3000SWXL, catalog #08541, 7.8 mm x 30 cm, 5 μm , 250Å column on an Agilent 1100 HPLC system (Agilent Technologies, Palo Alto, CA). The column was loaded with 20 μL of protein at 2.5 mg/mL. The samples were eluted at ambient temperature with a mobile phase of 10 mM Na_2HPO_4 , 250 mM NaCl, pH 7.3 with an isocratic flow rate of 0.75 mL/min. The elution peaks were monitored at 280 nm by a UV multi-wavelength detector (Agilent Technologies).

CATION EXCHANGE CHROMATOGRAPHY (CEX-HPLC): Cation exchange chromatography experiments were conducted using a Dionex ProPac WCX-10, catalog #054993, 4 mm x 250 mm, column on an Agilent 1100 HPLC system (Agilent Technologies, Palo Alto, CA). The column was loaded with 35 μL of protein at ~2 mg/mL. In preparation for injection, all antibody samples were diluted into the initial mobile phase (mobile phase A). The samples were eluted at ambient temperature using an isocratic flow rate of 1 mL/min, following a specific elution gradient between mobile phase A (10 mM MES pH 6.5) and mobile phase B (10 mM MES pH 6.5, 400 mM NaCl). The elution step consisted of the following gradient. At time 0 to 5 minutes the gradient was 100% mobile phase A and 0% mobile phase B. From five minutes to 50 minutes, the gradient changed and eventually consisted of 50% mobile phase A and 50% mobile phase B. The gradient then changed, from 50 minutes to 55 minutes, to 0% mobile phase A and 100% mobile phase B. Finally, the gradient changed abruptly, from 55 minutes to 56 minutes, to 100% mobile phase A and 0% mobile phase B, ending with

this final gradient after 75 minutes of total run time. The elution peaks were monitored at 280 nm by a multi-wavelength UV detector (Agilent Technologies).

ACHRO-K PEPTIDE MAPPING: The reduction/alkylation step was performed in 2 mL Starstedt vials using a total of 500 μ L of protein at a concentration of 2 mg/mL. The volume of the reduced and alkylated preparation was brought to 750 μ L with a final DTT concentration of 3.125 mM. The 1 M stock solution of DTT was made up prior to use and stored at -20 °C until needed. The volume was then adjusted to 1 mL with a solution of 6 M guanidine hydrochloride (GdnHCl), 50 mM Tris-HCl, pH 8.2, and the samples were incubated in a 40 °C heating block for one hour. The reduced samples were removed from the heating block and alkylated by adding 100 μ L of freshly prepared 1 M iodoacetic acid (IAA) solution for a final IAA concentration of 5.5 mM. The samples were then incubated in the dark at ambient temperature for an additional hour and the reaction was quenched by the addition of 5 μ L of the 1 M DTT stock solution. To remove excess reagents, the entire volume of each reduced and alkylated antibody sample was then buffer exchanged into 50 mM Tris-HCl, pH 9.0 using two Amersham Biosciences HiTrap Desalt columns in series. The resulting protein concentration was then determined by UV absorbance, using the mobile phase (50 mM Tris-HCl, pH 9.0) to blank the instrument. The digestion step followed with approximately 60 μ g of the protein sample mixed with Achro-K, at an enzyme substrate concentration of 1:20, and brought up to a total volume of 1 mL using 50 mM Tris-HCl, pH 9.0. The final chromatography step was performed using a Waters Symmetry C18, catalog #WAT106151, 4.6 mm x 250 mm, column on an Agilent 1100 HPLC system (Agilent Technologies, Palo Alto, CA). The column was loaded with 900 μ L of protein for a total

sample load of 54 µg. The samples were eluted at 30 °C using a flow rate of 1 mL/min, following a specific elution gradient between mobile phase A (0.05% TFA (v/v) in water) and mobile phase B (0.05% TFA (v/v) in 95% acetonitrile). The elution step consisted of the following gradient. At time zero to five minutes the gradient was 96% mobile phase A and 4% mobile phase B. From 5 minutes to 100 minutes, the gradient changed and eventually consisted of 60% mobile phase A and 40% mobile phase B. The gradient then changed, from 100 minutes to 100.1 minutes, to 0% mobile phase A and 100% mobile phase B and ran to 102 minutes. The gradient then was changed again, from 102 minutes to 102.1 minutes, to 96% mobile phase A and 4% mobile phase B, ending with this final gradient after 120 minutes of total run time. The elution peaks were monitored at 214 nm by a UV multi-wavelength detector (Agilent Technologies).

N-LINKED OLIGOSACCHARIDE ANALYSIS: The oligosaccharide analysis was performed by initially diluting the protein samples to approximately 2 mg/mL using 25 mM ammonium formate pH 7.4. The samples additionally were buffer exchanged into the same volatile buffer using Amicon Ultra 30,000 MWCO protein concentrators. After recovery, each sample was digested with 5 µL of PNGase F (NEB, glycerol free) and incubated overnight at 37 °C. The samples then were dried down by speed vacuum centrifugation and reconstituted in purified water. Samples were then analyzed using High pH Anion Exchange Chromatography on an all PEEK Agilent 1100 HPLC system (Agilent Technologies, Palo Alto, CA) with Pulsed Electrochemical Detection (HPAEC-PED) analysis. Separation on the HPAEC-PED system was performed with a Dionex CarboPac[®] PA100 guard column (2 mm x 50 mm) and an analytical column (2 mm x 250 mm). A linear gradient was used throughout the 60 minute run consisting of mobile

phase A (100 mM NaOH) and mobile phase B (100 mM NaOH, 500 mM sodium acetate). The elution progress was monitored using a Dionex ED-40 electrochemical detector (Dionex Corporation, Sunnyvale, CA).

Opalescence Characterization

Preparation of Sample

Solutions of Mab 1, Mab 2 and Mab 3 antibodies used in the opalescence characterization were prepared by dialyzing the stock protein solution for 24 hours in 10 mM Histidine, Sigma Chemical Co. Lot 113H5725, pH 6, using Pierce Slide-A-Lyzer[®] 10K MWCO Dialysis Cassettes. Samples were then similarly prepared by dialysis into 10 mM Histidine buffer, pH 6, containing the various NaCl concentrations used throughout this study. After dialysis, the pH was checked and the solution was sterilized using a Whatman Anotop[®] 25 mm, 0.20 μm , PES syringe mount filter, Catalog #6809-2022. The protein concentration was determined by measuring the absorbance at 280 nm using a Spectramax Plus UV-Vis spectrophotometer equipped with a plate reader. The absorbance was determined at a wavelength of 280 nm and was corrected for light scattering by subtracting the absorbance at 320 nm. The concentration was then calculated using an extinction coefficient of 1.55 ($\text{mL mg}^{-1}\text{cm}^{-1}$) for Mab 1, 1.36 ($\text{mL mg}^{-1}\text{cm}^{-1}$) for Mab 2 and 1.45 ($\text{mL mg}^{-1}\text{cm}^{-1}$) for Mab 3 as determined theoretically by quantitative amino acid analysis.

Visual Appearance and Description

Although it was initially thought to be of great importance to properly characterize the degree of protein opalescence, the scope of this study shifted to examine the unique opalescence of a single model antibody. The degree at which the actual opalescence assignments are used throughout this study is minimal but it is important to understand how the assignments were derived and subsequently used for opalescence comparison between the three model antibodies examined.

The method to assess and describe the visual appearance of the unique protein self-association characterized in the study was based on the guidelines employed by the European Pharmacopeia (Ph. Eur, 1980). The guidelines describe a test for clarity and degree of opalescence of liquids that are specific in terms of visual description. It is important to note that this method does not attempt to distinguish between the types of particles that are giving rise to the observed opalescence.

PREPARATION OF REFERENCE SUSPENSION: The reference suspensions were prepared as described in the European Pharmacopeia (Ph. Eur, 1980) with the following modifications:

- A. Hydrazine sulfate solution: 1.0 g hydrazine sulfate (J.T. Baker, cat #2177-04, "Baker analyzed") was dissolved in 100 mL deionized reverse osmosis water and allowed to stand for four-six hours.
- B. Hexamethylenetetramine solution: 2.5 g hexamethylenetetramine (Aldrich Chemical Co. cat #H1,130-0) was dissolved in 25 mL deionized reverse osmosis water.

- C. Primary opalescent suspension: 15 mL of solution A was added to 25 mL of solution B and the mixture was allowed to stand for 24 hours.
- D. Standard of opalescence: 15 mL of the primary opalescence suspension (C) was diluted to 1000 mL with deionized reverse osmosis water. [This suspension was prepared fresh and stored for 24 hours at most].
- E. Reference suspensions: 5 mL of solution D was added to 95 mL of deionized reverse osmosis water to produce reference suspension I, 10 mL of solution D was added to 90 mL of deionized reverse osmosis water to produce reference suspension II, 30 mL of solution D was added to 70 mL of deionized reverse osmosis water to produce reference suspension III, 50 mL of solution D was added to 50 mL of deionized reverse osmosis water to produce reference suspension IV.

The protein sample in question was then compared visually to the freshly prepared reference suspensions using identical vials of colorless, transparent, neutral glass with a flat base and an internal diameter of 15 to 25 mm, the depth of the solution layer being at least 40 mm. All solutions were compared in a specially prepared light box which had light holes designed to illuminate each vial equally from the bottom. The samples were compared approximately five minutes after preparation and viewed vertically against a black background. These conditions insured that each of the reference suspensions could be easily distinguished for accurate opalescence assignments.

DESCRIPTION OF THE RESULTS OF THE VISUAL INSPECTION: The European Pharmacopeia has characterized opalescence in four very specific categories.

1. Clear (Ph. Eur, 1980) “A liquid is considered clear if its clarity is the same as that of purified water or of the solvent used when examined under the conditions as described above, or if its opalescence is not more pronounced than that of reference suspension I”.
2. Slightly Opalescent (Ph. Eur, 1980) “A liquid is slightly opalescent if its opalescence is more pronounced than in the preceding case, but not more pronounced than that of the reference suspension II”.
3. Opalescent (Ph. Eur, 1980) “A liquid is considered opalescent if its opalescence is more pronounced than in the preceding case, but not more pronounced than that of the reference suspension III”.
4. Very Opalescent (Ph. Eur, 1980) “A liquid is considered very opalescent if its opalescence is more pronounced than in the preceding case, and may be more pronounced than that of the reference suspension IV”.

UV SPECTROSCOPY TO DETERMINE CATEGORY OF OPALESCENCE:

In contrast to the European Pharmacopea methods of visual characterization of opalescence, UV spectroscopy allowed a less subjective measure of the degree of opalescence. UV spectroscopy was carried out using a Spectramax Plus UV-Vis spectrophotometer equipped with a plate reader. The protein samples and reference suspensions were placed in individual wells in a 96 well plate along with a well containing purified water. The relative optical density (OD) of the reference suspension and protein solutions were measured against the purified water at a wavelength of 400 nm and recorded. In order to determine the degree of opalescence, the OD values of the

protein samples were then compared to the OD values of the reference suspensions to allow placement into the appropriate category.

Static Multi-Angle Light Scattering (MALS) Studies

SIZE EXCLUSION CHROMATOGRAPHY-MALS: Size exclusion chromatography experiments were conducted using a TosoHaas G3000SWXL, catalog #08541, 7.8 mm x 30 cm, 5 μm , 250 \AA column on an Agilent 1100 HPLC system (Agilent Technologies, Palo Alto, CA). The column was loaded with 100 μL of protein at 1 mg/mL. The samples were eluted at ambient temperature with a mobile phase of 10 mM Na_2HPO_4 , 100 mM NaCl, pH 7.15 with an isocratic flow rate of 0.2 mL/min. The elution peaks were monitored at 280 nm by a UV multi-wavelength detector (Agilent Technologies), a DAWN[®]-HELEOS Multi Angle Light Scattering (MALS) detector (Wyatt Technology, Santa Barbara, CA) equipped with a 60 mW GaAs linearly polarized laser, operating at a wavelength of 658 nm, and an Optilab rEX[™] differential refractive index detector (Wyatt Technology, Santa Barbara, CA) that utilizes an LED light source operating at a wavelength of 658 nm. The data from the UV, MALS and dRI were collected and analyzed using Astra[®] V software (Wyatt Technology, Santa Barbara, CA). The complete static light scattering data set at multiple angles (10° - 160°) and the dRI data (using a dn/dc value of 0.185 mL/g) then was used to create a Debye plot to derive the absolute weight average molecular weight for the eluting SEC species.

BATCH-MALS: The weight average molecular weight of the antibody samples as a function of protein and salt concentration were measured along with the root mean square radius (R_g) at ambient temperature and at multiple angles (10° - 160°) using a

DAWN[®]-EOS[™] Multi Angle Light Scattering (MALS) detector and an Optilab DSP[™] differential refractive index detector. The samples were introduced into the MALS detector, with the flow cell still in place, using a Razel[™] syringe pump model #A-99, and a 3 mL Norm-Ject[®] all polymer syringe, VWR part number 53548-006, flowing at 0.2 mL/min. A buffer blank was initially injected to establish a baseline and then the protein samples were injected in adequate volumes to establish a flat plateau for each concentration. In addition to Debye plots, Zimm Plots we also generated from the excess Raleigh ratio of the protein solutions to measure the effects of non-ideality, also known as second virial coefficient or A_2 .

FIELD FLOW FRACTIONATION-MALS: In order to overcome the significant separation limitation of size exclusion chromatography, asymmetric flow field flow fractionation (AFFF) was also employed. An Eclipse[™] II field flow fractionation instrument (Wyatt Technology, Santa Barbara, CA) was coupled to a UV multi-wavelength detector (Agilent Technologies), a DAWN[®]-HELEOS Multi Angle Light Scattering (MALS) detector and an Optilab rEX[™] differential refractive index detector. The solvent flow through the AFFF was achieved by the use of an HPLC isocratic pump and autosampler (Agilent Technologies) and delivered to the separation channel by the use of two needle valves. The protein samples were loaded onto the AFFF in various quantities depending on the degree of opalescence. Samples with a lower degree of opalescence were loaded at 50 μ g to 100 μ g and samples with a higher degree of opalescence were loaded at 10 μ g to 50 μ g. Separation was achieved at ambient temperature using a 21 cm aqueous channel with a 10 KDa regenerated cellulose membrane and a 350 μ M standard width spacer. To examine the salt dependence on the

protein opalescence, two buffers were used in the AFFF analysis consisting of 10 mM Histidine, pH 6, and 10 mM Histidine, 100 mM NaCl, pH 6. After the injection, the samples were initially focused for two minutes at a cross flow of 0.2 mL/min and then eluted using a channel flow of 1 mL/min and a cross flow of 5 mL/min over ten minutes, followed by a cross flow gradient to 0.1 mL/min over 30 minutes.

Sedimentation Velocity Studies

All sedimentation velocity experiments were conducted using a Beckman XL-I analytical ultracentrifuge equipped with an on-line Raleigh optical system (Laue, 1992), a UV absorption optical system and a An-50 Ti 8-hole titanium rotor. The cells consisted of a 2-sector, 12 mm charcoal-filled Epon, velocity centerpiece and matched quartz windows contained in wide-aperture window holders. Protein samples were diluted to 1, 0.5 and 0.125 mg/mL using a buffer containing 10 mM Histidine, 10 mM NaCl, pH 6 and another buffer containing 10 mM Histidine, 150 mM NaCl, pH 6. The samples then were filled into the velocity cells along with their appropriate buffer blanks and allowed to equilibrate before running. Centrifugation was run at 35,000 rpm at 20 °C, and the scans were collected using the UV-absorption optical scanning system, scanning at a wavelength of 280 nm. Data were collected using the Beckman XL-I version 4.5 program and the distribution of the different species was obtained using the non-linear curve fitting program SEDFIT (Schuck, 2000). The program Sednterp was used to calculate the partial specific volume (v) of the antibodies in solution and the buffer density (ρ), for each ionic strength, as described (Laue, 1992). The data were arranged

using ORIGIN™ to graph the C(S_{20,w}) distribution overlays for each antibody concentration.

Electro-Separation

A unique method of inducing opalescence was initially derived to study the opalescence phenomenon. This method used an apparatus that was built in the lab using a 15 mL conical tube with the conical end removed. The tube was further modified by drilling nine, 1/16" diameter holes along the length of the tube in linear, equidistant spacing, used for sampling purposes. The two open ends of the tube were fitted with #00 rubber stoppers that were modified with platinum electrodes passing through, and the electrodes at the wide end of the stopper were connected to a power supply using wires fitted with alligator clips. Prior to fitting the modified stoppers into the ends of the tube, a 12,000 MWCO Spectra/Por® 1 Molecularporous Regenerated Cellulose Dialysis Membrane was draped over each so that once inserted, the electrodes at the narrow end of the stopper would not come into contact with the contents of the tube. The tube was filled carefully with the antibody sample at a concentration of approximately 10 mg/mL and held horizontally during the experiment using a ring stand and ring stand clamps

Figure 2.1. Constant voltage (80 volts) then was applied to the apparatus using a Heofer PS-1200 DC power supply until the current stabilized and the opalescence phenomenon was observed (approximately ten minutes). The power supply then was turned off and a 10 uL sample was removed at each sampling port for further analysis. The samples were diluted 1:10 and the optical density (OD₂₈₀) was measured along with the pH and

Figure 2.1: The Electroseparation Device Designed to Induce Opalescence

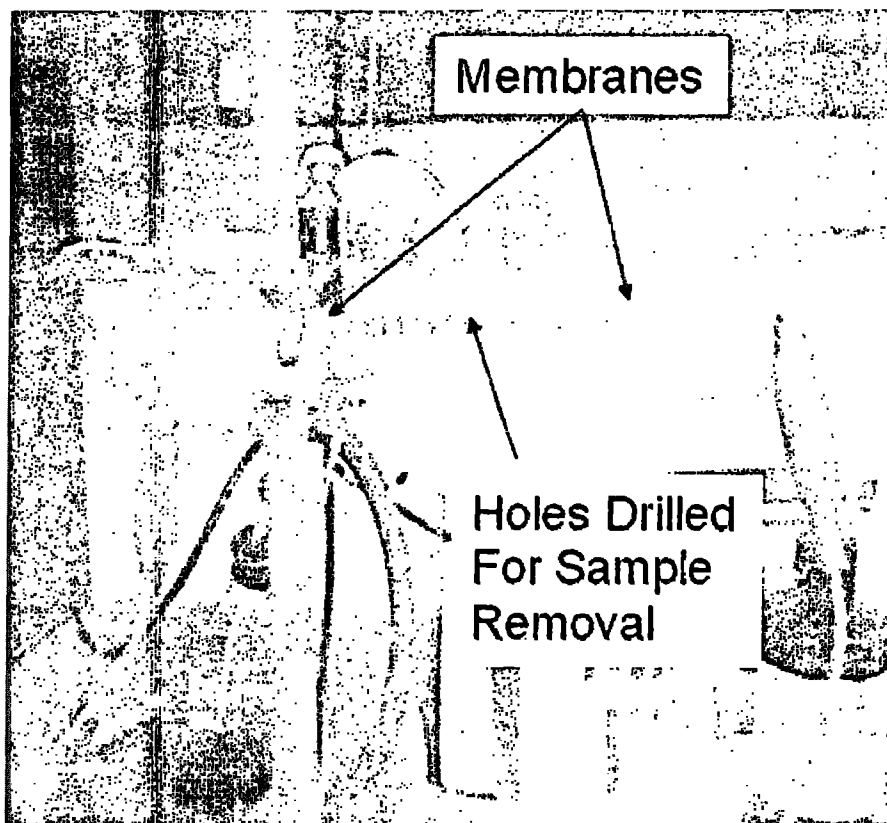


Figure 2.1: The electroseparation device was designed to induce opalescence by passing an electrical current through the IgG 1 sample solution. The platinum electrodes were isolated from the sample solution by the use of semi-permeable membranes. Once opalescence was induced the holes drilled along the top of the device allowed a sample of the solution to be recovered for further analysis. It should be noted that although a fair amount of time was placed on conducting these unique experiments, the results were merely used to study the opalescence phenomenon through manual induction and to craft further analysis of the naturally occurring opalescence, through more traditional biophysical techniques.

conductance. Attempts were made to further analyze each sample using sedimentation velocity but were unsuccessful.

Salt Induced Opalescence

Salt induced opalescence was examined after the results of the Electro-Separation experiments. Solutions of Mab 1, Mab 2 and Mab 3 antibodies used in the salt induced opalescence characterization were prepared by dialyzing the stock protein solution for 24 hours in 10 mM Histidine, Sigma Chemical Co. Lot 113H5725, pH 6, using Pierce Slide-A-Lyzer[®] 10K MWCO Dialysis Cassettes. Samples were similarly prepared by dialysis into 10 mM Histidine buffer, pH 6, containing the various NaCl concentrations used throughout this study. In addition to NaCl dependence, other salts also were examined in the 10 mM Histidine buffer including 100 mM KCl and 100 mM Sodium Citrate. The resulting opalescence that occurred was used for all subsequent characterization results in this study.

Dynamic Light Scattering Studies

The hydrodynamic radius of the IgG 1 samples in this study were measured using a DynaPro[™] Titan (Wyatt Technology, Santa Barbara, CA) and the DynaPro[™] Plate Reader Plus (Wyatt Technology, Santa Barbara, CA). Both of the DLS instruments employed a solid state GaAs laser tuned to λ_{830} , and operating at an output power between 5 and 50 mW. When required, the filtration of samples was performed using a Whatman Anotop[®] 10, 0.1 μ M pore size Anopore syringe tip filter, catalog #6809-1012 (Whatman plc, Maidstone, KY), fitted to a 3 mL Norm-Ject[®] all polymer syringe, VWR

part number 53548-006. Data were collected using a proprietary multi-mode optical fiber and analyzed using Dynamics™ software, that utilizes a multi-tau correlator collecting 248 channels at 0.48 μs.

DYNAPRO™ TITAN ANALYSIS: The Titan sample cell holder consisted of a 12 μL quartz cuvette with a one cm path length, and a built in air-cooled Peltier with condensation control. During analysis, the IgG 1 samples were prepared over a range of concentrations and NaCl conditions used throughout this study and the sample temperature was maintained at 25 °C (± 0.03 °C). The scattered light intensity was collected at an angle of 90° and the laser power was adjusted manually until there was a total scattering intensity of approximately 8×10^5 counts/second. Data were collected over a 20 second time frame with five data sets averaged together to give a total collected time of 100 seconds.

DYNAPRO™ PLATE READER PLUS: The Plate Reader Plus sample holder consisted of a Greiner™ Bio-One 384 SensoPlate, catalog #781892, 50 μL microplate that was black with a clear flat glass bottom (Greiner Bio-One, Inc, Monroe, NC), and a built in air-cooled Peltier with condensation control. During analysis, the Mab 1 sample was diluted from a stock solution of 77 mg/mL in 10 mM Histidine, pH 6 to a concentration range of 2, 4 and 6 mg/mL, each, in buffers containing 10 mM Histidine, pH 6, with 0, 25 and 50 mM NaCl. To examine the temperature dependence on the NaCl concentration for the Mab 1, the temperature of the Plate Reader was increased from 4 °C to 70 °C in 4 °C increments, waiting at each increase for the temperature of the plate to equilibrate. Each sample was prepared three times and the data were collected over a two second time

frame with five data sets averaged together to give a total collected time of ten seconds. Additionally, the temperature dependence on the viscosity of the solvent was corrected for based on an aqueous model.

Digestion / Fragmentation

PEPSIN DIGEST: This preparation describes the procedure for peptic digestion of IgG 1 molecules and the subsequent purification of their F(ab')₂ fragments by SEC-HPLC.

To prepare the digestion buffer, 20 mM sodium acetate pH 4.0 was prepared dissolving 1.64 g of sodium acetate (Fluka catalog #94318) in ~900 mL of water, using acetic acid to titrate the solution to pH 4.0. The volume was brought up to one liter, the buffer was filtered with a 0.2 μm (pore size) bottle-top filter and stored at room temperature.

The IgG 1 samples (10 mg/mL each in 10 mM Histidine, pH 6) were buffer exchanged into the digestion buffer (4 mL × 2) using centrifugal filter devices (Millipore catalog #UFC801024), and the final volumes were adjusted to 1 mL. For each Mab, 0.25 mL of immobilized pepsin (Pierce catalog #20343) (50% slurry) was equilibrated with digestion buffer (4 mL × 2) in a glass borosilicate test tube and the final volume was adjusted to 0.5 mL. The IgG 1 samples in the digestion buffer were combined with the immobilized pepsin in a 16 x 100 mm borosilicate glass tube (Fisher catalog #14-961-29) along with a stir bar, and sealed with parafilm. Samples were incubated at a temperature of 37 °C with constant stirring (Pierce Reacti-Therm heating/stirring module). Based on time course experiment results, all IgG 1s were digested in 20 mM sodium acetate pH

4.0, at 37 °C for 12 hours. Immobilized pepsin was separated by centrifugation, and the supernatant was buffer exchanged into 10 mM Na₂HPO₄, 100 mM NaCl, pH 7.15, and the final volume was ~0.5-1 mL.

PURIFICATION OF THE PEPSIN DIGEST: SEC-HPLC was chosen for the purification of the F(ab')₂ fragments because it is a mild separation technique which operates independently from small changes in their environment such as ionic strength, pH and temperature. The buffer-exchanged crude peptic digest, in PBS-CMF, was filtered using a Whatman Anotop[®] 10, 0.1 μM pore size Anopore syringe tip filter, fitted to a 3 mL Norm-Ject[®] all polymer syringe, into an HPLC vial. The analytical scale SEC-HPLC was run by injecting 50 μg of intact IgG 1 followed 50 μL of crude digest to estimate the extent of digestion and retention time relative to the undigested IgG 1. SEC-HPLC purification was performed using a TosoHaas G3000SWXL, catalog #08541, 7.8 mm x 30 cm, 5 μm, 250Å column on an Agilent 1100 HPLC system (Agilent Technologies, Palo Alto, CA). The samples were eluted in 20 minutes at ambient temperature with a mobile phase of 10 mM Na₂HPO₄, 100 mM NaCl, pH 7.15 using an isocratic flow rate of 0.75 mL/min. The elution peaks were monitored at 214 nm by a UV multi-wavelength detector (Agilent Technologies). For the preparative SEC-HPLC, the injection volume was increased according to the height of the F(ab')₂ peak (major peak) observed in analytical scale chromatograms. The F(ab')₂ fraction was manually collected from multiple injections and pooled. Protein concentration was determined spectrophotometrically (A₂₈₀) using calculated absorptivity (mg/mL)⁻¹cm⁻¹ for the F(ab')₂ fragments.

PAPAIN DIGEST: The preparation of Fab, (Fab)₂, and Fc fragments, followed Pierce protocol #20341 “Procedure for IgG 1 Digestion to Generate Fab Fragments”, exceptions are noted.

To start the sample preparation, the IgG 1 samples were dialyzed into the papain sample buffer (20 mM sodium phosphate, Na₂HPO₄, 10 mM EDTA, pH 7.0) before papain digestion using an Amicon 10 kDa MWCO membrane spin tube. Approximately 11 mg of each of the samples (250 μL of 45 mg/mL) were spun at 6500 x g for 30 minutes for two buffer exchange cycles. The final volume of the sample after the buffer exchange was brought to approximately 350 μL, the samples were diluted 1:10 and the optical density (OD₂₈₀) was measured. The antibody samples were then diluted to a final concentration of approximately 33 mg/mL in preparation of the digest step.

The bead immobilized papain (Pierce catalog #20341) was shipped in a storage solution containing 50% glycerol, 0.1 M sodium acetate, 0.05% sodium azide, pH 4.4. The bead immobilized papain solution was dialyzed into a papain digest buffer containing 20 mM cysteine-HCL added to the papain sample buffer with the pH adjusted to 7.0 before use. The wash volume ratio recommended by Pierce was 0.5 mL immobilized papain to 4 mL papain digest buffer. The following modified procedure was followed:

1. Added 1.5 mL immobilized papain to a 15 mL conical tube
2. Added 12 mL papain digest buffer and mixed by inversion
3. Spun at 3500 x g for three minutes
4. Removed supernatant
5. Repeated with another 12 mL papain digest buffer

6. Resuspended immobilized papain with 0.5 mL papain digest buffer so the final volume was ~1 mL (0.5 mL papain + 0.5 mL papain digest buffer)

The digestion of the antibody samples was performed by mixing 300 μ L of each antibody sample (~10 mg) with 67 μ L of papain sample buffer and 500 μ L of the papain digest buffer. The digests were placed in starstedt tubes allowing for space in the tubes for the digest volume to mix and then placed on a table top shaker for 24 hours at room temperature. After the digestion was complete, the samples were stored at 2-8 $^{\circ}$ C for two days. The papain was then separated from the sample by spinning the starstedt tubes on a bench top centrifuge at 8000 RPM for three minutes. Supernatant was removed and the immobilized papain was discarded. Theoretical concentration after the papain digestion was calculated to be approximately 6 mg/mL for each of the antibody samples but the optical density (OD₂₈₀) was not measured.

PURIFICATION OF THE PAPAIN DIGEST: The purification of the papain digested IgG 1 samples was then performed by Protein-A HPLC. The theory is that the Fab and (Fab)₂ fragments elute in the flow through and the Fc fragment binds to the protein-A column allowing for the first step in purification of the antibody fragments. The chromatography was performed using an Applied Biosystems PA Immuno-Detection Sensor Cartridge, catalog #2-1001-00, column on a Waters 2695 HPLC system (Waters Corporation, Milford, MA). The column was loaded with 50 μ L of protein for a total sample load of 300 μ g. The samples were eluted at 4 $^{\circ}$ C using a flow rate of 1 mL/min, following a specific elution gradient between mobile phase A (50 mM NaH₂PO₄, 150 mM NaCl, pH 7.0) and mobile phase B (0.5% H₃PO₄, 100 mM NaH₂PO₄, 400 mM

NaCl). The elution step consisted of the following gradient. At time zero to five minutes the gradient was 100% mobile phase A and 0% mobile phase B. From seven minutes to 12 minutes, the gradient changed to 0% mobile phase A and 100% mobile phase B. Finally, the gradient was changed back to 100% mobile phase A and 0% mobile phase B and the elution continued for a total run time of 15 minutes. The elution peaks were monitored at 280 nm by a UV variable-wavelength detector (Waters Corporation). Both the flow through and the elution fraction were collected from multiple injections. The collected fractions were pooled, buffer exchanged into the appropriate buffer system and concentrated. Buffer exchange and concentration was performed using Amicon 10 kDa MWCO membrane spin tubes spun at 6500 X g to reduce the initial volume to ~100 μ L. Then 4 mL of the 10 mM Histidine, pH 6, buffer was added and spun for two exchange cycles until the final volumes were approximately 500 μ L. Finally, the optical density (OD_{280}) for each fractionated sample was measured using a Spectramax Plus UV-Vis spectrophotometer equipped with a plate reader. The absorbance was determined at a wavelength of 280 nm and was corrected for light scattering by subtracting the absorbance at 320 nm. The concentration was then calculated using an extinction coefficient of 1.65 ($\text{mL mg}^{-1}\text{cm}^{-1}$) for Fab (Mab 1), 1.37 ($\text{mL mg}^{-1}\text{cm}^{-1}$) and for Fc (Mab 1) as determined theoretically by quantitative amino acid analysis. The Fab and Fc samples that were analyzed for Mab 2 and Mab 3 were supplied by a collaborator.

PURIFICATION OF THE POST PROTEIN-A PAPAIN DIGEST BY SEC-

HPLC: The final purification was performed using a TosoHaas G3000SWXL, catalog #08541, 7.8 mm x 30 cm, 5 μ m, 250 \AA column on an Agilent 1100 HPLC system (Agilent Technologies, Palo Alto, CA). The column was loaded initially with an analytical load of

10 μg and then with a purification load of 300 μg of the fractionated samples. The samples were eluted in 20 minutes at ambient temperature with a mobile phase of 10 mM Na_2HPO_4 , 100 mM NaCl, pH 7.15 using an isocratic flow rate of 0.75 mL/min. The elution peaks were monitored at 280 nm by a UV multi-wavelength detector (Agilent Technologies). Since each fragment had some undigested material, the fragments were further purified into Fab, $(\text{Fab})_2$, and Fc. The fragments were collected from several runs, pooled, and concentrated using Amicon 10 kDa MWCO membrane spin tubes, spun at 6500 x g to reduce volume. Solutions of the purified Fab, $(\text{Fab})_2$, and Fc fractions were then dialyzed for 24 hours in 10 mM Histidine, Sigma Chemical Co. Lot 113H5725, pH 6, using Pierce Slide-A-Lyzer[®] 10K MWCO Dialysis Cassettes. Samples were then similarly prepared by dialysis into 10 mM Histidine buffer, pH 6, containing the various NaCl concentrations used throughout this study. The protein fraction concentration was determined as previously described.

Differential Scanning Calorimetry (DSC) Studies

The thermal stability of the antibody samples and the fractionated protein samples was assessed using a MicroCal VP-Capillary Differential Scanning Calorimeter (Microcal LLC, Northampton, MA). Samples were run at a volume of 350 micro liters and a concentration of approximately 1.5 mg/mL using a 90 $^\circ\text{C/hr}$ scan rate spanning the temperature range from 20 to 90 $^\circ\text{C}$. Triplicate scans were performed at each temperature with a ten minute equilibration at 20 $^\circ\text{C}$ and no equilibration at 90 $^\circ\text{C}$. It is also important to note that the system was completely washed out after each protein run. Samples were buffer subtracted and converted into concentration normalized scans. The

data was then analyzed using Origin™ software ver. 7.0 in order to fit the thermal transitions.

Non-Ideality Analysis

INSTRUMENTATION: An experimental instrument known as the Calypso was developed by Wyatt Technology to deliver a series of un-fractionated samples of different concentrations in order to characterize the affinities of macromolecular interactions, or virial coefficients. The Calypso system comprises three computer-controlled syringe pumps that utilize dc-servo motors for a smooth, pulse-free delivery and a built-in multi-channel vacuum degasser. The three syringe pumps were able load buffer and stock sample solutions, subsequently dispensing them at different pre-programmed rates so as to generate a succession of concentration ratios. The syringes delivered the sample mixtures through a four port union, an in-line Whatman Anotop 25, 0.1 µM filter to a mixing chamber and finally to a DAWN®-EOS™ Multi Angle Light Scattering (MALS) detector and an Optilab DSP™ differential refractive index detector, installed in parallel as indicated schematically in **Figure 2.2**. The flow rate to each of the two detectors connected in parallel was adjusted using a metering valve to ensure that the refractive index measured at a particular time point corresponded to the composition of solution scattering light at the same point. The data was collected and analyzed using the CALYPSO data analysis program and Astra® V software.

EXPERIMENTAL PROCEDURE: The setup employed in this study consisted of one syringe containing our IgG 1 sample and one syringe containing the buffer of interest so that the desired dilutions could be made. Following baseline measurements of the

Figure 2.2: The Parallel Detector Configuration of the Calypso Instrument with the MALS and Concentration Detector

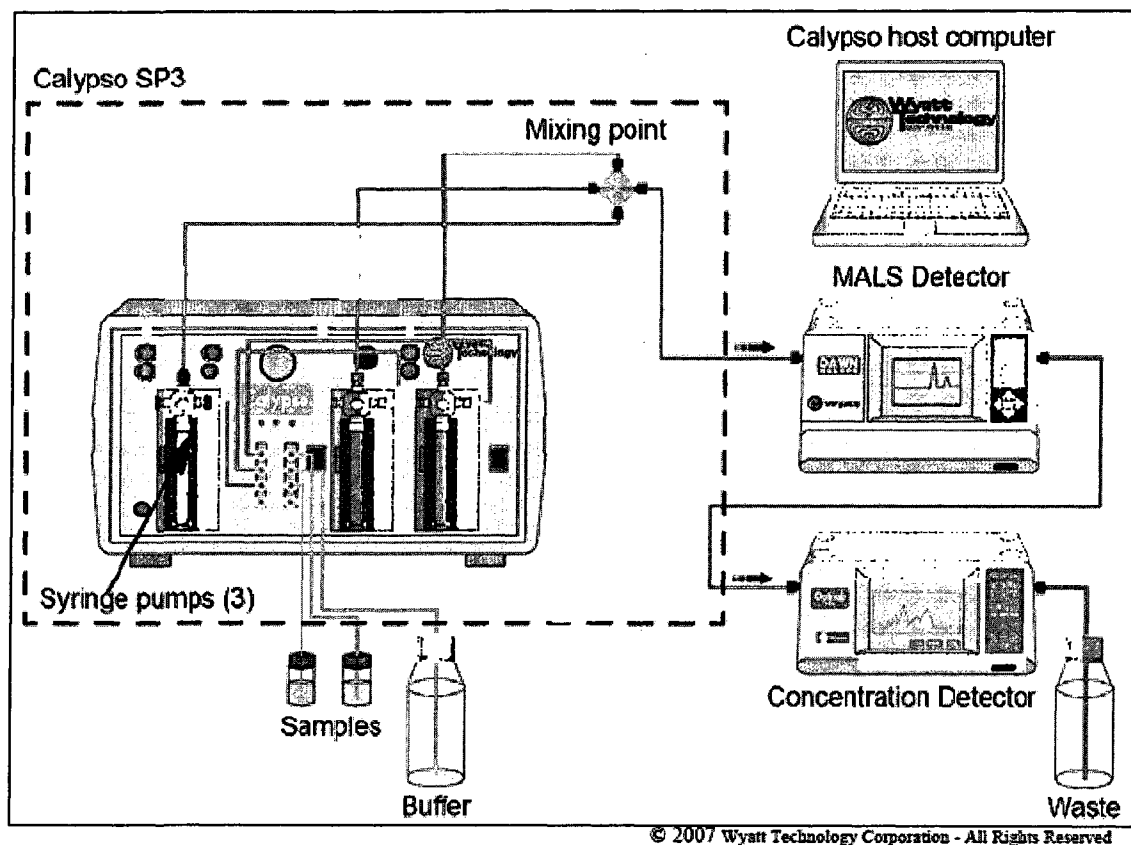


Figure 2.2: The Calypso instrument comprises a set of three computer-controlled syringe pumps and a built in multi-channel vacuum degasser, together with associated tubing, filters and valves. The schematic displays a Calypso instrument which is configured in the parallel configuration. In the parallel configuration, the sample flow is first mixed and then split between the two detectors at a fixed ratio which is optimized to guarantee equal concentrations in each detector upon injection.

buffer alone, there was a stepwise change of solute concentration that varied linearly upward from zero concentration (pure buffer) to the concentration of the IgG 1 stock solution, and then downward from the concentration of the IgG 1 stock solution to zero concentration, typically over a series of ten concentrations. Upon collecting the data, the resulting plateaus are assigned a concentration based on the refractive index detector, and the multi-angle light scattering data was used to assign the value of the Rayleigh ratio at a zero scattering angle. This data was then combined to generate a Zimm plot which is capable of calculating values of M_w , R_g and A_2 for the IgG 1 species.

Viscosity Measurement

The viscosity of the antibody samples was measured using an Anton PAAR rheometer (Anton PAAR, Ashland, VA) equipped with a CP 25-1 cone/plate measuring system. Approximately 100 μ L of sample was loaded onto the lower measuring plate and allowed to come to thermal equilibrium. The rheometer was set at a constant shear rate of 898 s^{-1} , speed 150 min^{-1} , and a constant temperature of $25\text{ }^\circ\text{C}$. Ten points were averaged per sample and the data was measure in units of centipoise. The viscosity of Mab 1 was measured over a concentration range of 1, 5, 10, 20, 30, 40, 50, 55 and 60 mg/mL at 4 and $25\text{ }^\circ\text{C}$ in a buffer containing 10 mM Histidine, 50 mM NaCl, pH 6. The viscosity effects of NaCl on the three IgG 1 antibody samples were also measured at a concentration of 5 mg/mL in a buffer containing 10 mM Histidine, pH 6 with 0, 50 and 100 mM NaCl.

Circular Dichroism Analysis

The CD spectra were recorded on JASCO J-815 spectropolarimeter (JASCO Inc. Easton, MD) equipped with peltier-controlled temperature regulation and a one cm path length cuvette for recording near-UV spectra. The antibody samples to be tested were dialyzed for 24 hours in 10 mM Histidine, Sigma Chemical Co. Lot 113H5725, pH 6, using Pierce Slide-A-Lyzer[®] 10K MWCO Dialysis Cassettes. Samples were then similarly prepared by dialysis into 10 mM Histidine buffer, 100 mM NaCl, pH 6 and brought to a final concentration of 4 mg/mL. The near-UV CD spectra were recorded at a temperature of 25 °C from 250 to 360 nm (in 0.5 nm steps) with an integration time of two seconds at each wavelength and the baseline was corrected against a cuvette containing buffer alone. The CD data thus obtained were expressed in terms of molar ellipticity ($\text{deg cm}^2 \text{ dmol}^{-1}$) $[\theta]$ and graphed against wavelength (nm).

Congo Red Studies

The binding of Congo Red (CR), Sigma Chemical Co. Lot C6767, to the IgG 1 samples was examined at room temperature in buffer conditions of 10 mM Histidine, pH 6, \pm 100 mM NaCl. The samples were diluted to \sim 1 mg/mL and incubated in 50 μ M CR for two hours (Chiti et. al. 2001) (Sirangelo et. al. 2002) (Srisailam et. al. 2002) and then filtered using a Whatman Anotop[®] 10 mm, 0.20 μ m, PES syringe mount filter. Absorption spectra were acquired using a Spectramax Plus UV-Vis spectrophotometer equipped with a plate reader at 25 °C in 2 nm increments, from 300 nm to 650 nm, at a scan rate of 300 nm/min. The protein samples and were placed in individual wells in a 96 well plate with the spectra of corresponding buffer without CR, used as a blank.

Urea Analysis

Urea was used to study the nature of the self association observed in the IgG 1 samples. A 5 mg/mL solution of Mab 1 used in the urea characterization was prepared by dialyzing the stock protein solution for 24 hours in 10 mM Histidine, 100 mM NaCl, pH 6, using Pierce Slide-A-Lyzer[®] 10K MWCO Dialysis Cassettes. After dialysis, the pH and concentration was checked and the solution was sterilized as described previously. For the study, a range of urea concentration from 0 mM, 0.03 mM (1:1), 0.3 mM (10:1) and 200 mM (6000:1), were mixed into the Mab 1 sample to study the effects of hydrogen bond disruption. In addition, 200 mM Arginine was also mixed into the Mab 1 sample to compare the effects of urea to lower the viscosity. The samples were incubated for one hour at room temperature and the hydrodynamic radius of the IgG 1 samples in this study were measured using a DynaPro[™] Titan as previously described. The Mab 1 samples were then incubated for 24 hours at 4 °C and the dynamic light scattering measurements were repeated. The urea study was not performed on the Mab 2 and the Mab 3 samples due to the fact that they did not display significant levels of high-order association when analyzed by dynamic light scattering under the initial buffer conditions.

FTIR Structural Analysis

The structural analysis was performed on the three IgG 1 antibodies using Fourier Transform Infrared (FTIR) spectroscopy. Mab 1, Mab 2 and Mab 3 were analyzed at a concentration of 77 mg/mL, 60 mg/mL and 54 mg/mL respectively, in a buffer containing 10 mM Histidine, pH 6 ± 100 mM NaCl. Samples were stored at 4 °C and

analysis run with the samples at both 4 °C and 20 °C. All FTIR spectra were recorded on a Bruker Tensor 27 from 1000-4000 cm⁻¹ using a resolution of 2 cm⁻¹ and 128 scans. The crystal was cleaned with water, and ethanol prior to sample solution application. The temperature of the ATR unit was maintained at 4 °C and 20 °C with an external water bath and purged continuously with nitrogen or house air. After a 40 minute equilibration, 200 ul of sample was spread uniformly over the germanium crystal. A blank buffer spectra was also collected. The data were collected with OPUS software (Ver. 5) and the spectra of the three antibody runs were overlaid for each experiment.

Capillary Electrophoresis Studies

Capillary electrophoresis was used in the valence determination of the IgG 1 samples in this study. The instrument used to conduct the electrophoresis experiments was the Beckman Coulter ProteomeLab™ PA800 (Beckman Coulter, Inc. Fullerton, CA), using an eCAP amine capillary (part #477431), that was rinsed with the amine regeneration solution (part #477433) as per the protocol described by Beckman. Data were acquired using the 32 Karat software (ver. 7.0) and further analyzed using ZUtilities (ZUtilities: <http://rasmb.bbri.org/rasmb/AOS/ZUtilites>).

Initially, the expected valence of the antibody samples was calculated based on the amino acid sequences, in the buffer solutions, using the program Sednterp (Sednterp: www.jphilo.mailway.com/download). Then following the setup recommended by Beckman, the total length of the capillary was determined as was the length of the capillary to the detector. Additionally, the maximum voltage to be used with each buffer

in the study was determined by constructing an Ohm's law plot. A typical valence measurement protocol is as follows:

1. Determine the expected valence of the molecule from the amino acid composition at the pH of the buffer solution selected for the study. For positively charged molecules, use an amine capillary and for negatively charged molecules, use a bare capillary. If the valence is entirely unknown, start with a bare capillary.
2. Record the total length of your selected capillary and the length to the detector as well as the maximum voltage (measured by the Ohm's law plot) that can be used with the running buffer.
3. Run the samples with and without the electroosmotic flow (eof) marker (e.g. DMSO, benzyl alcohol at 0.02%) at the highest voltage measured using the Ohm's law plot. A good protein concentration is between 0.3 and 0.5 mg/mL and a typical time of injection to get a good peak is between five and ten seconds.
4. After the first attempt, if the sample and the marker peak are not easily identifiable and/or do not have adequate resolution, try lowering the run voltage or increasing the ionic strength of the running buffer.
5. An option is to perform additional runs including the sample and the eof marker using several different voltages. Record the migration time for each sample and eof marker peak plus the voltage used.
6. Using dynamic light scattering, determine the hydrodynamic radius (R_h) and the diffusion coefficient of the sample in the CE running buffer.

7. Measure the ionic strength, and the radius of the counter-ion in the running buffer.
8. Calculate the velocity of the sample by determining the migration time of each peak and subtracting the migration time of the eof marker. This result is the mobility of the sample corrected for the electro-osmotic flow of the CE run.
9. Calculate the final valence (Z^* and Z) of the samples using the software program ZUtilities.

The conditions that were used for the valence determination are as follows, with a typical 32 Karat software experimental protocol shown in **Figure 2.3**.

The conditions used for this study:

1. Solvent: Buffer A contained 100 mM MES buffer, 100 mM NaCl, pH 6. Buffer B contained 100 mM MES buffer, 10 mM NaCl, pH 6. The conductivity of Buffer A was measured to be 14.5 mS/cm and the conductivity of Buffer B was measured to be 0.28 mS/cm. In addition, 0.1 mM urea was spiked into each of the buffers to study the resulting effects on charge.
2. Sample concentrations: The samples that were used in this study consisted of the intact IgG 1 antibodies with Mab 1 = 0.511 mg/mL, Mab 2 = 0.532 mg/mL and Mab 3 0.55 mg/mL and the $F(ab')_2$ fragments (see section on Digestion / Fragmentation) with Mab 1 $F(ab')_2$ = 0.569 mg/mL, Mab 2 $F(ab')_2$ = 0.631 mg/mL, Mab 3 $F(ab')_2$ = 0.782 mg/mL.

Figure 2.3: A Typical CE Method Used For Valence Determination

Initial Conditions		UV Detector Initial Conditions		Time Program					
Time (min)	Event	Value	Duration	Inlet vial	Outlet vial	Summary	Comments		
1	Rinse - Pressure	25.0 psi	1.00 min	BI:C1	BO:B1	forward	0.1M NaOH		
2	Rinse - Pressure	25.0 psi	1.00 min	BI:B1	BO:B1	forward	water		
3	Rinse - Pressure	25.0 psi	1.00 min	BI:D1	BO:B1	forward	amine regeneration soln.		
4	Rinse - Pressure	25.0 psi	0.50 min	BI:B1	BO:B1	forward	water		
5	Rinse - Pressure	25.0 psi	3.00 min	BI:E1	BO:B1	forward	run buffer		
6	Inject - Pressure	0.5 psi	5.0 sec	SI:A1	BO:B1	No override, forward	cod marker		
7	Wait		0.00 min	BI:A1	BO:A1				
8	Inject - Pressure	0.5 psi	5.0 sec	SI:B1	BO:B1	Override, forward	sample		
9	Separate - Voltage	5.0 KV	60.00 min	BI:A3	BO:A3	0.17 Min ramp, reverse polarity, In / Out vial inc 5			
10	Autzero								
11	Wait		0.00 min	BI:A1	BO:A1				
12	End								
13									

Figure 2.3: Typical method for valence determination using the 32 karat software (v.7.0) with an amine capillary.

3. Sample Valence (based on AA sequence at pH 6): Mab 1 = 22.162, Mab 2 = 28.288, Mab 3 = 42.378; Mab 1 $F(ab')_2$ = 9.297, Mab 2 $F(ab')_2$ = 17.5, Mab 3 $F(ab')_2$ = 31.892.
4. Neutral marker: 0.02% dimethyl sulfoxide (Pierce, Rockford, IL)
5. Run temperature: 20 °C
6. Detector wavelength: 214 nm
7. Total capillary length: 61.6 cm
8. Length to detector: 50.8 cm
9. Voltage used: 10 kV for buffer A and 30 kV for buffer B
10. Diffusion coefficient: Mab 1 = 3.45×10^{-7} cm²/sec, Mab 2 = 4.74×10^{-7} cm²/sec, Mab 3 = 4.48×10^{-7} cm²/sec; Mab 1 $F(ab')_2$ = 3.38×10^{-7} cm²/sec, Mab 2 $F(ab')_2$ = 2.85×10^{-7} cm²/sec, Mab 3 $F(ab')_2$ = 3.62×10^{-7} cm²/sec, determined from dynamic light scattering data using a DynaPro™ Plate Reader Plus..
11. Stokes radius (Rh): Mab 1 = 5.1 nm, Mab 2 = 5.1 nm, Mab 3 = 5.1 nm; Mab 1 $F(ab')_2$ = 4.6 nm, Mab 2 $F(ab')_2$ = 4.6 nm and Mab 3 $F(ab')_2$ = 4.7 nm, calculated from the molecular weight of the AA sequence as determined using Sednterp and using the Stokes Einstein relationship for a globular model as implemented in Dynamics™. The Rh for NaCl = 0.122 nm.

CHAPTER III

RESULTS

Antibody Purification

Characterization of Protein Purity

For this study, the three recombinant humanized IgG 1 monoclonal antibodies were expressed in the CHO cell lines, purified by a series of chromatography steps and then finally brought to a concentration of ~75 mg/mL. To assess protein purity, several characterization techniques were employed however, due to the aim of this study, only the results from the Mab 1 are shown. It is important to note that both Mab 2 and Mab 3 were assessed, with similar results of purity.

SDS-PAGE: **Figure 3.1** shows the migration position of the purified Mab 1 using SDS-PAGE analysis following non-denaturing and denaturing preparation. It was evident from the non-reducing preparation that the most abundant species present was the purified Mab 1 monomer. The reducing preparation shows two major, distinct bands, representing that of the light chain (~25 kDa) and the heavy chain (~48 kDa). However, due to the impurity of the initial protein isolate, several other minor bands appear on the gel which represents both small Mw species and non-dissociable aggregated species.

These minor bands were seen routinely in all the non-reduced SDS-PAGE analysis of the

Figure 3.1: Reducing and Non-Reducing SDS-PAGE Results of Mab 1

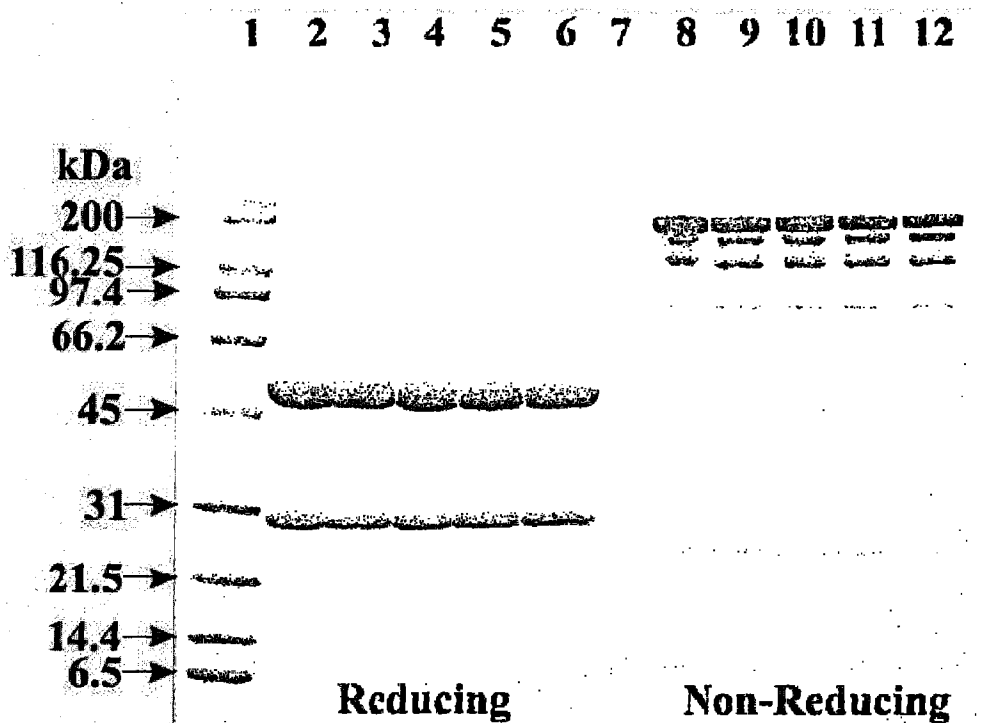


Figure 3.1: Lane 1 represents the Mw markers, lanes two through six represent reduced purified Mab 1 and lanes eight through 12 represent non-reduced purified Mab 1 (each 10 μ L injection was repeated five times). The overall banding pattern of the Mab 1 in each reducing lane is similar and indicates that in addition to the bands representing the purified Heavy Chain and Light Chain, there are non-dissociable aggregates present (bands migrating around 116 to 200 kDa). The overall pattern of the Mab 1 in each non-reducing lane is also similar with small amounts of low Mw species present. It should be noted that the non-dissociable aggregates were removed in a subsequent cHA purification step.

three IgG 1 samples and their origins are currently unknown. Therefore, a clean separation of the IgG 1 samples from the impurities using an additional hydroxyapatite chromatography (cHA) step was required prior to subsequent opalescence characterization. It is also important to note that the majority of the minor bands seen in the non-reduced preparation were eliminated following the reducing preparation, indicating disulfide bonding.

SEC-HPLC: To further assess purity of the CHO expressed recombinant humanized IgG 1 monoclonal antibodies, SEC-HPLC was performed. Five samples of the Mab 1 were examined after the additional cHA purification step and the chromatograms overlaid in **Figure 3.2**. In general, the profiles show approximately 98% monomer and about equal amounts of low Mw and high Mw species present. The subtle run to run variations that are displayed in the chromatograms are considered normal and well within the error of the technique. These results indicate that the cHA purification step was adequate to purify the IgG 1 samples for further opalescence characterization.

CEX-HPLC: A total of five samples of the Mab 1 antibody were also analyzed by CEX-HPLC in order to assess the degree of basic and acidic species that remained after the additional cHA purification step. The resulting chromatograms are shown in **Figure 3.3** with labels to indicate the main species from the acidic and basic species. Although there is a fair amount of acidic and basic species present, the results are considered typical for the degree of purification used for this study.

ACHRO-K PEPTIDE MAPPING: The peptide mapping step was performed on only three batches of the final cHA purified Mab 1. The results of the peptide mapping

Figure 3.2: Overlay Details of the SEC-HPLC Profiles of Mab 1

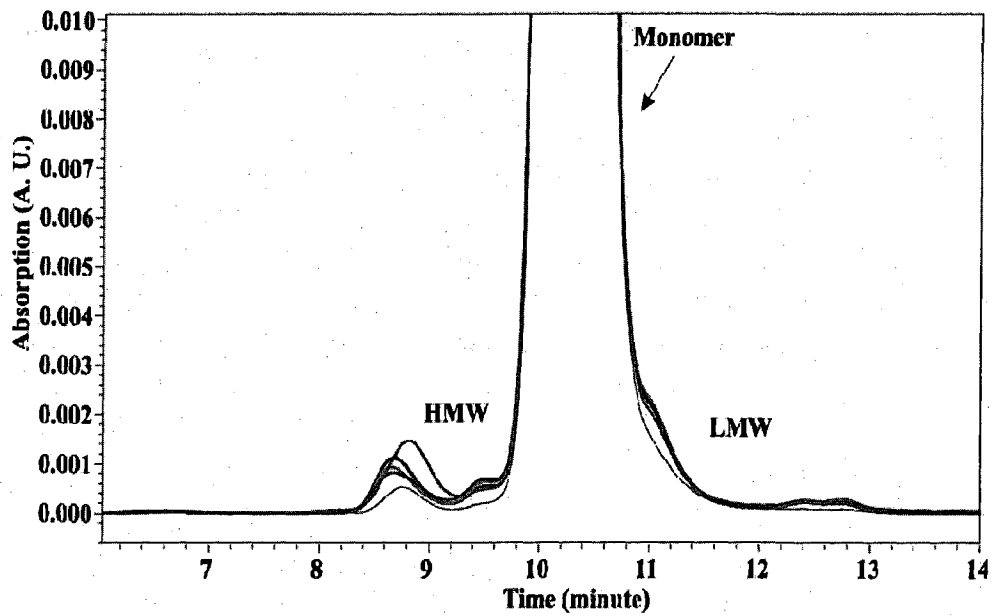


Figure 3.2: The SEC elution profiles of the five purified Mab 1 samples following the cHA step as recorded at an absorbance wavelength of 280 nm. It is clear from these results that the cHA purification step was successful in purifying the Mab 1 monomer to around 98% pure, with approximately 1% LMW and 1% HMW species also identified.

Figure 3.3: CEX-HPLC Profile of Mab 1

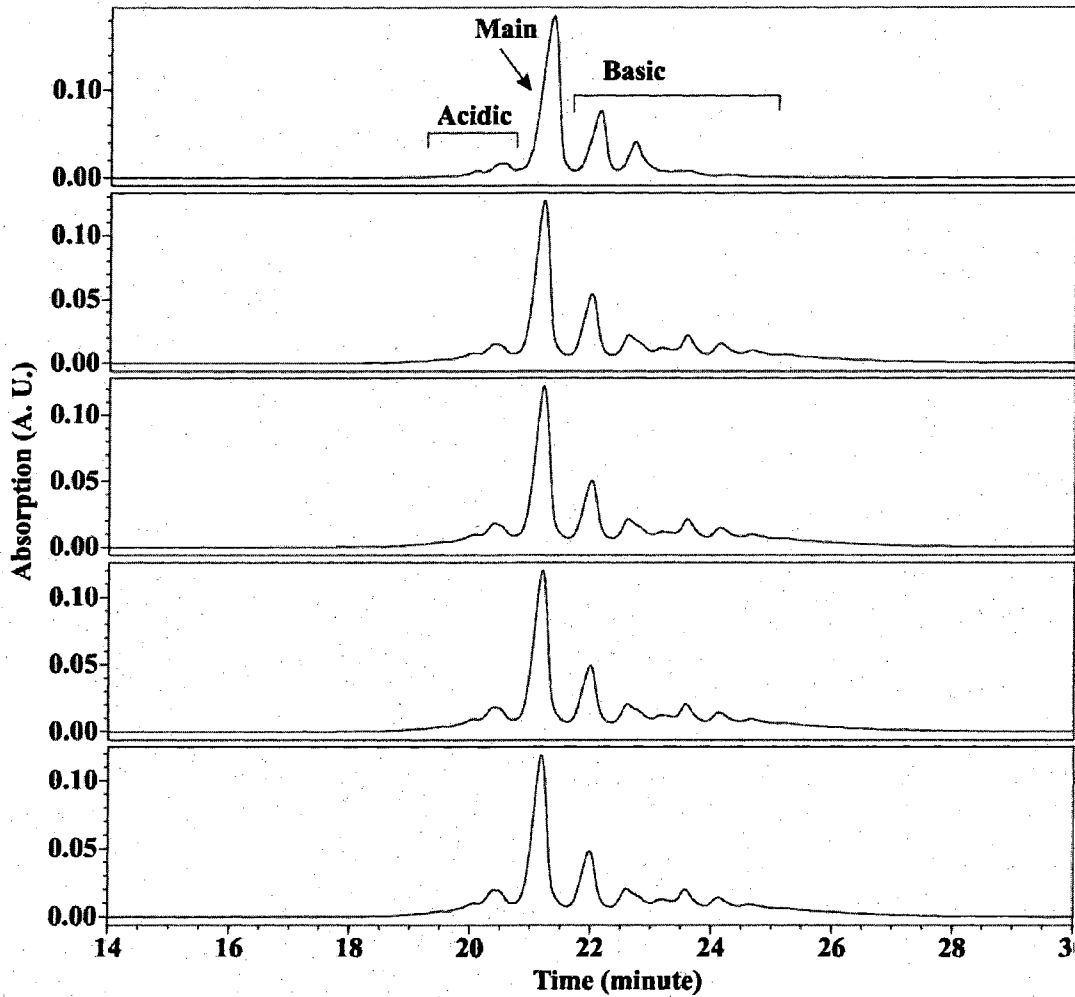


Figure 3.3: Comparison CEX-HPLC runs for five of the Mab 1 sample after final cHA purification. The results indicate that in addition to the main IgG 1 peak, there are some basic and acidic species that remain. These results are typical for the purification steps that were employed and were similar for all of the IgG 1 samples that were used throughout this study.

were then compared to show that the final IgG 1 samples are identical in the amino acid composition (**Figure 3.4**). It should be noted that the results were also similar for both the Mab 2 and Mab 3 samples.

N-LINKED OLIGOSACCHARIDE ANALYSIS: The three types of complex *N*-linked biantennary glycans that are associated with the Mab 1 antibody are the G0, G1 and G2 structures, which respectively contain zero, one or two galactose residues on their outer *N*-linked biantennary arms. The three samples tested by high pH anion exchange chromatography (HPAEC-PED) in **Figure 3.5** show the presence of three peaks representative of the G0, G1 and G2 glycoforms, and are comparable to Mab 1 that has been analyzed previously (data not shown). Although the samples do appear to have varying levels of glycoforms present, the difference is not considered to be significant. The IgG 1 samples used in this study, including Mab 2 and Mab 3, were therefore considered comparable in their degree of glycosylation.

Opalescence Characterization

Visual Appearance and Description

The visual appearance of the IgG 1 samples used in this study was originally examined and characterized through the use of the European Pharmacopeia reference suspensions as described in **Figure 3.6**. With the use of these standards, it was possible to assign a degree of protein opalescence (although somewhat subjectively) when initially characterizing the effects of NaCl and pH. **Figure 3.7** shows the opalescence assignments that were performed on Mab 1 at the start of this study. Vial A contained

Figure 3.4: Peptide Mapping Chromatograms of Mab 1

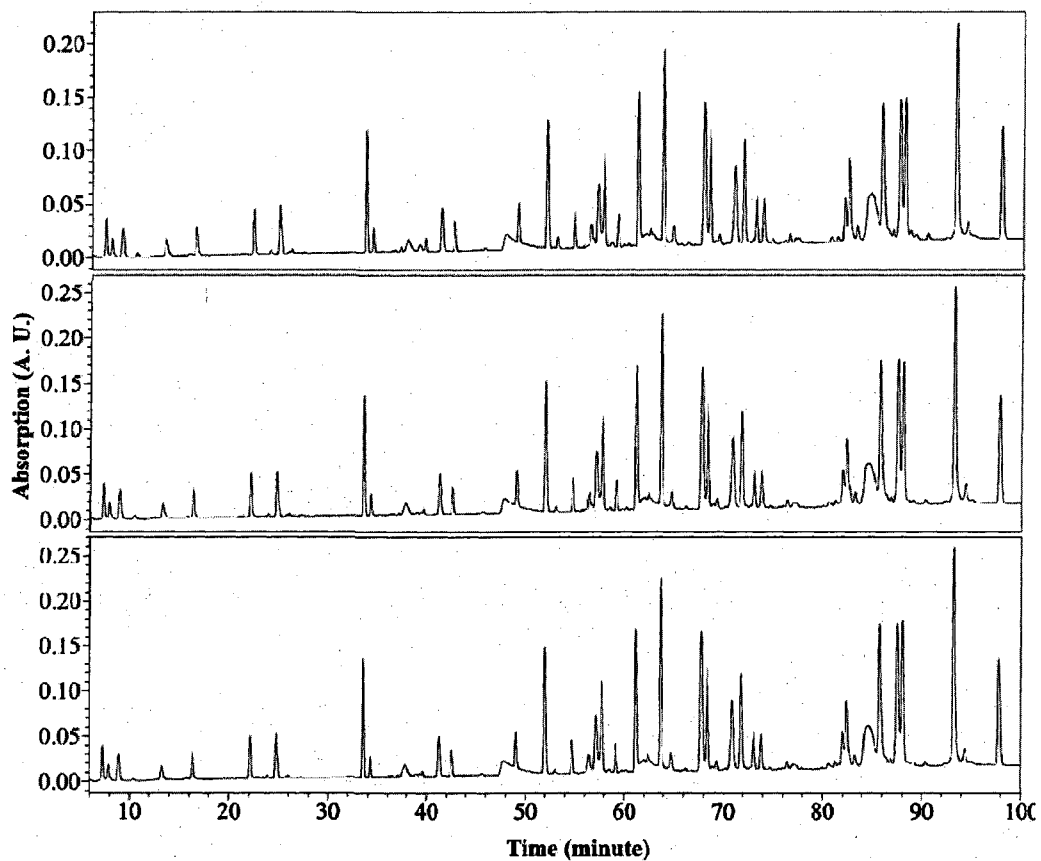


Figure 3.4: A peptide map was performed on three of the final purified Mab 1 samples. It is important to note that each of the samples were reduced, alkylated, desalted and run on the same day for this comparison. From the chromatographic results, it appears as though all three Mab 1 samples tested were comparable in their amino acid sequence.

Figure 3.5: HPAEC-PED Chromatograms of Mab 1

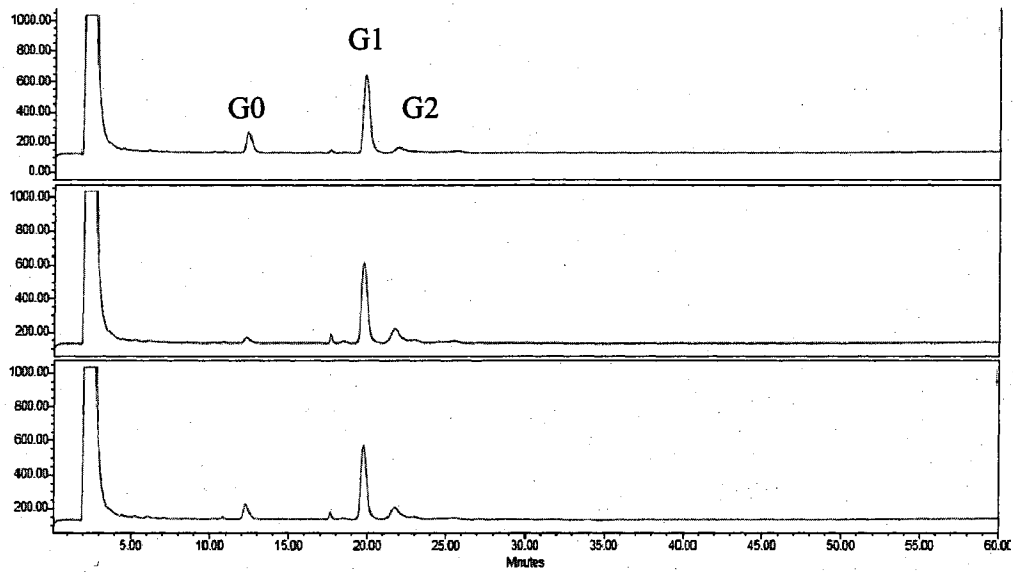


Figure 3.5: The *N*-linked oligosaccharide “fingerprint” profiles of Mab 1 were compared for glycosylation heterogeneity. The profiles show the three major peaks associated with the G0, G1 and G2 structures on the *N*-linked biantennary arms. Although the three samples tested do not appear to have identical glycoform levels, the difference is not thought to be significant. Therefore, the samples of Mab 1 tested are considered comparable.

Figure 3.6: Visual Appearance of EP Reference Suspensions

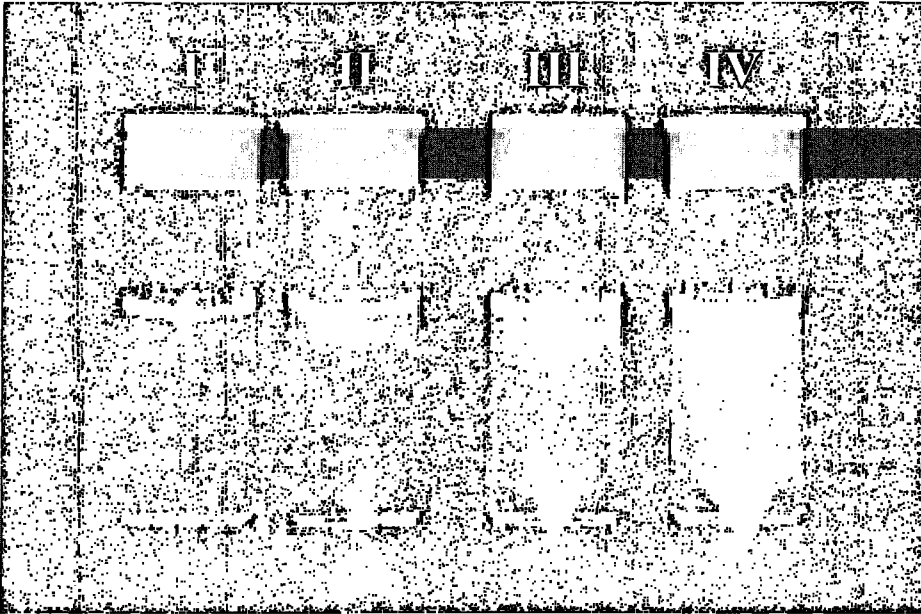


Figure 3.6: The European Pharmacopeia reference suspensions are seen here labeled as I, II, III and IV. The opalescence assignments went as I was considered “clear”, II was assigned as “slightly opalescent”, III was considered “opalescent” and IV was labeled as “very opalescent”. The EP standards were prepared fresh, stored in neutral glass vials with a flat base, and illuminated with a specially prepared light box so that they could be used to characterize the degree of protein opalescence. It is important to note that although these standards were helpful in initially assigning the degree of antibody opalescence, they were subject to interpretation and were quickly replaced by less subjective optical measurement.

Figure 3.7: Initial Antibody Opalescence Assignment Using EP Standards

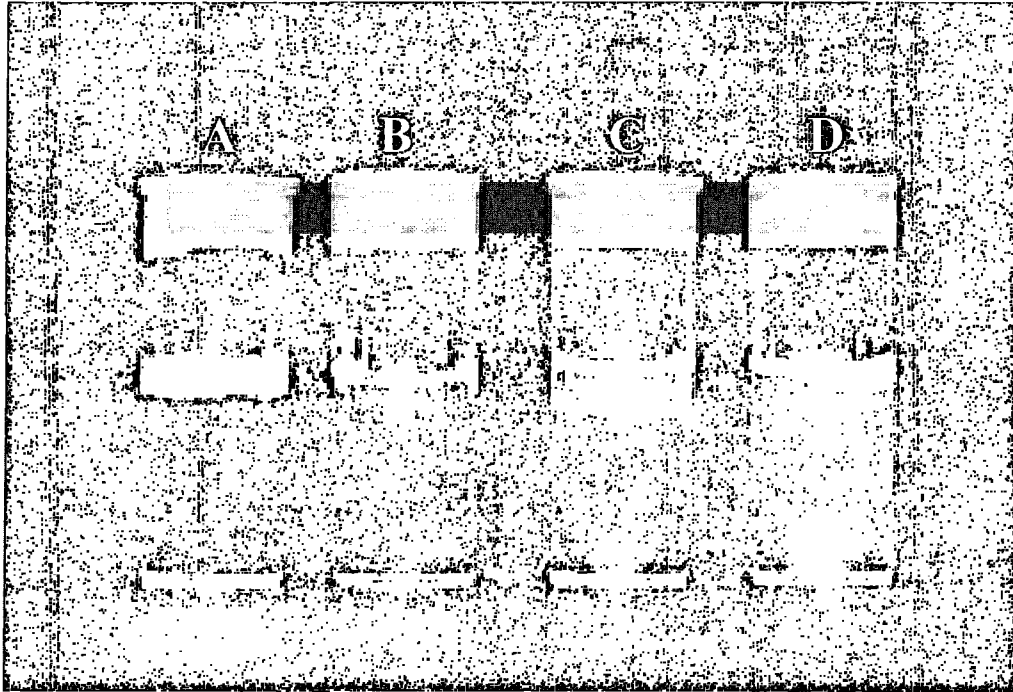


Figure 3.7: This figure is an example of the initial characterization of the Mab 1 antibody. Vial A contains the storage buffer of 10 mM Histidine, pH 6, there is slight foam on the top due to shaking. Vial B contains the Mab 1 antibody at an approximate concentration of 60 mg/mL and a purity of >99% (it was assigned an opalescence rating of II or slightly opalescent). Vial C and D contain the EP reference suspensions III and IV respectively.

just the storage/formulation buffer (10 mM Histidine, pH 6) used throughout the study and is seen as a control as it does not display any appreciable opalescence. Vial B is the Mab 1 antibody in 10 mM Histidine, pH 6, at a concentration of 60 mg/mL and a purity of >99%. This sample already appears to display a degree of opalescence and through the use of the EP reference suspensions III and IV in vials C and D respectively. Vial B is labeled as slightly opalescent and therefore is assigned an EP rating of II. This figure was intended to show the difficulty and limited nature of initially using the EP reference suspensions as the only way of assigning the degree of opalescence. In Figure 3.8, an attempt was made to characterize the effects of NaCl and Tween 80 on the opalescence of Mab 1, using the EP reference suspensions. Initially, a 1 M stock solution of NaCl was added into a solution of Mab 1 which was at a protein concentration of 65 mg/mL in 10 mM Histidine, pH 6 (Figure 3.8 A). Results indicate that at a NaCl concentration of only 2 mM, the degree of opalescence was already increasing, changing the initial EP appearance from <III to III. As the concentration of NaCl that was added to the Mab 1 increased, from 1 to 8 mM, the opalescence also increased, with a final EP value of >IV was assigned to the protein solution at 8 mM NaCl. Using the Mab 1 in 10 mM Histidine, pH 6 (assigned an EP value of <III), Tween 80 was added from a stock solution to examine the ability of the polysorbate to remove the opalescence (Figure 3.8 B). It was shown that the initial EP value did not change with the addition of the Tween 80 (from 0% to 32%) even though the protein concentration of Mab 1 was diluted from 65 mg/mL to 55.4 mg/mL. Figure 3.9 was a further attempt to characterize the opalescence dependence of Mab 1 on pH and NaCl concentration. Mab 1 was examined at a concentration of 10 mg/mL and assigned a degree of opalescence in each solvent

Figure 3.8: Characterizing the Effect of NaCl and Tween 80 on Mab 1 Opalescence Using EP Reference Suspensions

A

Concentration of NaCl (mM)	Appearance (E.P.2.2.1)
0	< III
1	< III
2	III
3	< IV
4	< IV
5	< IV
6	IV
7	IV
8	> IV

B

Theoretical % PS 80	Sample Volume (µL)	Theoretical Protein Conc. Based on Increased Vol. (mg)	Appearance (E.P. 2.2.1)
0	3000	65.0	< III
0.0005	3003	64.9	< III
0.001	3006	64.8	< III
0.0015	3009	64.8	< III
0.002	3012	64.7	< III
0.0025	3015	64.7	< III
0.005	3030	64.4	< III
0.01	3060	63.7	< III
0.02	3120	62.5	< III
0.04	3240	60.2	< III
0.08	3480	56.0	< III
0.16	3500	55.7	< III
0.32	3520	55.4	< III

Figure 3.8: Using EP standards to characterize the effects of NaCl and Tween on opalescence, stock solutions of 1 M NaCl or Polysorbate 80 (0.5% and 10%) were spiked into Mab 1 at a protein concentration of 65 mg/mL in 10 mM Histidine, pH 6. Initially the opalescence of Mab 1 was explored over a NaCl range of 0 to 8 mM (A). Also, the ability of Polysorbate 80 to remove the subsequent opalescence was explored using Mab 1 in 10 mM Histidine, pH 6, with an opalescence value of III (B).

Figure 3.9: Characterization on the Effect of NaCl and pH on Opalescence of Mab 1 Using EP Reference Standards

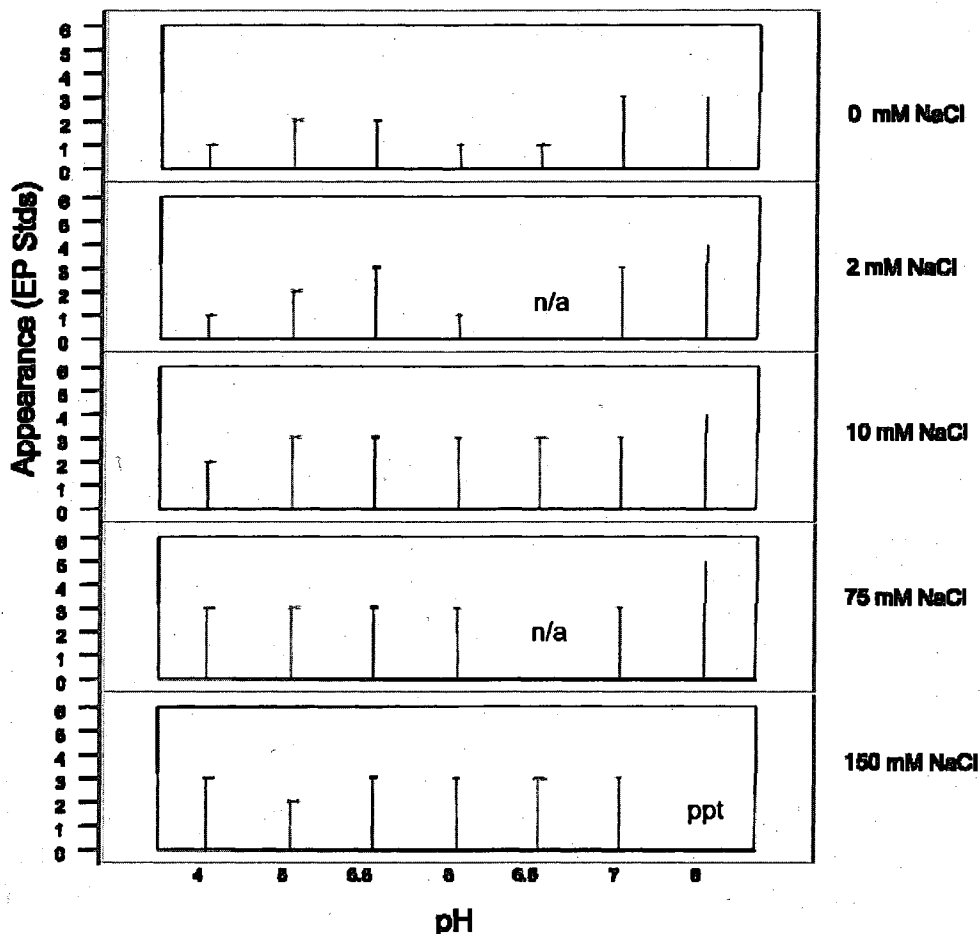


Figure 3.9: The effects of NaCl and pH on the opalescence of Mab 1 was examined at a protein concentration of 10 mg/mL and assigned a degree of opalescence based on the EP standards. Note that in some cases, it was necessary to extend the EP values to that of “5” and “6” due to the high degree of opalescence.

condition based on the EP standards. It is important to note that in some cases, it was necessary to extend the EP values to that of “5” and “6” due to the high degree of opalescence (these values were arbitrarily assigned). Samples at pH 4.0 through 6.0 generally had less opalescence at NaCl concentrations of 0 and 2 mM NaCl, with the pH effect essentially lost at ≥ 10 mM NaCl. In the presence of 75 and 150 mM NaCl, most samples between pH 4 and 7 had the same degree of opalescence and eventually precipitated at 150 mM NaCl. Overall, samples measured at pH 8 scored high in opalescence at any NaCl level but precipitated immediately upon the addition of 150 mM NaCl. Based on these results, it was then decided that the initial “formulation” buffer of 10 mM Histidine, pH 6 was the most appropriate for use in this study.

Static Multi-Angle Light Scattering (MALS) Studies

The effects of NaCl on the opalescence of Mab 1 were analyzed using multi-angle static light scattering. The weight average molecular weights of the antibody solutions were measured at 25 °C using static light scattering at angles of 32° to 147° combined with concentration detection by UV or RI, measured in series.

SIZE EXCLUSION CHROMATOGAPHY-MALS: The effects of NaCl on the self-association of Mab 1 was analyzed by SEC-MALS and a typical graphical presentation of the experimental results is shown in **Figure 3.10**. The chromatographic profile is a result of the light scattering signal at an angle of 90° and is seen with the Mw distribution of each of the selected peaks in the elution. The monomer peak is clearly

Figure 3.10: SEC-MALS Chromatogram of Mab 1 at 100 mM NaCl

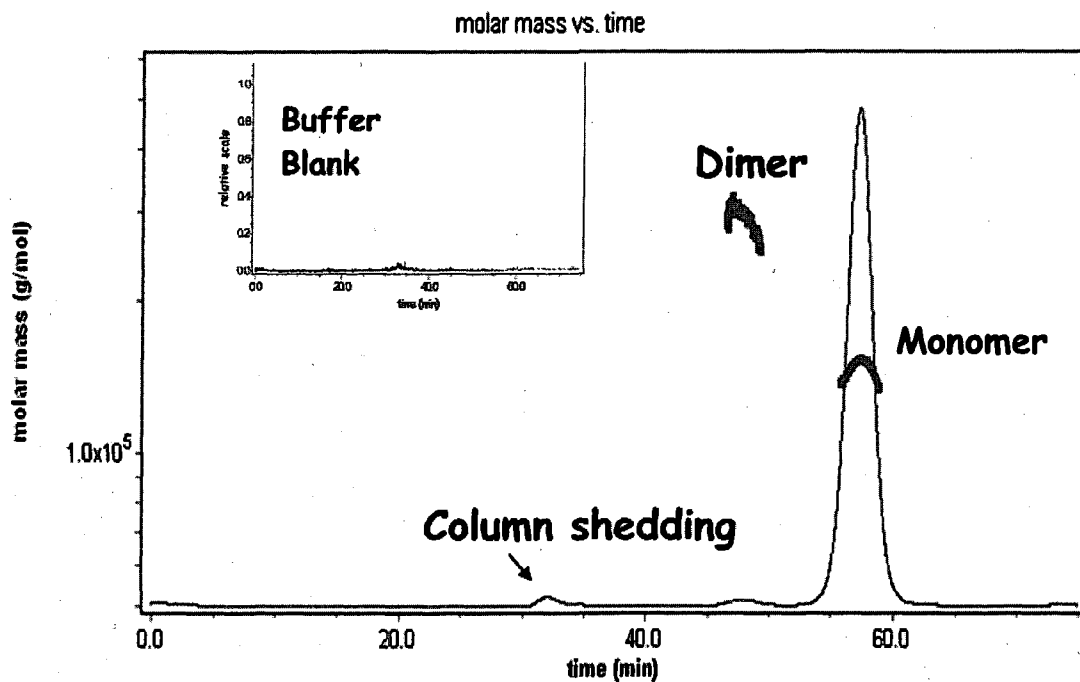


Figure 3.10: The effects of NaCl on Mab 1 opalescence was analyzed using SEC-MALS. The TosohHaas G3000SWXL column was loaded with 100 μg of protein with a mobile phase of 10 mM Na_2HPO_4 , 100 mM NaCl, pH 7.15, with an isocratic flow rate of 0.2 mL/min. The results of the analysis were then plotted as molar mass (g/mol) vs. time (min), with the Mw distribution shown for the selected peak regions. A buffer blank was also performed to identify the “ghost peak” that appeared during each injection. It is important to note that after each injection, the pressure of the HPLC system would increase gradually, limiting the use of the column to ~25 injections.

seen at ~57 minutes at around 98% of the material in solution along with the dimer peak at ~47 minutes, at around 2% of the total material in solution. There is an additional peak at ~32 minutes and is due to the column shedding the silica matrix as is clearly seen in the inlayed chromatogram of the buffer blank. The SEC-MALS results indicate that even in buffer conditions containing 100 mM NaCl, the Mab 1 antibody does not appear to contain any higher order associated material beyond the dimer. It is important to note that these results were consistently seen by Mab 2 and Mab 3 at all NaCl concentrations tested. It should also be noted that after each Mab 1 injection, the pressure of the HPLC system would increase gradually, limiting the use of the TosoHaas G3000SW_{XL} column to ~25 injections before reaching the pressure limit of the column. This may indicate fouling of the guard column by large aggregates.

BATCH-MALS: In order to examine the presence of any additional higher order species present in the Mab 1 sample, batch-MALS was also employed. **Figure 3.11** shows the light scattering profile of the 90° detector along with the RI concentration profile for each of the five concentrations tested, in the 10 mM Histidine buffer, pH 6. The results for each of the concentrations tested show a weight average molecular weight that represents the monomer and dimer species in solution. In addition, the RMS radius was also measured by angular dependence for each of the concentrations tested and indicated that there is an average RMS radius from 11 to 14 nm. **Figure 3.12** shows the light scattering profile of the 90° detector along with the RI concentration profile for each of the five concentrations tested, in the 10 mM Histidine buffer, 150 mM NaCl, pH 6. As with **Figure 3.11**, the results for each of the concentrations tested show a weight average molecular weight that represents the monomer and dimer species in solution. However,

Figure 3.11: Batch Multi-Angle Light Scattering Analysis of Mab 1 (No NaCl)

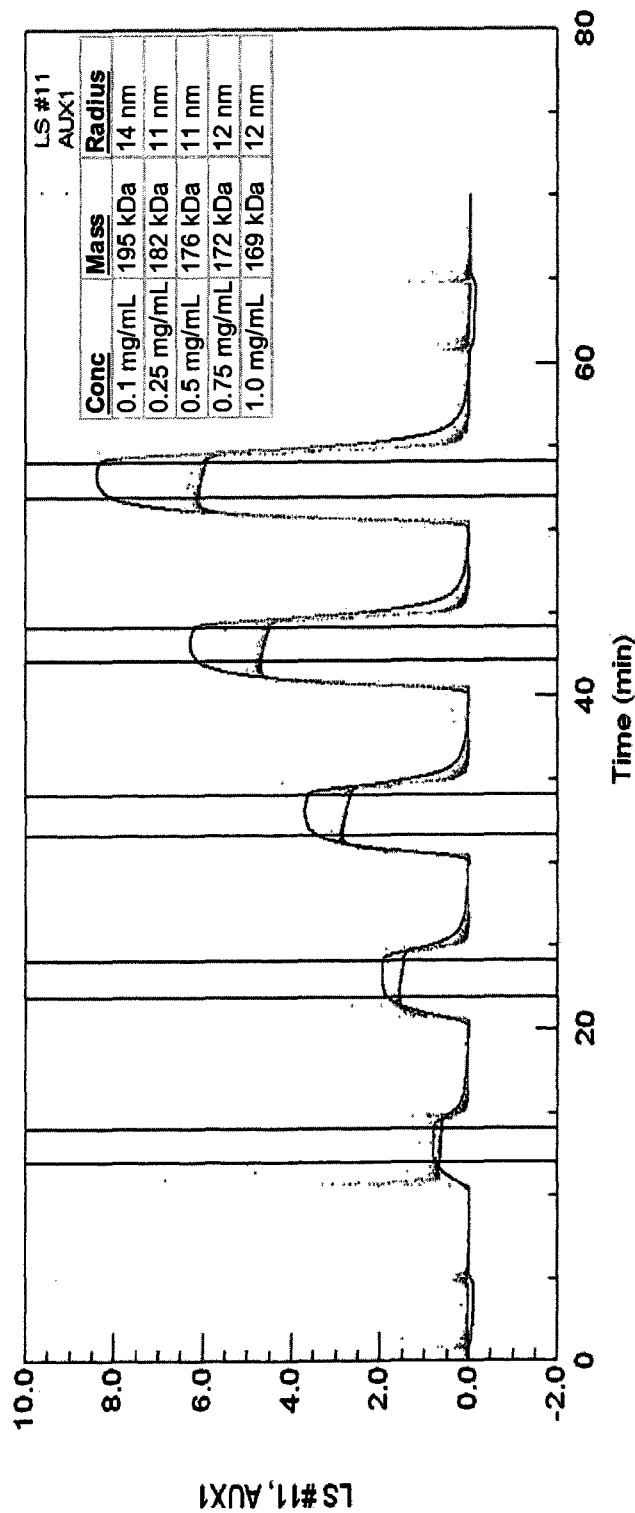


Figure 3.11: The NaCl dependence of Mab 1 was analyzed using batch MALS. The volume for each injection was approximately 1 mL, and the injections were performed using a syringe pump, at a flow rate of 0.2 mL/min. After each injection plateau was established, a syringe containing only buffer was introduced to bring the signal back to baseline. In this study, five samples were injected at the concentrations listed, without any NaCl in the Histidine buffer, and the Mw and RMS radius calculated for each using MALS.

Figure 3.12: Batch Multi-Angle Light Scattering Analysis of Mab 1 (150 mM NaCl)

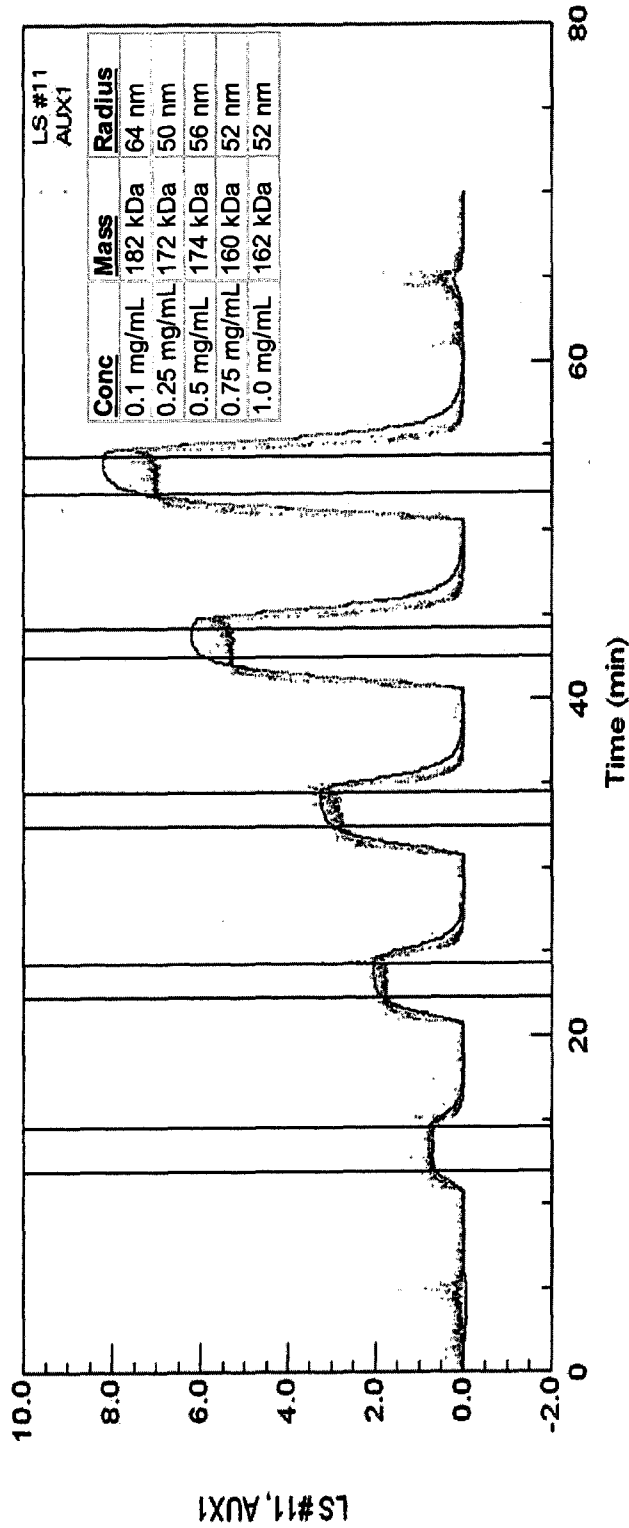


Figure 3.12: The NaCl dependence of Mab 1 was analyzed using batch MALS. The volume for each injection was approximately 1 mL, and the injections were performed using a syringe pump, at a flow rate of 0.2 mL/min. After each injection plateau was established, a syringe containing only buffer was introduced to bring the signal back to baseline. In this study, five samples were injected at the concentrations listed, with 150 mM NaCl in the Histidine buffer, and the Mw and RMS radius calculated for each using MALS.

unlike Figure 3.11, the RMS radius measured for each of the concentrations tested shows an increased size varying from 50 to 64 nm.

FIELD FLOW FRACTIONATION-MALS: In order to characterize the apparent higher order species seen in the batch-MALS analysis, FFF-MALS was also employed. While the Mw distribution of the antibody samples had been determined using SEC-MALS, the analysis was limited due to the potential interaction with the column stationary phase. **Figure 3.13** shows the weight average molecular weight distribution for Mab 1 in 10 mM Histidine, 100 mM NaCl, pH 6, overlaid on the light scattering profile of the 90° detector. The results indicate that in addition to the monomer peak (at ~150 KDa) there is an additional “aggregate” peak that spans a Mw distribution from 10^6 to over 10^8 Daltons. The distribution of the RMS radius was also measured (data not shown) resulting in a Rg range for the “aggregate” peak from 20 to 200 nm.

Sedimentation Velocity Studies

Sedimentation velocity analysis was carried out on the Mab 1 antibody at three concentrations and in a buffer containing 10 mM Histidine, pH 6, \pm 150 mM NaCl. The $C(S_{20}, w)$ profile is seen in **Figure 3.14** for the sedimentation velocity run performed without NaCl. At each of the concentrations tested, the majority of the species in solution appeared to be that of the monomer with the average Mw of the “aggregate” species approaching only a dimer. In **Figure 3.15**, the $C(S_{20}, w)$ profile is seen for the sedimentation velocity run performed with 150 mM NaCl. As in **Figure 3.14**, the majority of the species in solution, at each of the concentrations tested, appeared to be that of the monomer with only a small amount of dimer present. These results indicate

Figure 3.13: Field Flow Fractionation with Multi-Angle Light Scattering Analysis of Mab 1

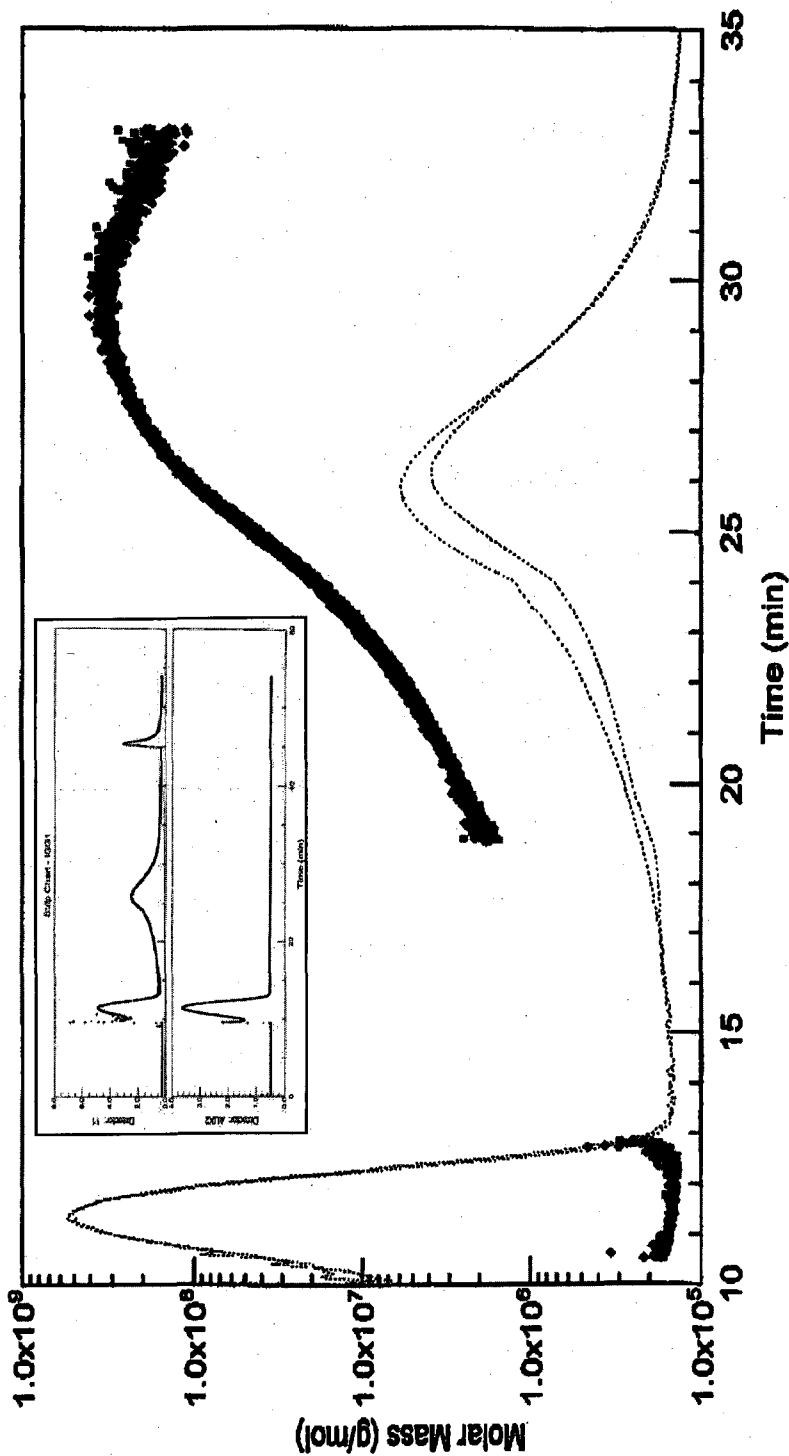


Figure 3.13: This figure represents the weighted averaged molar mass vs. time of Mab 1 in Histidine buffer with 100 mM NaCl. The main antibody monomer peak is easily identified, as is a high Mw "aggregate" peak. The sample injection amount was 50 μ g, with two samples overlaid to show reproducibility. The inlay image shows the 90° light scattering trace on the top graph and the differential refractive index trace on the bottom graph.

Figure 3.14: Sedimentation Velocity Study of Mab 1 Without NaCl

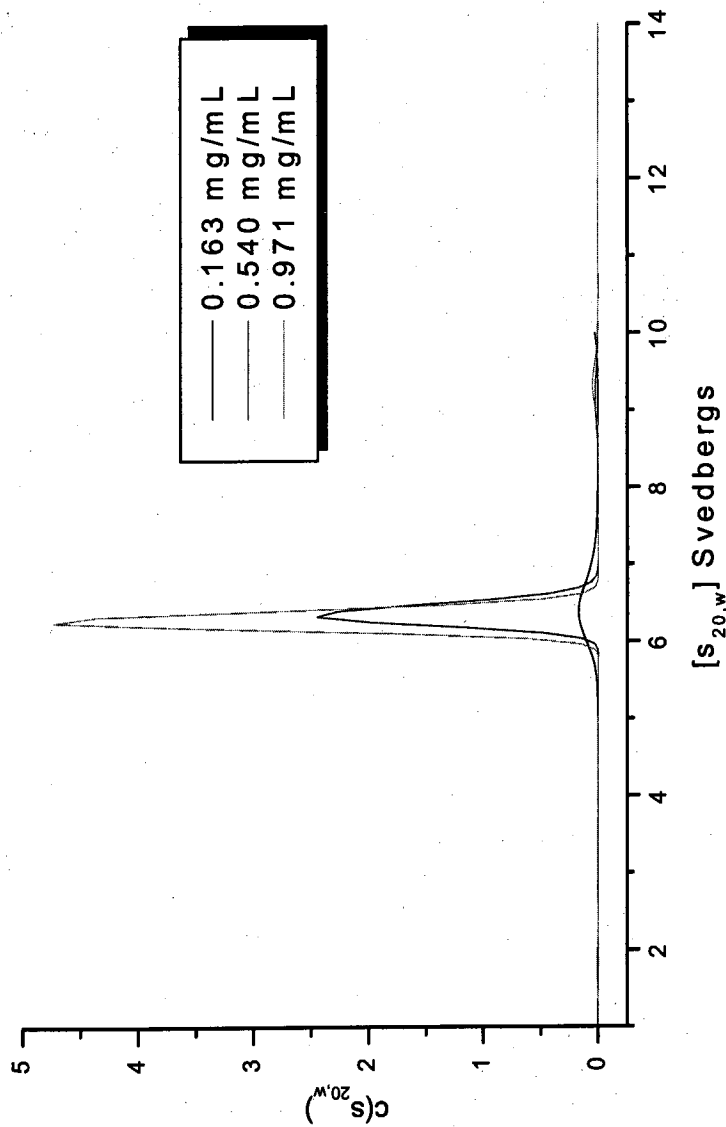


Figure 3.14: Analytical ultracentrifugation sedimentation velocity analysis of Mab 1 in 10 mM Histidine, pH 6, at loading concentration of 0.163, 0.540 and 0.971 mg/mL. The sedimentation value, in units of Svedbergs, are normalized for water at 20 °C and are plotted in the X axis against the normalized concentration of each sample in the Y axis.

Figure 3.15: Sedimentation Velocity Study of Mab 1 With 150 mM NaCl

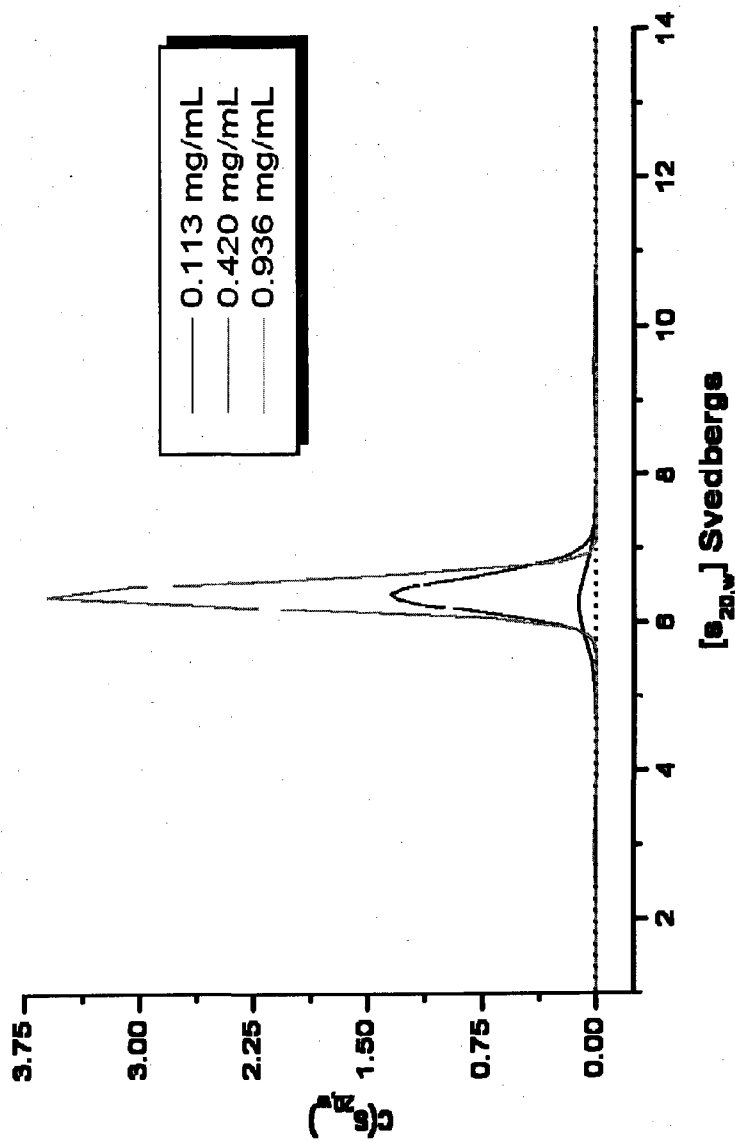


Figure 3.15: Analytical ultracentrifugation sedimentation velocity analysis of Mab 1 in 10 mM Histidine, 150 mM NaCl, pH 6, at loading concentration of 0.113, 0.420 and 0.936 mg/mL. The sedimentation value, in units of Svedbergs, are normalized for water at 20 °C and are plotted in the X axis against the normalized concentration of each sample in the Y axis.

that the percent of high molecular weight material did not increase with an increase in Mab 1 concentration or the addition of NaCl. Similar results were seen in all of the sedimentation velocity runs performed on Mab 2 and Mab 3 under the same conditions. It should be noted that there was no apparent loss of material due to potentially aggregated species in solution.

Electro-Separation

The results of the electro-separation experiments were neither very scientifically rigorous, nor were they used to any great extent beyond the initial attempts to induce and understand the opalescence phenomenon. **Figure 3.16** shows a cartoon depiction of the opalescence behavior of Mab 1 while being fractionated (or induced) by the electric field, in different NaCl concentrations. At 0 mM NaCl (**Figure 3.16 A**), the results of the experiment produced an opalescence “cloud” at the cathode shortly after the electric field was established. It should also be noted that after the appearance of the opalescent “cloud” the electric field was reversed, the opalescent cloud disappeared, and then it reformed at the other end of the chamber. When the pH was taken at the ends, it appeared as though the protons in the buffer had moved against the electric field and were collecting near the anode. The conductivity taken at each of the ends of the chamber also suggested that there was a severe imbalance of the buffer ions. It should also be noted that the initial concentration of the Mab 1 (10 mg/mL) had now increased in the opalescent “cloud” approximately 5 X and there was a negligible amount of protein at the opposite end of the chamber. When the same experiment was performed in a buffer containing 500 mM NaCl (**Figure 3.16 B**), the opalescence “cloud” appeared very rapidly

Figure 3.16: Electroseparation Induced Opalescence of Mab 1

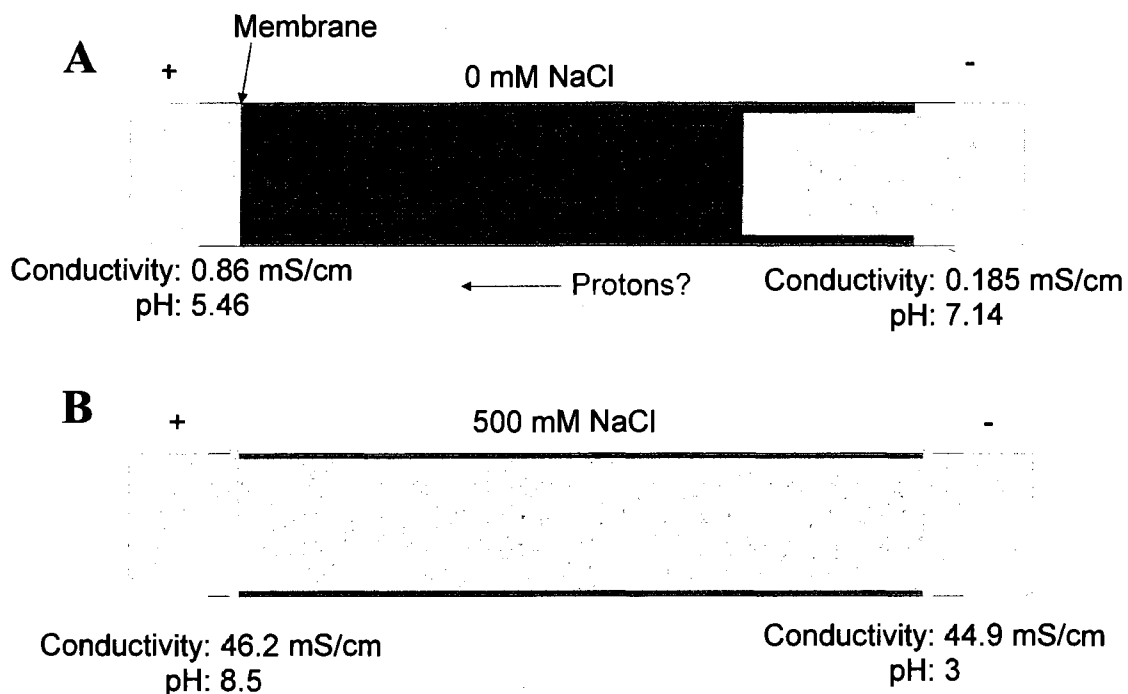


Figure 3.16: The effects of an electric field on Mab 1 is depicted. The first sample contained Mab 1 at an initial concentration of 10 mg/mL in 10 mM Histidine, pH 6 (A). The second sample contained Mab 1 at an initial loading concentration of 10 mg/mL in 10 mM Histidine, 500 mM NaCl, pH 6 (B). The figure depicts the opalescence of the sample (in gray) as it was induced by the electric field. The samples were run at a constant voltage of 80 volts until the current stabilized (approximately ten minutes). The conductivity and pH was then measured at each end of the device and recorded.

and evenly dispersed across the length of the chamber. The pH and conductivity measured at each end of the chamber reflected a routine (and expected) migration pattern of ions in the buffer with the pH being acidic at the anode, and basic at the cathode. The conductivity was also measured at each end of the chamber and appeared to represent a balanced distribution of buffer ions in solution. It is unclear exactly what the results seem to indicate following this experiment and, in fact, the data leave more questions than answers. Although the subsequent experimentation avoided further utilization of this technique, the results helped to craft a framework of characterization based on charge determination as a factor in the opalescence phenomenon.

Salt Induced Opalescence

The effects of salt on the opalescence of Mab 1 was further explored visually, and the results are seen in **Figure 3.17**. For this study, the control was the antibody sample in buffer containing 10 mM Histidine, pH 6. After one hour at room temperature, the effects of the salt on the opalescence are already apparent (**Figure 3.17 A**). Each of the salts in the study appear to drive opalescence to some degree, however, it is clear that the sample in 100 mM NaCl was the most opalescent. In order to examine if the sodium or chloride ion had more of an effect on the opalescence, 100 mM Na₂HPO₄ and 100 mM CaCl₂ were specifically chosen as alternative salts. However, it is clear from these results that after one hour, the alternative salts that were tested do not contribute to the opalescence of Mab 1 as strongly as NaCl. The same vials were then stored overnight at 2-8 °C and re-examined (**Figure 3.17 B**). The vial containing the NaCl appeared to have formed a firm, but turbid, gel while the opalescence seen in the 100 mM CaCl₂ did not

Figure 3.17: Salt Induced Opalescence of Mab 1

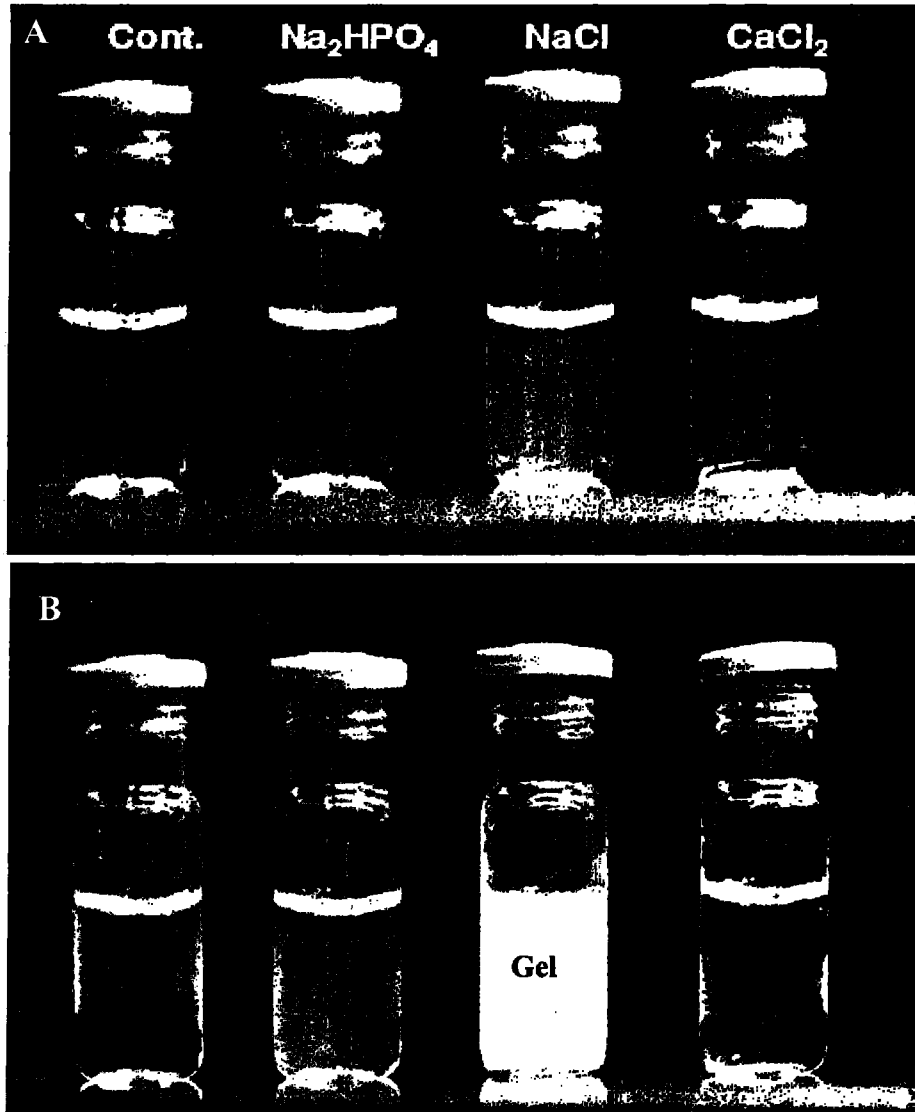


Figure 3.17: The salt induced opalescence of Mab 1 was studied as a function of differing salts. The protein concentration used in this study was 63 mg/mL, and the buffer was 10 mM Histidine, pH 6, with all salts at 100 mM. The samples were prepared and examined after one hour at room temperature (A) and then the samples were stored overnight at 2-8 °C (B) and re-examined. It should be noted that the same samples were stored at 2-8 °C for two additional weeks with the result of a gel also forming in the buffer containing Na₂HPO₄.

appear to increase and the opalescence in the 100 mM Na₂HPO₄ appeared to increase only slightly. It should be noted that the same samples were stored for an additional two weeks at 2-8 °C with the result of a similar gel also forming in the vial containing 100 mM Na₂HPO₄. The opalescence in the sample containing 100 mM CaCl₂ did not appear to change from the initial examination. It is also important to note that the individual ion concentration in each of the salts chosen was not equal, and these differences alone may have contributed to the observed changes in opalescence.

Further characterization on the opalescence effect of NaCl on Mab 1 was characterized and the results are seen in **Figure 3.18**. From the initial study (**Figure 3.18 A**), there appears to be a linear effect on the opalescence from 0 to 20 mM NaCl as measured by the apparent OD₄₀₀. However, as the NaCl concentration was increased from 0 to 150 mM NaCl, and compared to a known salt that does not appreciably increase opalescence (CaCl₂), the dramatic effect of NaCl on the opalescence is evident (**Figure 3.18 B**). The opalescence as measured by OD₄₀₀ appears to reach a maximum opalescence of ~0.55 OD at a NaCl concentration of ~40 mM but then gradually declines back to an opalescence value of ~0.20 OD at a NaCl concentration of 150 mM NaCl. All this while the opalescence of the Mab 1 in CaCl₂ does not appear to rise above ~0.18 OD regardless of the salt concentration. To further examine the unique behavior of the NaCl induced opalescence of Mab 1, a comparison was made to the Mab 2 antibody in **Figure 3.19**. It is easy to visualize the effects of NaCl on the opalescence of Mab 1 as they are examined in 15 mL conical tubes (**Figure 3.19 A**). In 0 mM NaCl, the antibody is clear, then, quickly changes to form two distinct phases in 25 mM NaCl, where the bottom

Figure 3.18: Measuring the Opalescence of Mab 1 as a Function of Salt Concentration

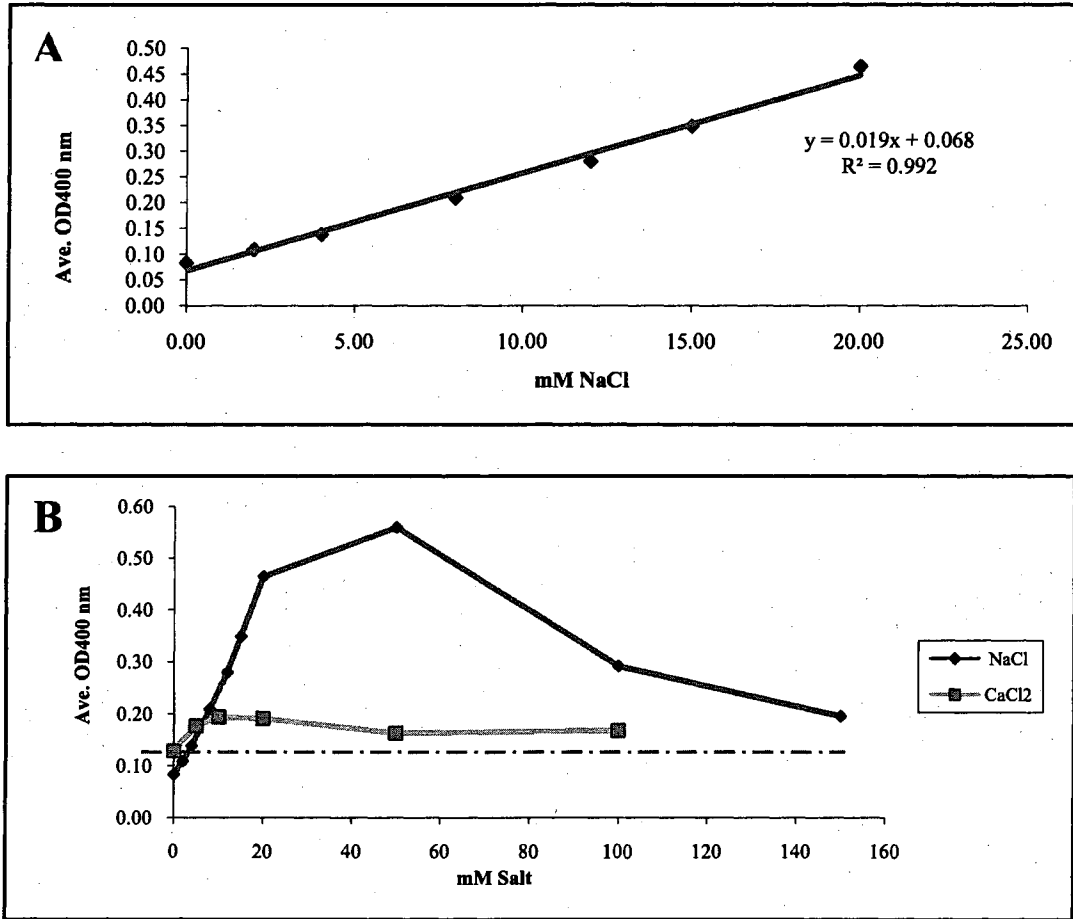


Figure 3.18: Opalescence was monitored as a function of NaCl concentration for Mab 1 at a concentration of 30 mg/mL, using UV detection at 400 nm (A). The OD_{400nm} was plotted against several NaCl concentrations to examine the linearity. Opalescence was further examined as a function of both NaCl and CaCl₂ for Mab 1 over an extended salt concentration range after each sample was dialyzed and kept at 4-8 °C for 24 hours (B).

Figure 3.19: Comparison of NaCl Induced Opalescence of Mab 1 and Mab 2

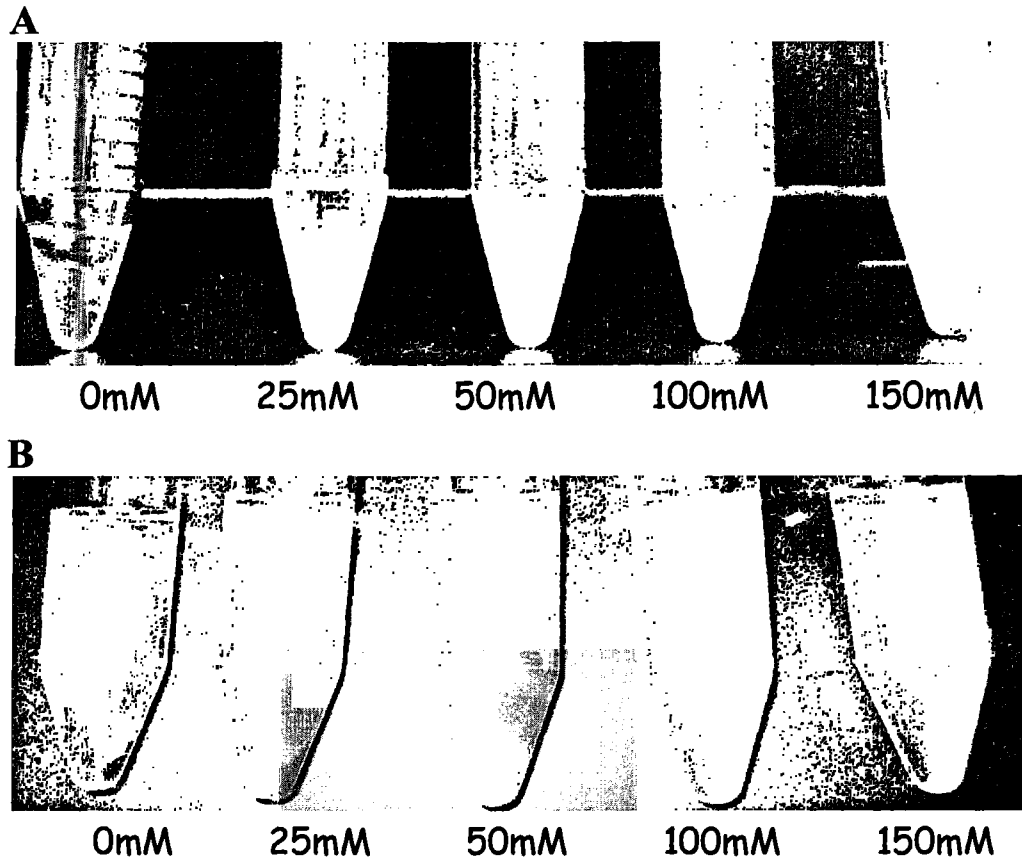


Figure 3.19: The effect of NaCl on the opalescence of Mab 1 and Mab 2 were compared. Both Mab 1 (A) and Mab 2 (B) were tested at a concentration of 30 mg/mL in 10 mM Histidine, pH 6, at the NaCl concentration listed. The samples were dialyzed overnight at room temperature and stored at 4 °C prior to the measurements. It is important to point out that Mab 1 at 25 mM and 50 mM NaCl separated into two distinct phases at the top and bottom of the conical tube, but remained homogeneous and highly opalescent at 100 mM and 150 mM NaCl. Mab 2 remained clear throughout all of the NaCl concentration.

phase is starting to appear opalescent. At 50 mM NaCl, the two phases are opalescent but the bottom phase appears to be more opalescent. Finally, at 100 and 150 mM NaCl, the tubes appeared homogeneous but highly opalescent, even forming the initial stages of a gel state at 150 mM NaCl. In contrast, the Mab 2 antibody remained visually clear throughout all of the NaCl concentrations tested (Figure 3.19 B).

Following the visual characterization of NaCl induced opalescence of Mab 1, the concentration was measured (for each phase if applicable) along with the conductivity, chloride content and pH and the results are seen in **Table 3.1**. In the concentration column, the tube at 0 mM NaCl reflects the starting concentration of 43.7 mg/mL with no “phase separation”. At 25 mM NaCl, there already appears to be a phase separation with the top phase at 9.6 mg/mL and the bottom phase at 103.5 mg/mL. At 50 mM NaCl, there is also a phase separation with the top phase at 10.9 mg/mL and the bottom phase at 75.3 mg/mL. At 100 mM NaCl, there does not appear to be a phase separation but the top of the tube was measured to be 17.8 mg/mL, while the concentration at the bottom of the tube was measured to be 52.2 mg/mL. At 150 mg/mL, the antibody solution was too viscous to be drawn into the pipette, as it was already developing the initial stages of gel formation, and therefore the concentration was not measured.

In the column containing the measured chloride ion concentration, the tube at 0 mM NaCl had a chloride ion content of 7.2 mM. At 25 mM NaCl, the top phase contained a chloride ion concentration of 26 mM, and the bottom phase contained a chloride ion concentration of 31.2 mM. At 50 mM NaCl, the top phase contained a chloride ion concentration of 50.4 mM, and the bottom phase contained a chloride ion concentration of 54.8 mM. At 100 mM NaCl, the top of the tube contained a chloride ion

Table 3.1: Conductivity of NaCl Induced Opalescence of Mab 1

	Conc. mg/mL		Cl ⁻ content mM		Cond. mS/cm		pH	
	<u>top</u>	<u>bottom</u>	<u>top</u>	<u>bottom</u>	<u>top</u>	<u>bottom</u>	<u>top</u>	<u>bottom</u>
Mab 1 (10mM His)								
0mM NaCl	NA	43.7	NA	7.2	NA	0.59	NA	6.05
25mM NaCl	9.6	103.5	26	31.2	2.6	2.1	6.05	6.14
50mM NaCl	10.9	75.3	50.4	54.8	5.3	3.8	5.96	6.05
100mM NaCl	17.8	52.2	94.4	100.4	8.6	8.4	5.89	5.96
150mM NaCl	gel	NA	NA	NA	NA	13.4	NA	6.04

Table 3.1: Following the NaCl induced opalescence of Mab 1, the concentration was measured along with the conductivity, chloride content and pH, at a protein concentration of ~30 mg/mL.

concentration of 94.4 mM, and the bottom of the tube contained a chloride ion concentration of 104.4 mM. As previously stated, at 150 mg/mL, the antibody solution was too viscous to be drawn into the pipette, as it was already developing the initial stages of gel formation, and therefore the chloride ion concentration was not measured.

In the column containing the measured conductivity, the tube at 0 mM NaCl had a conductivity of 0.59 mS/cm. At 25 mM NaCl, the top phase had a conductivity of 2.6 mS/cm, and the bottom phase had a conductivity of 2.1 mS/cm. At 50 mM NaCl, the top phase had a conductivity of 5.3 mS/cm, and the bottom phase had a conductivity of 3.8 mS/cm. At 100 mM NaCl, the top of the tube had a conductivity of 8.6 mS/cm, and the bottom of the tube had a conductivity of 8.4 mS/cm. At 150 mg/mL, the antibody solution was very viscous but the overall conductivity was measured to be 13.4 mS/cm.

In the column containing the measured pH, the tube at 0 mM NaCl reflected the initial pH of 6.05. At 25 mM NaCl, the top phase had a pH of 6.05, and the bottom phase had a pH of 6.14. At 50 mM NaCl, the top phase had a pH of 5.96, and the bottom phase had a pH of 6.05. At 100 mM NaCl, the top of the tube had a pH of 5.96, and the bottom of the tube had a pH of 5.89. Finally, at 150 mg/mL, overall pH was measured, despite the solution viscosity, to have a value of 6.04.

In order to further explore the effect of NaCl on the antibody opalescence, a protein concentration dilution study was performed to assess the potential reversibility of Mab 1 as compared to Mab 2 and Mab 3, in 0 and 50 mM NaCl (**Figure 3.20**). Upon the serial dilution of Mab 2 and Mab 3, in 0 and 50 mM NaCl, and Mab 1, in 0 mM NaCl, from 80 mg/mL, the OD₄₀₀ appeared to be linear. During the serial dilution the Mab 1 antibody at 50 mM NaCl, the bottom phase dropped from an OD₄₀₀ value of ~1.5 (at 85

Figure 3.20: Measuring the Dilution Effect of Mab 1, Mab 2 and Mab 3

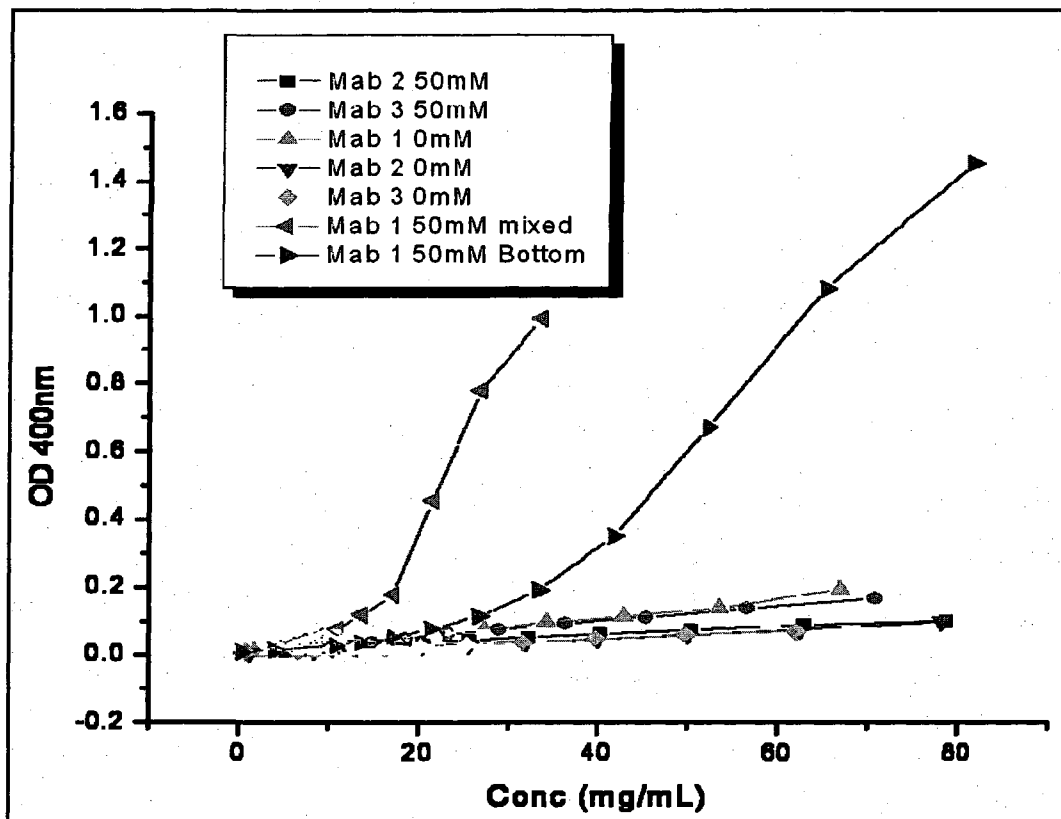


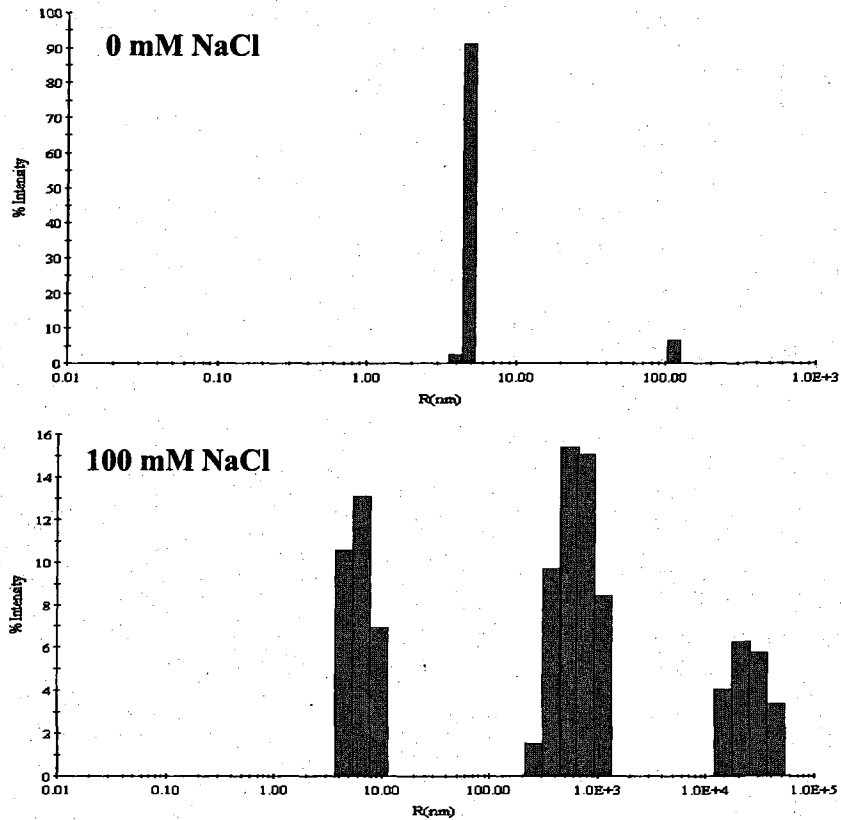
Figure 3.20: The dilution effect was measured for Mab 1, Mab 2 and Mab 3 using UV detection at 400 nm. The NaCl concentration range was chosen due to the fact that Mab 1 became very opalescent and eventually formed a gel in all solutions above 50 mM NaCl. The phase separation of Mab 1 was disrupted by gentle mixing prior to dilution. It is important to note that neither Mab 2 or Mab 3 became very opalescent at any of the NaCl concentrations tested.

mg/mL) to 0 in a non-linear fashion. When the two phases were gently mixed, the drop in OD₄₀₀ from a value of 1 (at ~30 mg/mL) to 0, was even more precipitous. These results are consistent with the Mab 1 forming reversible complexes.

Dynamic Light Scattering Studies

To further examine the solution characteristics of the association state of the antibodies when NaCl is added, dynamic light scattering was employed. The results for Mab 1 are seen in **Figure 3.21** at a protein concentration of 5 mg/mL and a NaCl concentration of 0 and 100 mM NaCl. At 0 mM NaCl, 100% of the material is in the monomeric form as is indicated by the Mw determination of 147 KDa. There is an additional peak that is seen in the histogram but the concentration is negligible (less than 0.1%). At 100 mM NaCl, ~96% of the material has a Mw of ~229 KDa, with a small percent at a Mw of $\sim 1.6 \times 10^7$ KDa and the remainder of the material at a Mw of 0.1×10^{12} KDa. It is important to note that each of the histogram peaks in the sample containing 100 mM NaCl were very polydisperse as is indicated by their overall width. The results for Mab 2 are seen in **Figure 3.22** at a protein concentration of 5 mg/mL and a NaCl concentration of 0 and 100 mM NaCl. At 0 mM NaCl, 100% of the material is in the monomeric form as is indicated by the Mw determination of 139 KDa. There is an additional peak that is seen in the histogram but the concentration is negligible. At 100 mM NaCl, 100% of the material is also in the monomeric form as is indicated by the Mw determination of 134 KDa. There is also an additional peak that is seen in the histogram with a negligible concentration. The results for Mab 3 are seen in **Figure 3.23** at a

Figure 3.21: Dynamic Light Scattering Characterization of the Mab 1 Association State as a Function of NaCl Concentration

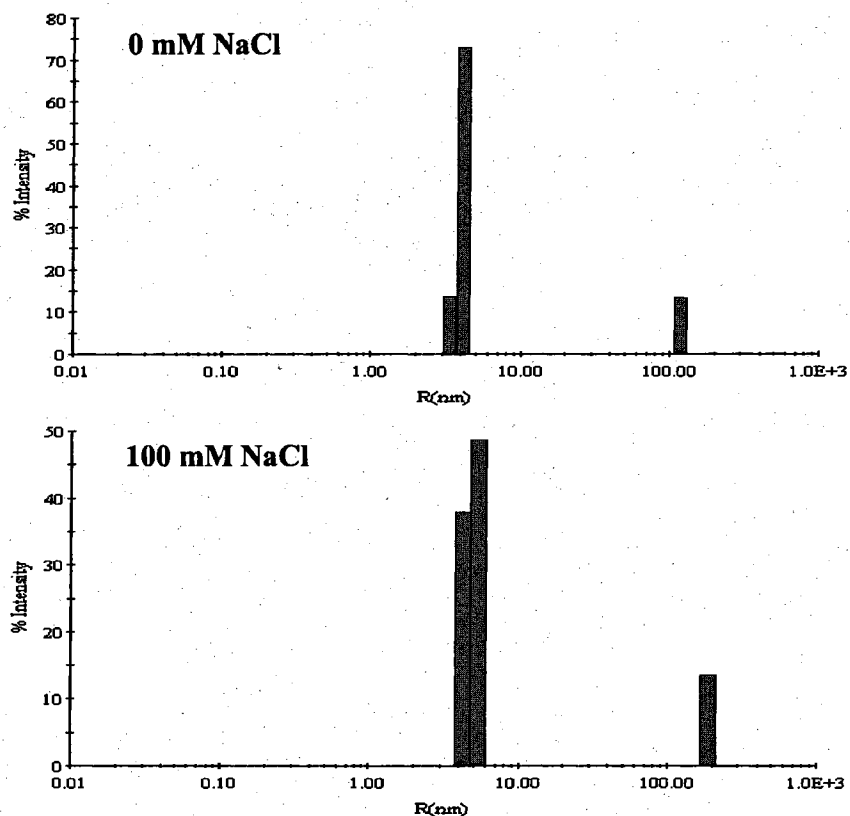


Time Zero

(diluted to 5mg/mL)	Peak 1		Peak 2		Peak 3	
	MW KDa	%Mass	MW KDa	%Mass	MW KDa	%Mass
0mM NaCl	147	100%	NA	NA	NA	NA
100mM NaCl	229	95.8%	1.6×10^7	0.2%	0.1×10^{12}	4.0%

Figure 3.21: The association state of Mab 1 as a function of NaCl concentration was measured using dynamic light scattering at the time of preparation. The antibody samples were diluted to 5 mg/mL in a buffer containing 10 mM Histidine, pH 6, and the same buffer containing 100 mM NaCl. The width of the histogram peaks represent the degree of polydispersity for each.

Figure 3.22: Dynamic Light Scattering Characterization of the Mab 2 Association State as a Function of NaCl Concentration

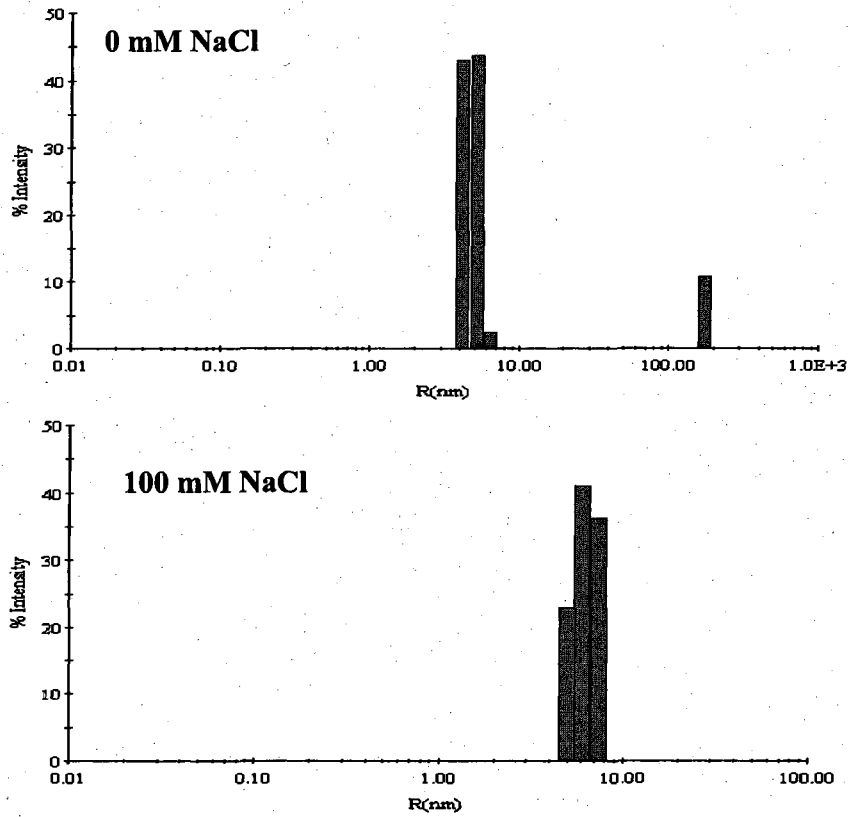


Time Zero

(diluted to 5mg/mL)	Peak 1		Peak 2		Peak 3	
	MW KDa	%Mass	MW KDa	%Mass	MW KDa	%Mass
0mM NaCl	139	100%	NA	NA	NA	NA
100mM NaCl	134	100%	NA	NA	NA	NA

Figure 3.22: The association state of Mab 2 as a function of NaCl concentration was measured using dynamic light scattering at the time of preparation. The antibody samples were diluted to 5 mg/mL in a buffer containing 10 mM Histidine, pH 6, and the same buffer containing 100 mM NaCl. The width of the histogram peaks represent the degree of polydispersity for each.

Figure 3.23: Dynamic Light Scattering Characterization of the Mab 3 Association State as a Function of NaCl Concentration



Time Zero

(diluted to 5mg/mL)	Peak 1		Peak 2		Peak 3	
	MW KDa	%Mass	MW KDa	%Mass	MW KDa	%Mass
0mM NaCl	131	100%	NA	NA	NA	NA
100mM NaCl	141	100%	NA	NA	NA	NA

Figure 3.23: The association state of Mab 3 as a function of NaCl concentration was measured using dynamic light scattering at the time of preparation. The antibody samples were diluted to 5 mg/mL in a buffer containing 10 mM Histidine, pH 6, and the same buffer containing 100 mM NaCl. The width of the histogram peaks represent the degree of polydispersity for each.

protein concentration of 5 mg/mL and a NaCl concentration of 0 and 100 mM NaCl. At 0 mM NaCl, 100% of the material is in the monomeric form as is indicated by the Mw determination of 131 KDa. As was seen in the earlier two antibody measurements, there is an additional peak that is seen in the histogram but the concentration is negligible. At 100 mM NaCl, 100% of the material is also in the monomeric form as is indicated by the Mw determination of 141 KDa, however, the width of the histogram peak suggests that the sample distribution is relatively polydisperse.

In order to explore the temperature dependence of Mab 1 aggregation as a function of NaCl concentration, a plate based DLS measurement was employed and the results are seen in **Figure 3.24**. For the Mab 1 sample at a concentration of 4 mg/mL (**Figure 3.24 A**), the results indicate that the addition of 150 mM NaCl lowers the thermal stability by ~ 5 °C as is seen by the change in the onset of the Rh increase from 48 °C to 53 °C. For the Mab 1 sample at a concentration of 6 mg/mL (**Figure 3.24 B**), the results are identical to the results of the 4 mg/mL experiment and indicate that the addition of 150 mM NaCl lowers the thermal stability by ~ 5 °C. For both concentrations, there also appears to be a decrease in the apparent Rh with an increase in temperature, by approximately 2 nm. It is important to note that the results of the DLS measurements were not corrected for changes in viscosity due to concentration and ionic strength but were corrected for the temperature dependence of the viscosity. Analysis results of the temperature dependence of Mab 1 as a function of NaCl concentration can be described as an apparent lowering of the overall free energy of the system that accompanies the mixing of a solution from its components in their pure state (Tanford, C., 1961). These theories of the transfer of free energies were also described in detail by Timasheff's

Figure 3.24: Plate Reader DLS Characterization of the Temperature Dependence of Mab 1 as a Function of NaCl Concentration

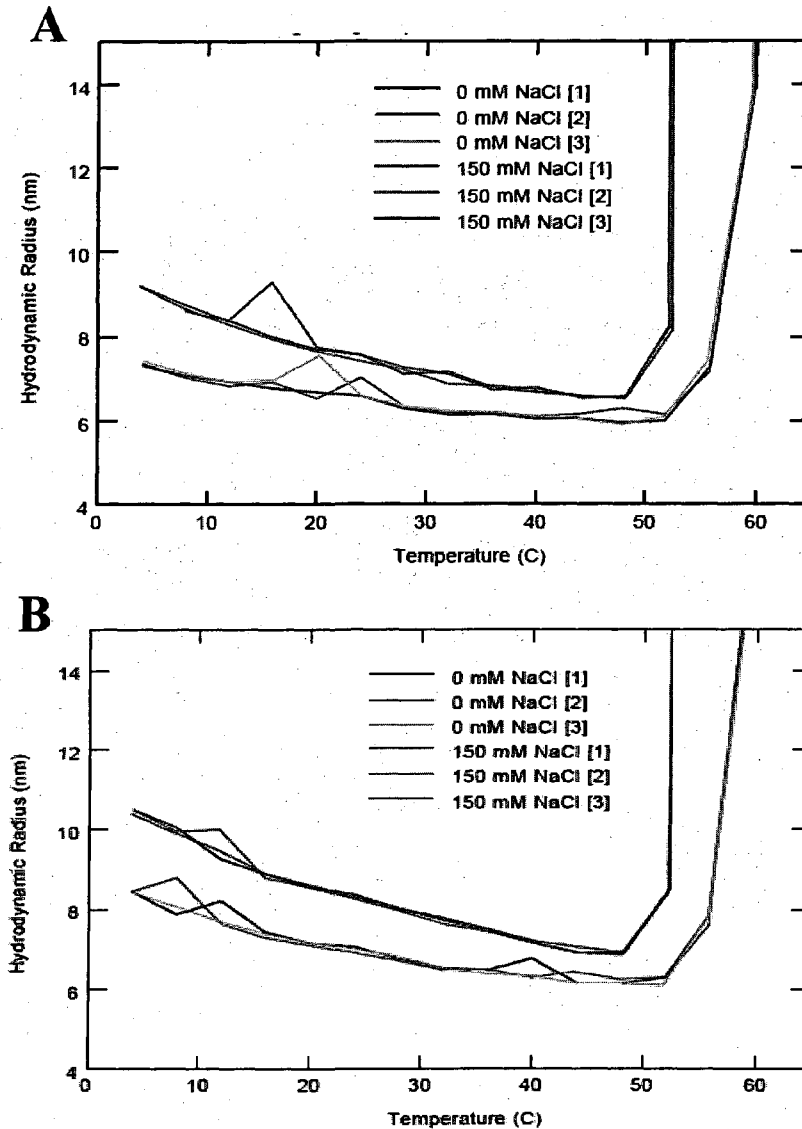


Figure 3.24: The temperature dependence (from 4 °C to 70 °C) of Mab 1 as a function of NaCl concentration was measured using a dynamic light scattering plate reader. The antibody samples were diluted to concentrations of 4 mg/mL (A) and 6 mg/mL (B) in a buffer containing 10 mM Histidine, pH 6, ± 150 mM NaCl. Each of the samples runs were performed in triplicate and the results were plotted as the apparent hydrodynamic radius (nm) vs. temperature (°C).

preferential interaction model that provides a thermodynamic treatment of protein stability as a function of solvent-solute interactions (Timasheff, 1998).

Digestion / Fragmentation

The results of the size exclusion chromatography separation of the pepsin digestion purification of the $f(ab')_2$ fragments are seen in **Figure 3.25**. The main SEC peaks were collected for Mab 1 as seen in chromatogram A, for Mab 2 as seen in chromatogram B, and for Mab 3 as seen in chromatogram C. In order to measure the hydrodynamic radius, dynamic light scattering was used (**Figure 3.26**). The measured hydrodynamic radius for Mab 1 was 4.6 nm (**Figure 3.26 A**), for Mab 2, the hydrodynamic radius was 4.6 nm (**Figure 3.26 B**), and for Mab 3, the hydrodynamic radius was 4.7 nm (**Figure 3.26 C**).

Differential Scanning Calorimetry (DSC) Study

The thermal profiles for the intact IgG 1 antibodies were performed using differential scanning calorimetry to assess any differences in the thermal stability. The thermograms of Mab 1, Mab 2 and Mab 3 from 25 °C to 90 °C, in 10 mM Histidine, pH 6 are seen in **Figure 3.27**. For Mab 1, there are three thermal transitions with the “T onset” at 55 °C, the first thermal transition at 69 °C, the second thermal transition at 76 °C and the third thermal transition at 84 °C. For Mab 2, there are three thermal transitions with the “T onset” at 59 °C, the first thermal transition at 70 °C, the second thermal transition at 75 °C and the third thermal transition at 84 °C. Finally, for Mab 3, there are also three thermal transitions with the “T onset” at 56 °C, the first thermal transition at 70 °C, the

Figure 3.25: SEC Chromatograms of the Pepsin Digestion Purification

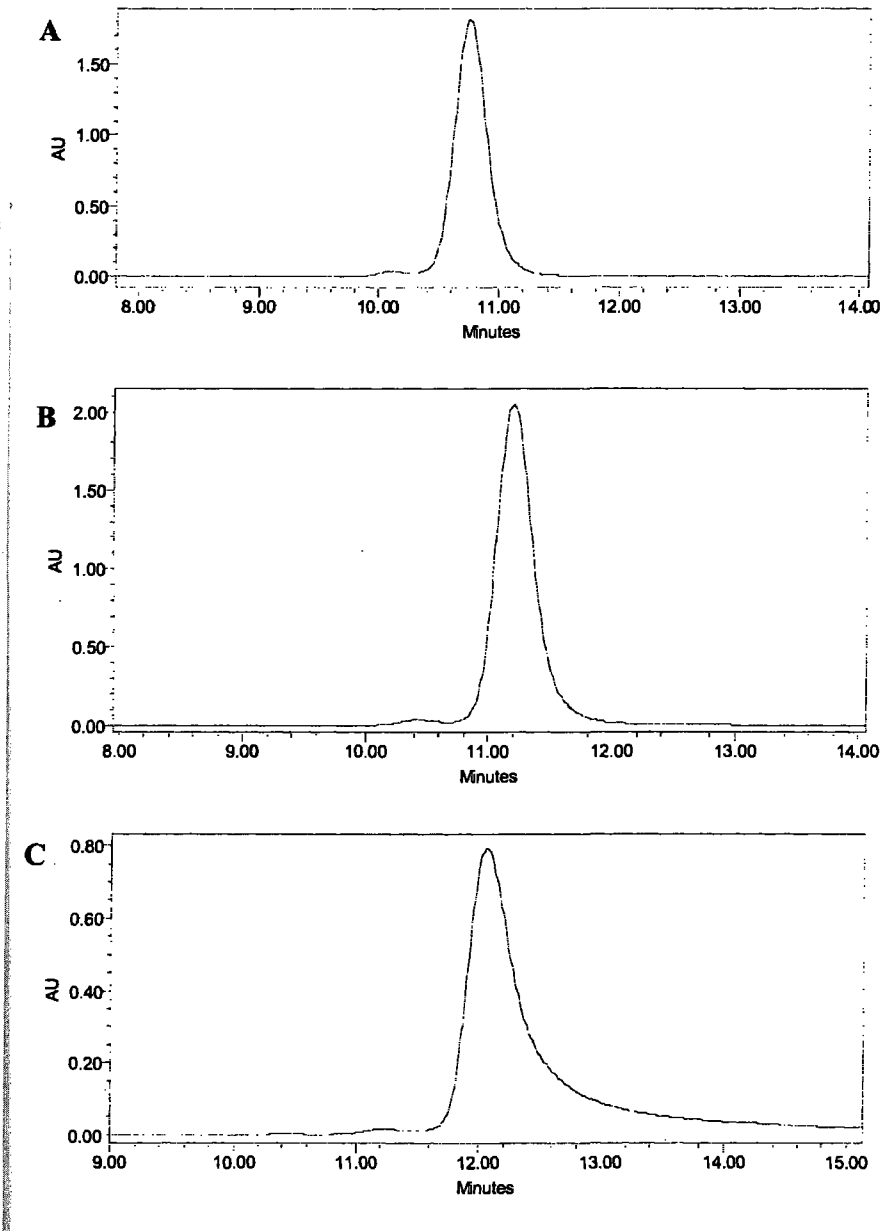


Figure 3.25: The pepsin digestion was performed on Mab 1 (A), Mab 2 (B) and Mab 3 (C). The SEC elution profile was monitored using UV detection at a wavelength of 214 nm. The main peaks were collected manually, pooled together and the protein concentration was determined spectrophotometrically (A_{280}) using calculated absorptivity ($\text{mg/mL}^{-1}\text{cm}^{-1}$) for the $F(ab')_2$ fragments.

Figure 3.26: Dynamic Light Scattering Characterization of F(ab')₂ Fragments

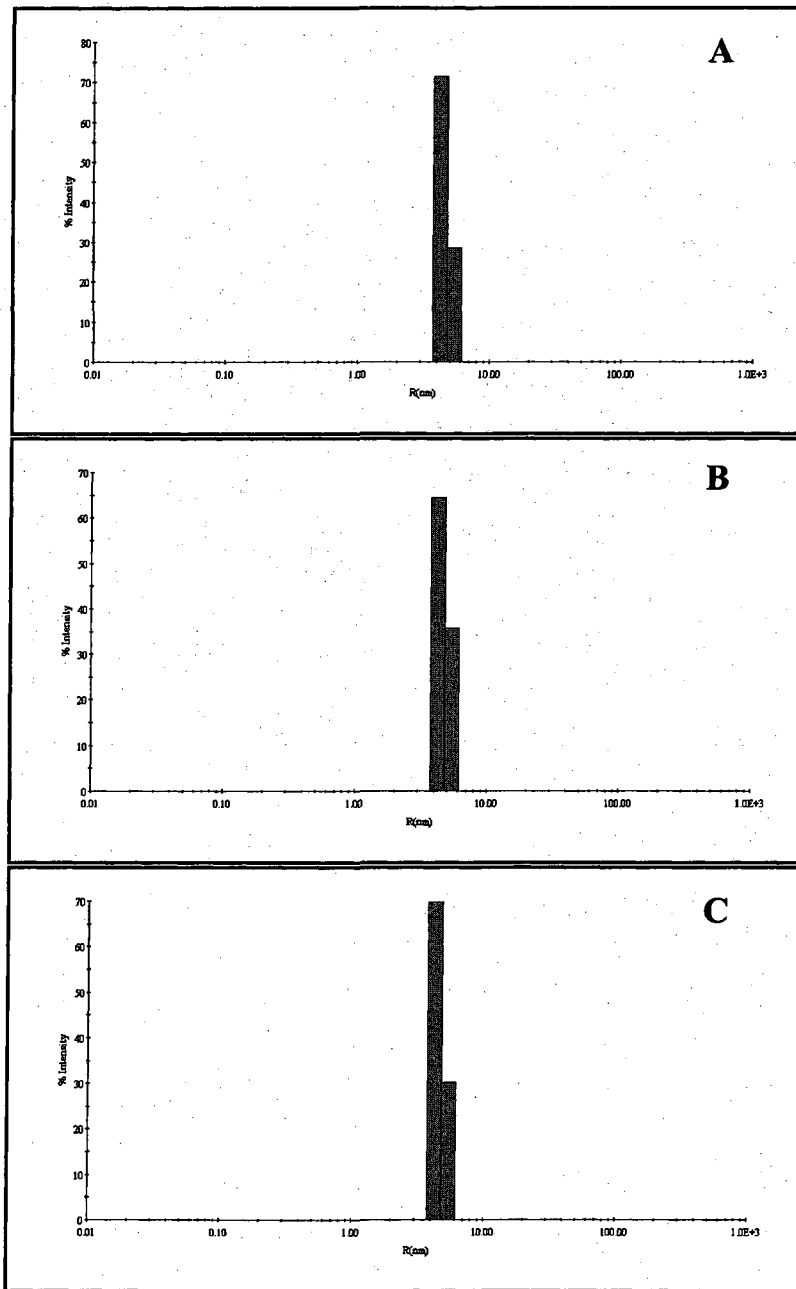


Figure 3.26: The dynamic light scattering results for the f(ab')₂ fragments are seen for Mab 1 (A) to be 4.6 nm, for Mab 2 (B) to be 4.6 nm and for Mab 3 (C) to be 4.7 nm.

Figure 3.27: Thermal Profiles of IgG 1 Antibodies Using Differential Scanning Calorimetry

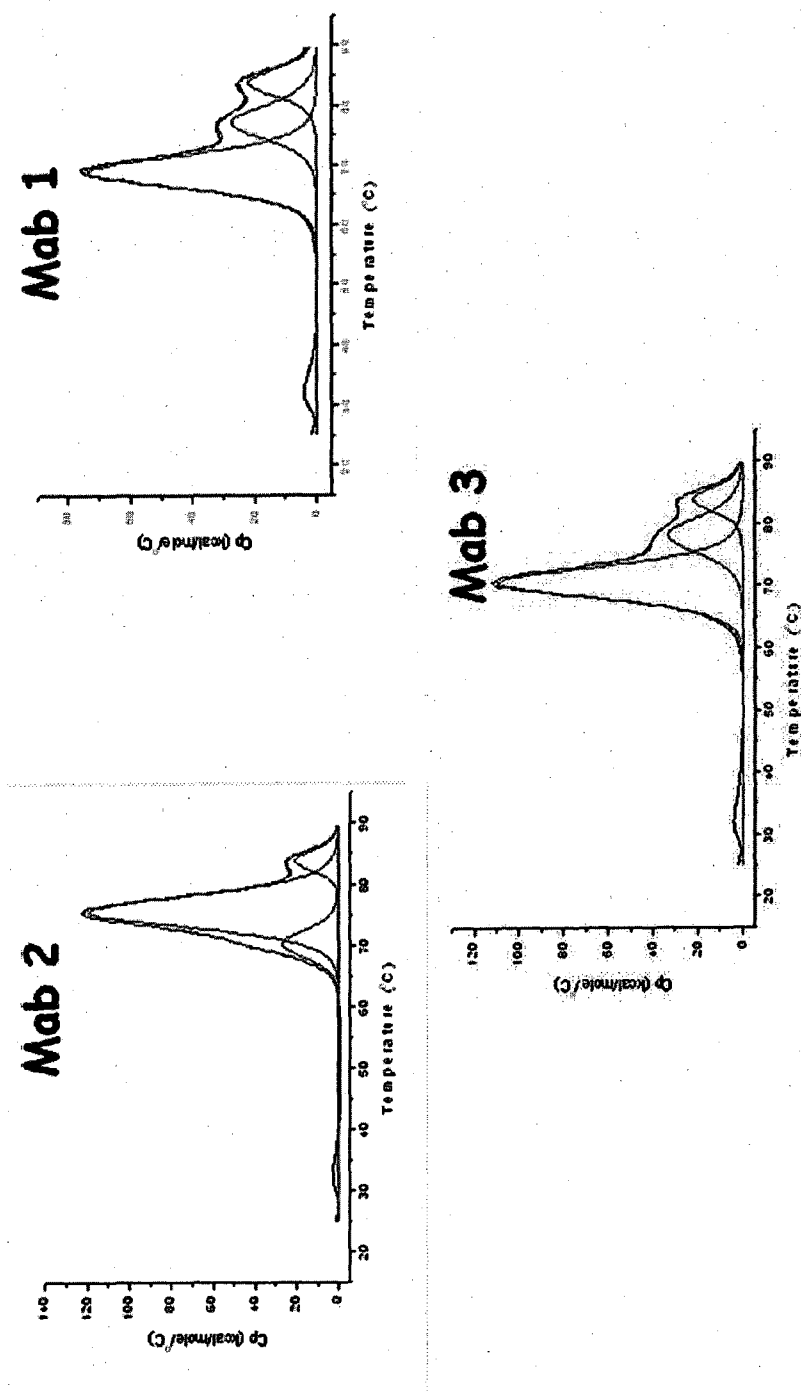


Figure 3.27: The thermal profile of Mab 1, Mab 2 and Mab 3 were characterized at a concentration of 1.5 mg/mL in 10 mM Histidine, pH 6. Scans were acquired using a 90 °C/hr scan rate spanning a temperature range from 25 to 90 °C. The data was analyzed using Origin™ software in order to fit the thermal transitions shown in red.

second thermal transition at 78 °C and the third thermal transition at 84 °C. The thermal scans of Mab 1, Mab 2 from 25 °C to 90 °C, in 10 mM Histidine, ± 150 mM NaCl, pH 6 were performed to assess any changes in the thermal stability with the addition of NaCl (Figure 3.28). The “T onset” and the thermal transitions (T_m) for Mab 1 and Mab 2 in 10 mM Histidine, pH 6 are similar to the results seen in Figure 3.27. For Mab 1 in 10 mM Histidine, 150 mM NaCl, pH 6 the “T onset” has decreased to 50 °C. There are now four thermal transitions with the first at 68 °C, the second thermal transition at 72 °C, the third at 77 °C and the final thermal transition at 85 °C. For Mab 2 in 10 mM Histidine, 150 mM NaCl, pH 6 the “T onset” has remained at 59 °C with much of the thermal profile remaining the same including a thermal transition at 68 °C, a second thermal transition at 77 °C and a third thermal transition at 84 °C. The Fab and Fc regions are also labeled in the figure based on results from scans taken for each of the isolated fragments. It is important to note that there appears to be two distinct thermal transitions for the $F(ab')_2$ region of Mab 1 in 0 and 150 mM NaCl, while the two distinct thermal transitions for the Fc region only appear in the buffer containing 150 mM NaCl.

The thermal stability (ΔT_m) for the $F(ab')_2$ and Fc regions of Mab 1 and Mab 2 were then measured as a function of NaCl concentration and the results are seen in Figure 3.29. The ΔT_m for the $F(ab')_2$ region of Mab 1 (the two $F(ab')_2$ thermal transitions were monitored and labeled as Mab 1 Fab 1 and Mab 1 Fab 2) show that there is little loss in the thermal stability from 0 to 150 mM NaCl. It is important to note that the two $F(ab')_2$ thermal transitions for Mab 2 had a similar ΔT_m profile and were therefore labeled as a single $F(ab')_2$. The results of the ΔT_m for the $F(ab')_2$ region of Mab 2 seem to indicate that there is an apparent loss in the thermal stability as the NaCl

Figure 3.28: Thermal Profiles of Mab 1 and Mab 2 Using Differential Scanning Calorimetry as a Function of NaCl Concentration

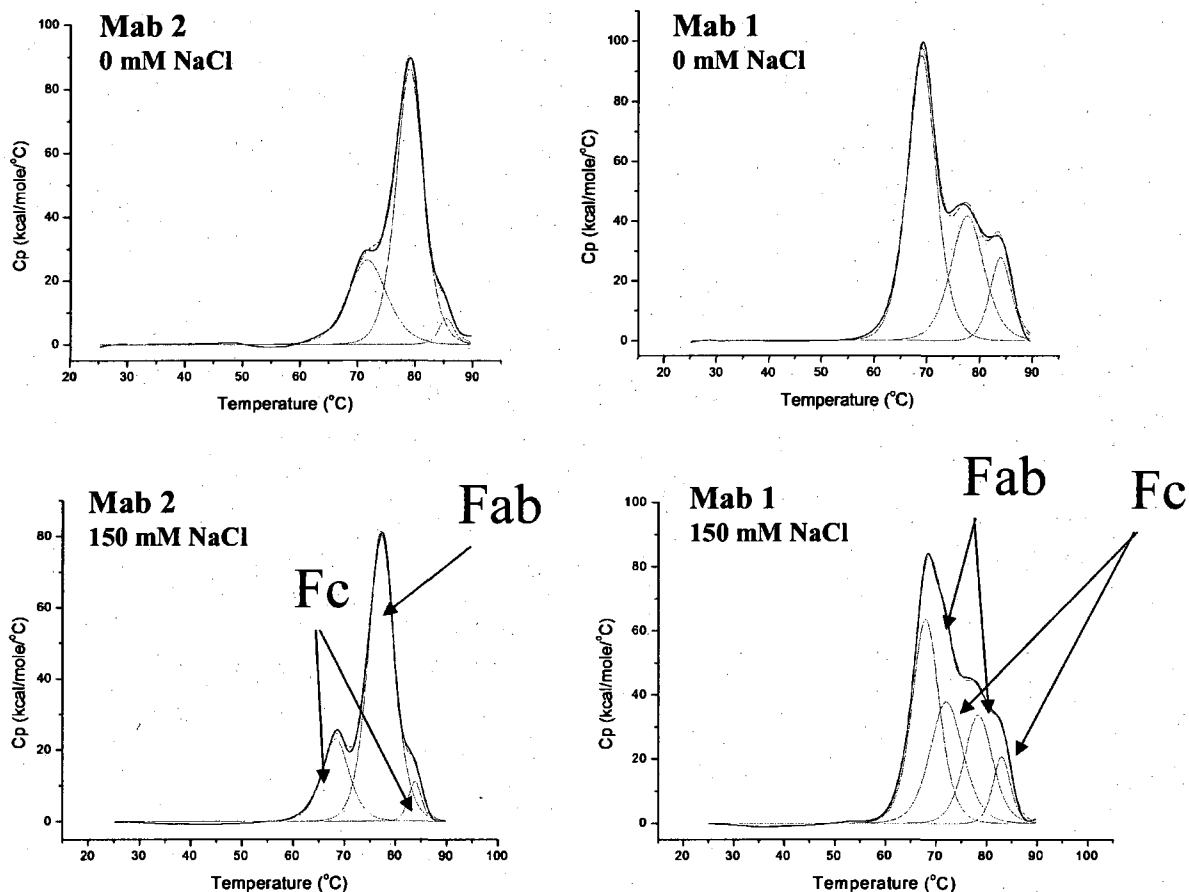


Figure 3.28: The thermal profile of Mab 1, Mab 2 were characterized at a concentration of 1.0 mg/mL in 10 mM Histidine, pH 6 and 10 mM Histidine, 150 mM NaCl, pH 6. Scans were acquired using a 90 $^{\circ}$ C/hr scan rate spanning a temperature range from 25 $^{\circ}$ C to 90 $^{\circ}$ C. The data was analyzed using OriginTM software in order to fit the thermal transitions shown in red.

Figure 3.29: Thermal Stability of Mab 1 and Mab 2 Fragments as a Function of NaCl Concentration

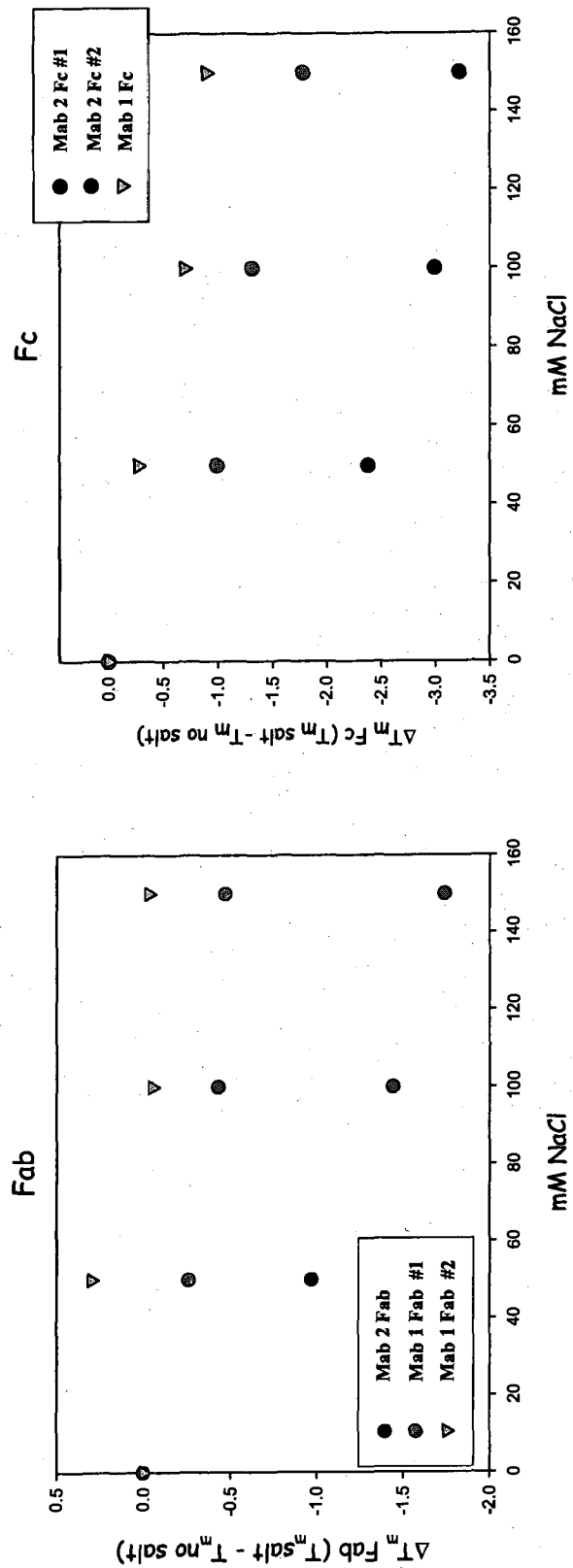


Figure 3.29: The thermal stability (ΔT_m) of the $F(ab')_2$ and Fc regions for Mab 1 and Mab 2 was measured as a function of NaCl concentration. The buffer used in this study was 10 mM Histidine, pH 6 with a range of NaCl concentrations including 0 mM, 50 mM, 100 mM and 150 mM NaCl. The two distinct thermal transitions seen in Mab 1 were measured and labeled as Fab #1 and Fab #2. Although there were also two distinct thermal transitions for the Fc region of Mab 1 and Mab 2, only one Fc transition was able to be measured for Mab 1.

concentration is increased from 0 to 150 mM NaCl. The results of the ΔT_m for the Fc region of Mab 1 and Mab 2 show that there is equivalent loss in the thermal stability, for the two antibody fragments, from 0 to 150 mM NaCl. It is important to note that the two Fc thermal transitions for Mab 2 were monitored and labeled as Mab 2 Fc 1 and Mab 2 Fc 2, however, the two Fc thermal transitions for Mab 1 followed the same ΔT_m and were therefore labeled as a single Fc. These results appear to be consistent with there being a specific charge effect on the Fc region with the addition of NaCl, leading to a decrease in the thermal stability.

The thermal profile for the $F(ab')_2$ and Fc domain of Mab 1, from 30 °C to 95 °C, in PBS-CMF (phosphate buffered saline, calcium and magnesium free), were examined and compared the intact antibody thermogram as a function of pH (Figure 3.30). The thermograms for intact Mab 1 were compared with the $F(ab')_2$ fragment at pH 7.2 and pH 4 (Figure 3.30 A). The pH 7.2 results show the two distinct thermal transitions for the $F(ab')_2$ fragments, along with the four thermal transitions for the intact Mab 1, as they appear in Figure 3.28. The pH 4 results show a distinct shift in the thermal profile of the $F(ab')_2$ fragment from two thermal transitions (at 66 °C and 77 °C) to a single thermal transition at 72 °C. The thermogram for the intact Mab 1 also shows a distinct shift from four thermal transitions to only three distinct thermal transitions at 56 °C, 72 °C and 92 °C. The thermograms for intact Mab 1 were then compared with the Fc fragment at pH 7.2 and pH 4 (Figure 3.30 B). The pH 7.2 results show the two distinct thermal transitions for the Fc fragments, along with the four thermal transitions for the intact Mab 1, as they appear in Figure 3.28. The pH 4 results show a distinct shift in the thermal profile of the Fc fragment from 72 °C and 84 °C to 56 °C and 75 °C. The thermogram

Figure 3.30: pH Dependent Domain Shifts in Mab 1

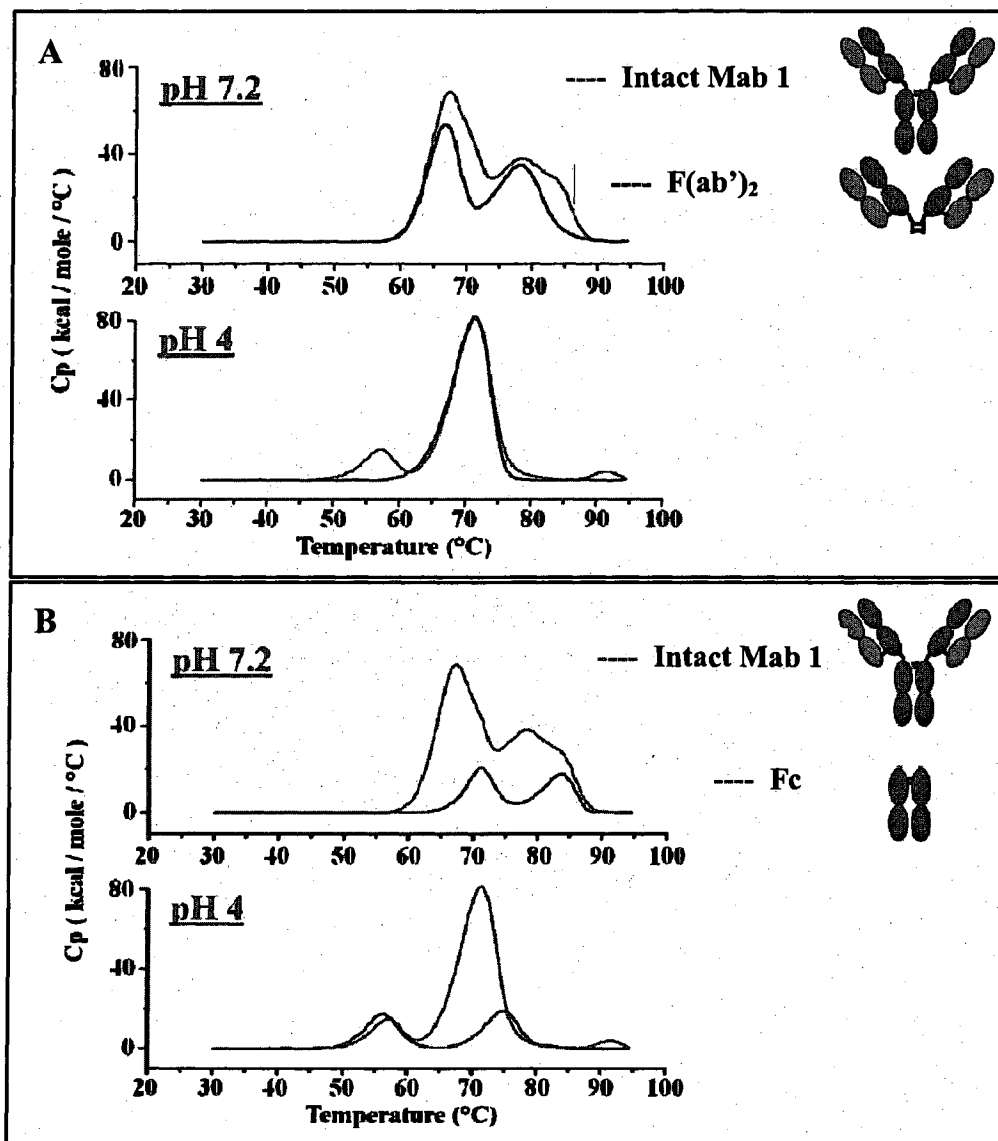


Figure 3.30: The thermal profile for the F(ab')₂ (A) and Fc domain (B) of Mab 1 were examined as a function of pH, and overlaid with the intact antibody thermogram. The two pH conditions were chosen to represent the most stable (pH 7) and the least stable (pH 4) thermal conditions for most IgG molecules. The thermal profiles were characterized at a concentration of ~1.0 mg/mL in PBS-CMF. Scans were acquired using a 90 °C/hr scan rate spanning a temperature range from 30 °C to 95 °C.

for the intact Mab 1 also shows a distinct shift as previously described. These results appear to be consistent with the results seen in Figure 3.29 where, at pH 4, there is higher charge on Mab 1 and a decrease in the thermal stability as the electrical free energy is reduced by unfolding (Stigter, 1990).

Non-Ideality Analysis

The non-ideality was measured using light scattering for the three IgG 1 antibodies as a function of NaCl concentration. The measurement was performed in a buffer containing 10 mM Histidine, pH 6 with the addition of 50, 100 and 150 mM NaCl. The results of these measurements are shown in Figure 3.31, labeled in units of 10^{-4} mol-mL/g². For Mab 1, all of the measurements were negative with a continued negative trend in the non-ideality from -3.6 in 0 mM NaCl, to -2.7 in 50 mM NaCl and -24.1 in 100 mM NaCl. The non-ideality for Mab 1 was not able to be measured at 150 mM NaCl due to viscosity limitation of the technique. It should be noted however that the non-ideality was eventually measured (1 X) for Mab 1 at 250 mM NaCl to have a value of -54.9 x 10^{-4} mol-mL/g². For Mab 2, all of the measurements were positive with somewhat of a positive trend in the non-ideality from 3.3 in 0 mM NaCl, to 3.1 in 50 mM NaCl, 9.0 in 100 mM NaCl and 6.8 in 150 mM NaCl. For Mab 3, all of the measurements were positive but there was a slightly negative trend in the non-ideality from 20.5 in 0 mM NaCl, to 18.5 in 50 mM NaCl and 12.9 in 150 mM NaCl and is consistent with a shielding of charge-charge interaction with the NaCl.

Figure 3.31: Non-Ideality (A_2) Measured as a Function of NaCl Concentration

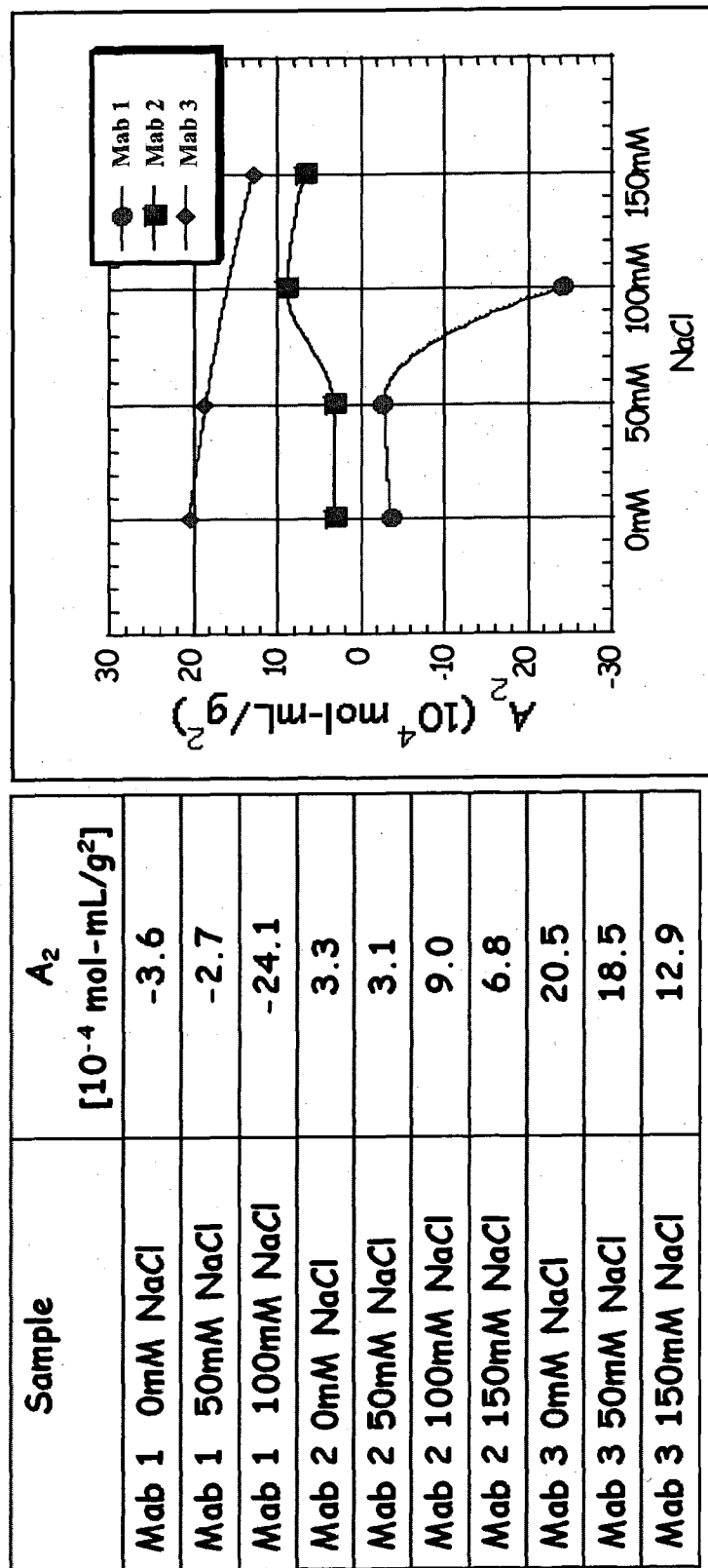


Figure 3.31: The non-ideality (A_2 or second virial coefficient) of Mab 1, Mab 2 and Mab 3 was measured as a function of NaCl concentration and recorded in units of mL-mol/gram². The data was then depicted graphically with Mab 1 in red circles, Mab 2 in blue squares and Mab 3 in green diamonds. The buffer used in this study was 10 mM Histidine, pH 6 with 0 mM, 50 mM, 100 mM and 150 mM NaCl. Each measurement was performed 3X with the standard deviation for each of the measurements $< 1.0 \times 10^{-4}$. It is important to note that Mab 1 was not able to be measured at 150 mM NaCl due to viscosity limitations of the technique. Eventually, a 1X measurement for Mab 1 in 10 mM Histidine, 250 mM NaCl, pH 6, revealed an A_2 of -54.9×10^{-4} mL-mol/g².

Viscosity Measurement

The viscosity and apparent optical density of Mab 1 was measured over a protein concentration range of 1, 5, 10, 20, 30, 40, 50, 55 and 60 mg/mL, at 4 °C and 25 °C in a buffer containing 10 mM Histidine, 50 mM NaCl, pH 6 (Figure 3.32). The viscosity appears to increase in a non-linear fashion with an increase in concentration at both 4 °C and 25 °C (Figure 3.32 A). The apparent optical density (OD_{400}) also appears to increase in a non-linear fashion with an increase in concentration (Figure 3.32 B). However, after 10 mg/mL, the increase in the apparent optical density at 4 °C increased more rapidly than the same sample measured at 25 °C.

The viscosity effects of NaCl on the three IgG 1 antibody samples were also measured at a concentration of 5 mg/mL in a buffer containing 10 mM Histidine, pH 6 with 0, 50 and 100 mM NaCl (Figure 3.33). The results of the viscosity for Mab 1 appeared to increase in a non-linear fashion from 1.2 cP at 0 mM NaCl to 1.48 cP at 50 mM NaCl and 1.62 cP at 100 mM NaCl. The results of the viscosity for Mab 2 also appeared to increase in a non-linear fashion from 0.94 cP at 0 mM NaCl to 1.02 cP at 50 mM NaCl and 1.07 cP at 100 mM NaCl. The results of the viscosity for Mab 3 again appeared to increase in a non-linear fashion from 0.94 cP at 0 mM NaCl to 0.95 cP at 50 mM NaCl and 1.02 cP at 100 mM NaCl. The higher specific viscosity of Mab 1 is consistent with protein-protein interactions in solution (Liu, 2005).

Figure 3.32: Viscosity of Mab 1 as a Function of Protein Concentration

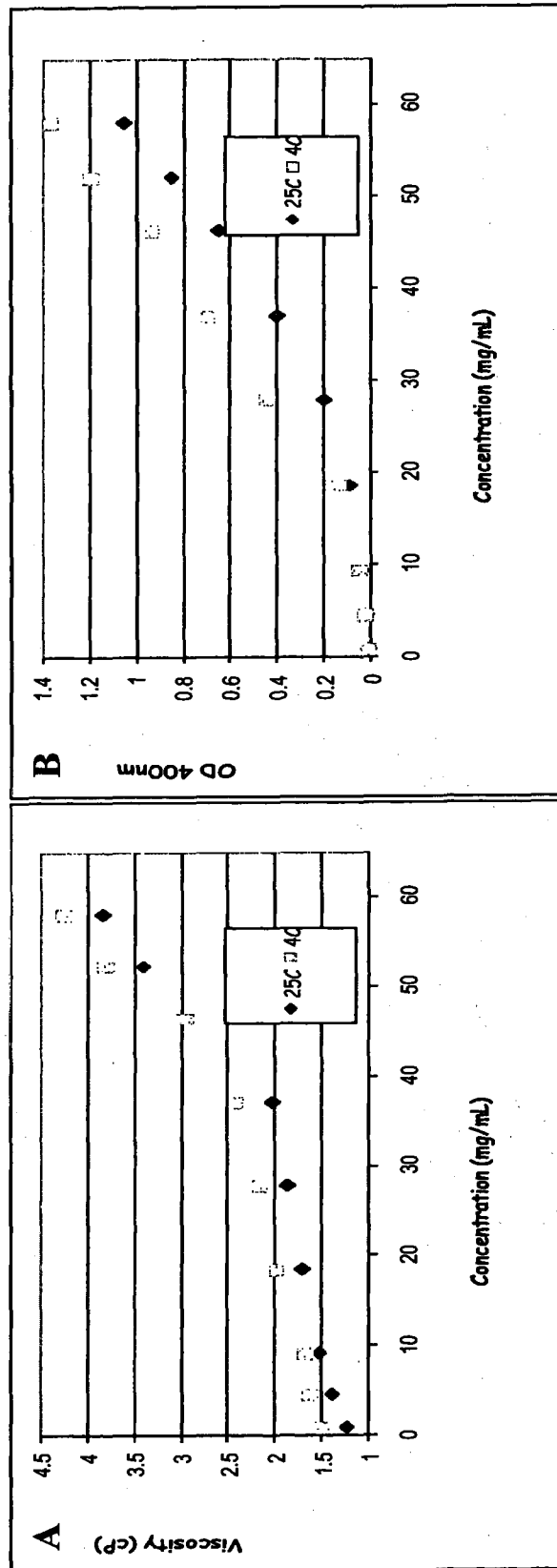


Figure 3.32: The viscosity of Mab 1 (A), as well as the apparent optical density (B), was measured as a function of protein concentration at 4 °C and 25 °C. Samples were measured in a buffer containing 10 mM Histidine, 50 mM NaCl, pH 6. The viscosity was measured in units of centipoise and the concentrations of Mab 1 used in this study were 1, 5, 10, 20, 30, 40, 50, 55 and 60 mg/mL.

Figure 3.33: Viscosity of Mab as a Function of NaCl Concentration

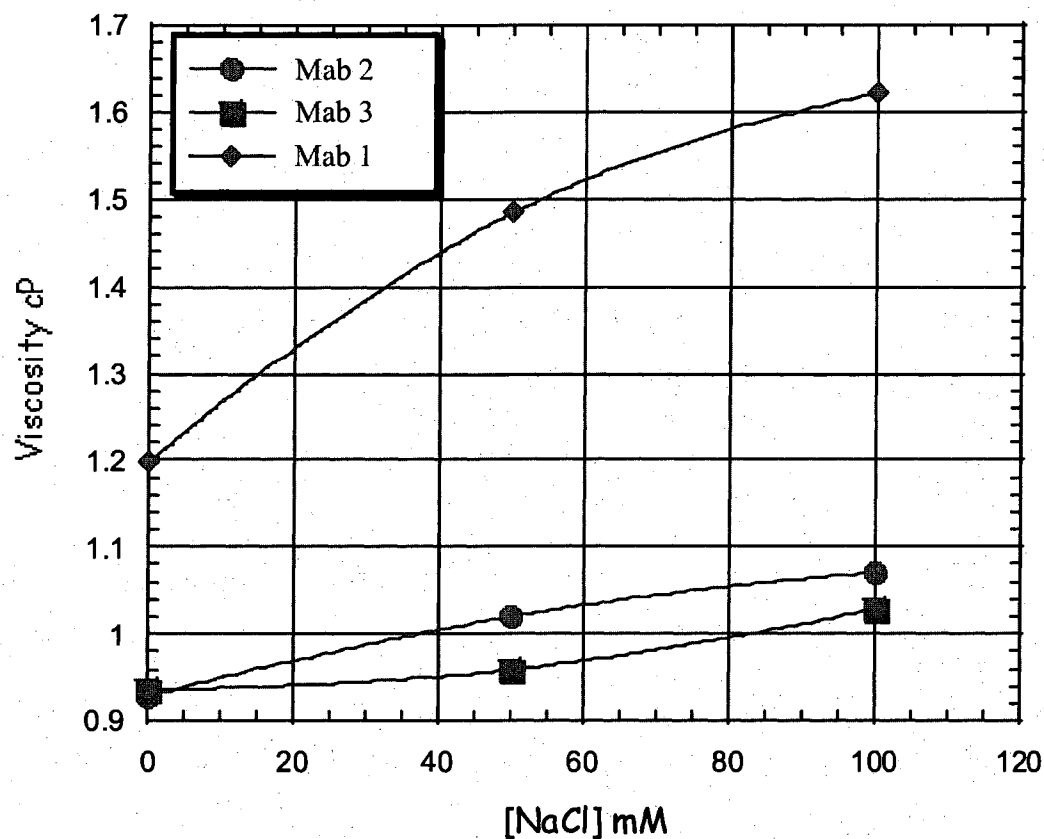


Figure 3.33: The viscosity effects of NaCl were examined for Mab 1 (green diamonds), Mab 2 (red circles) and Mab 3 (blue squares). The viscosity was measured in units of centipoise and the concentration of Mab used in this study was 5 mg/mL in a buffer containing 10 mM Histidine, pH 6 with 0, 50 and 100 mM NaCl. The data were fit using Origin™ software to a non-linear line using the data points available.

Circular Dichroism and Fluorescence Structural Analysis

The structural changes in Mab 1 were explored by the use of circular dichroism (along with fluorescence) in a buffer containing 10 mM Histidine, pH 6, ± 100 mM NaCl (Figure 3.34). The near UV-CD data (examined over a wavelength range of 250 to 360 nm) in the buffer containing 0 and 100 mM NaCl, appear to be identical and overlay perfectly for Mab 1. As a secondary method of determining structural changes the fluorescence of Mab 1 was also examined at an excitation wavelength of 280 nm and emission spectra from 300 to 450 nm. As with the CD data, the fluorescence emission spectra for Mab 1 also appear to be identical and overlay perfectly in the buffer containing 0 and 100 mM NaCl. These results indicate that there are no significant changes in the 2° or 3° structure with added NaCl.

Congo Red

Congo red (CR) was used to gain insight into the possibility of fibril formation during the Mab 1 opalescence phenomenon as a function of protein concentration, NaCl concentration and temperature (Figure 3.35). The concentrations of Mab 1 used in this study were 1 and 10 mg/mL in a buffer containing 10 mM Histidine, pH 6 ± 50 mM NaCl, with scans taken at 4 °C and room temperature. For the Mab 1 sample, run in the buffer without NaCl, under all the conditions tested, the OD maximum was ~500 nm. With the presence of NaCl in the buffer, the Mab 1 sample exhibited a slight “blue shift” in the OD maximum from ~500 nm to ~495 nm, under all conditions tested. It should be noted that when the same analysis was performed on Mab 2 and Mab 3, under similar

Figure 3.34: Structural Differences of Mab 1 as Measured by Circular Dichroism and Fluorescence

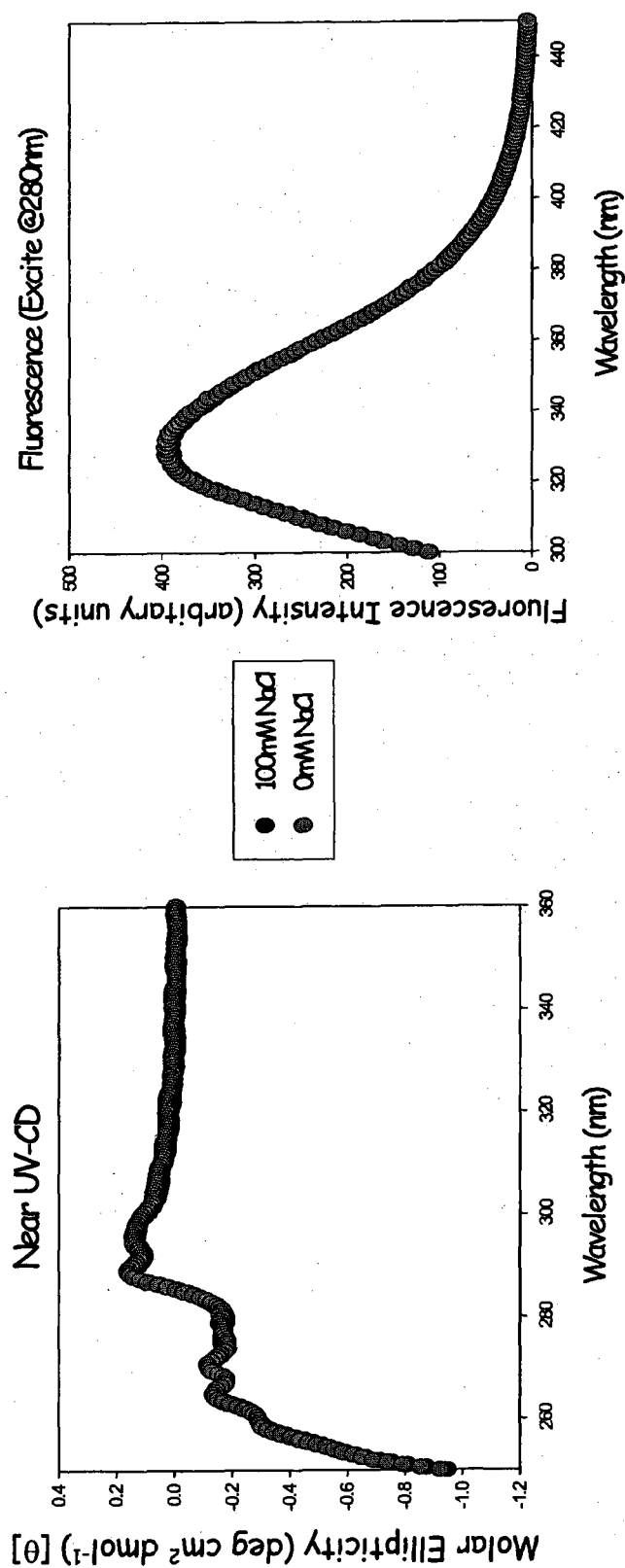


Figure 3.34: The structural changes of Mab 1 in a buffer containing 10 mM Histidine, pH 6 with 0 and 100 mM NaCl were examined by circular dichroism and fluorescence. The concentration of Mab 1 in this study was 4 mg/mL. The CD data was examined over a wavelength range of 250 to 360 nm and labeled in units of deg cm² dmol⁻¹. The excitation wavelength of the fluorescence was 280 nm, with the emission spectra measured from 300 to 450 nm.

Figure 3.35: Congo Red Analysis of Mab 1

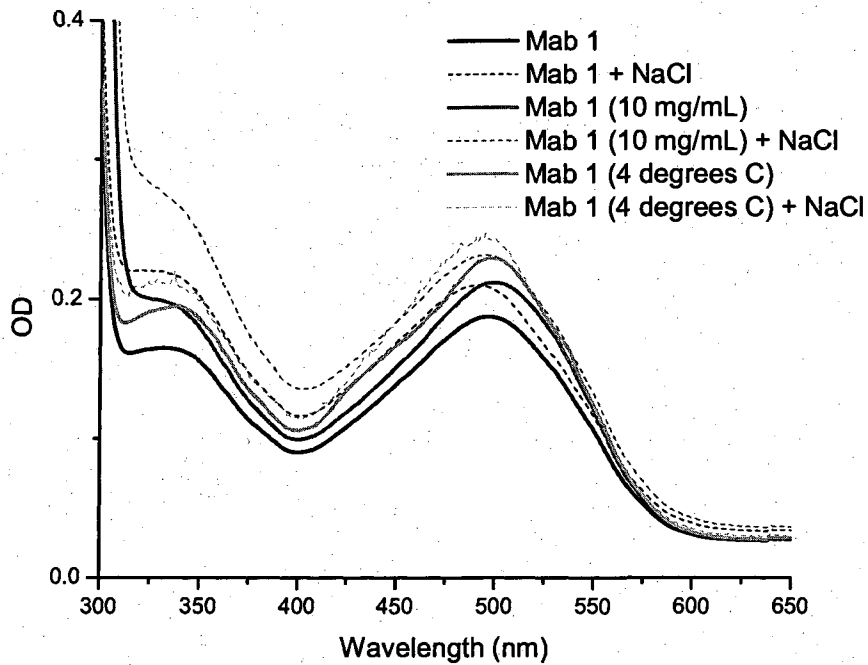


Figure 3.35: The results of the congo red analysis is displayed as apparent optical density versus wavelength. The concentrations of Mab 1 used in this study were 1 mg/mL and 10 mg/mL, in a buffer containing 10 mM Histidine, pH 6 ± 50 mM NaCl, at room temperature and 4 °C. The Mab 1 samples that were run without NaCl are represented by solid lines and the samples run with NaCl are represented by dotted lines. The absorption spectra were acquired in 2 nm increments from 300 to 650 nm at a scan rate of 300 nm/min. It is important to note that the same analysis was performed on Mab 2 and Mab 3 without significant differences in the scans with, and without NaCl.

conditions, there was not a “blue shift” in the OD maximum with NaCl in the buffer.

These results are consistent with the conclusion that there is no fibril formation in Mab 1, Mab 2 and Mab 3 under all of the conditions tested.

Urea Analysis

The ability for urea to break hydrogen bonds (and possibly disrupt the antibody opalescence) was tested on Mab 1 at a concentration of 5 mg/mL, in a buffer containing 10 mM Histidine, 100 mM NaCl, pH 6, using dynamic light scattering. In Table 3.2, the results of the molecular weight and the % Mass are listed for urea concentrations of 200 mM (6000:1), 0.3 mM (10:1) and 0.03 mM (1:1), for up to three R_h peaks after one hour (at room temperature) and then after 24 hours at 4 °C. At the urea concentration of 0.3 mM, the Mw of the most abundant peak (peak 1) decreased from 229 KDa (95.8% of the total) to ~135 KDa (100% of the total) after one hour at room temperature and after 24 hours at 4 °C. The urea also appeared to completely eliminate peak 2 (0.2% of the total) and peak 3 (4% of the total) that were apparent in the sample without urea. At the urea concentration of 0.3 mM, the Mw of peak 1 also remained low at 134 KDa (100% of the total) after one hour at room temperature. However, after 24 hours at 4 °C, the Mw of peak 1 increased to 165 KDa (99.5% of the total) with an additional high molecular weight peak re-appearing. At the urea concentration of 0.03 mM, the Mw of peak 1 was higher, at 160 KDa, but remained at 100% of the total after one hour at room temperature. However, after 24 hours at 4 °C, the Mw of peak 1 increased to 165 KDa

Table 3.2: The Effects of Urea on Mab 1 with NaCl as Measured by DLS

Sample Mab 1 (diluted to 5mg/mL)	Peak 1		Peak 2		Peak 3	
	MW KDa	%Mass	MW KDa	%Mass	MW KDa	%Mass
100mM NaCl	229	95.8%	1.6x10 ⁷	0.2%	1.1x10 ¹¹	4.0%
100mM NaCl + 200mM Urea	135	100%	NA	NA	NA	NA
100mM NaCl + 200mM Urea 24hrs 4C	136	100%	NA	NA	NA	NA
100mM NaCl + 0.3mM Urea	134	100%	NA	NA	NA	NA
100mM NaCl + 0.3mM Urea 24hrs 4C	165	99.5%	NA	NA	0.4x10 ¹¹	0.5%
100mM NaCl +0.03mM Urea	160	100%	NA	NA	NA	NA
100mM NaCl +0.03mM Urea 24hrs 4C	165	99.6%	NA	NA	0.1x10 ¹¹	0.4%

Table 3.2: The effects of urea on Mab 1 at a concentration of 5 mg/mL, in a buffer containing 10 mM Histidine, 100 mM NaCl, pH 6, were examined using dynamic light scattering. Urea at concentrations of 200 mM (6000:1), 0.3 mM (10:1) and 0.03 mM (1:1) was introduced to Mab 1 and measured after one hour at room temperature, and then after 24 hours at 4 °C. Scans of the samples were performed as ten, ten second scans that were globally fit for total of 100 seconds. The Mw was determined by comparison to globular standards of similar Rh, and the %Mass represents a quantitative measure of the peaks relative abundance.

(99.6% of the total) with an additional high molecular weight peak re-appearing, as seen with the 0.3 mM urea concentration.

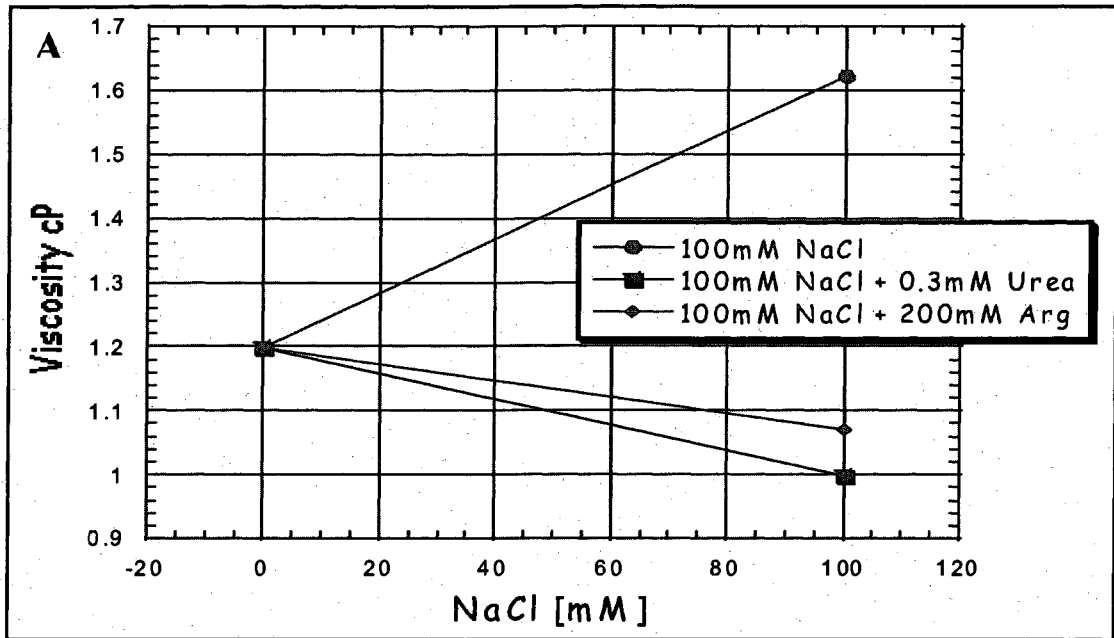
In addition to breaking hydrogen bonds, urea (0.3 mM) was compared to arginine (200 mM) to examine its effect in lowering the viscosity of Mab 1 at a concentration of 5 mg/mL, in a buffer containing 10 mM Histidine, pH 6 ± 100 mM NaCl (**Figure 3.36**). In addition to the measured viscosity (**Figure 3.36 A**), dynamic light scattering was also employed to examine and compare the effects of arginine in the disruption of high molecular weight species (**Figure 3.36 B**). The results of the viscosity of Mab 1 in the Histidine buffer containing 100 mM NaCl increased from 1.2 cP (in 0 mM NaCl) to 1.62 cP. However, when 0.3 mM urea was added to the Mab 1 sample, the viscosity dropped from 1.2 cP (in 0 mM NaCl) to 1.0 cP. Similarly, when 200 mM arginine was added to the Mab 1 sample, the viscosity dropped from 1.2 cP (in 0 mM NaCl) to 1.07 cP.

The results of the dynamic light scattering measurements in the Mab 1 sample containing 200 mM Arginine were similar to that seen in the sample containing 0.3 mM urea. The high molecular weight species appeared to be completely disrupted, resulting a single peak with a Mw of 143 KDa.

FTIR Structural Analysis

The results of the FTIR structural analysis of Mab 1, Mab 2 and Mab 3 indicate that there is little secondary structural difference between the three antibodies in the presence, or absence of 100 mM NaCl, at 4 °C and 20 °C. **Figure 3.37** shows the IR spectra for the most useful amide band in the analysis of the secondary structure of

Figure 3.36: The Effects of Urea and Arginine on Mab 1 in NaCl as Measured by Viscosity and Dynamic Light Scattering



Mab 1	Peak 1		Peak 2		Peak 3	
	MW KDa	%Mass	MW KDa	%Mass	MW KDa	%Mass
100mM NaCl	229	95.8%	1.6×10^7	0.2%	1.1×10^{11}	4.0%
100mM NaCl + 0.3mM Urea	134	100%	NA	NA	NA	NA
100mM NaCl + 200mM Arginine	143	100%	NA	NA	NA	NA

Figure 3.36: The viscosity of Mab 1 (5 mg/mL) in a buffer containing 10 mM Histidine, pH 6 ± 100 mM NaCl, was measured to examine the effects of urea (10:1) and Arginine (6000:1) (A). The same samples were then examined using dynamic light scattering at 25 °C, and the peak information displayed as Mw (KDa) and %Mass (B).

Figure 3.37: FTIR Structural Analysis of Mab 1, Mab 2 and Mab 3

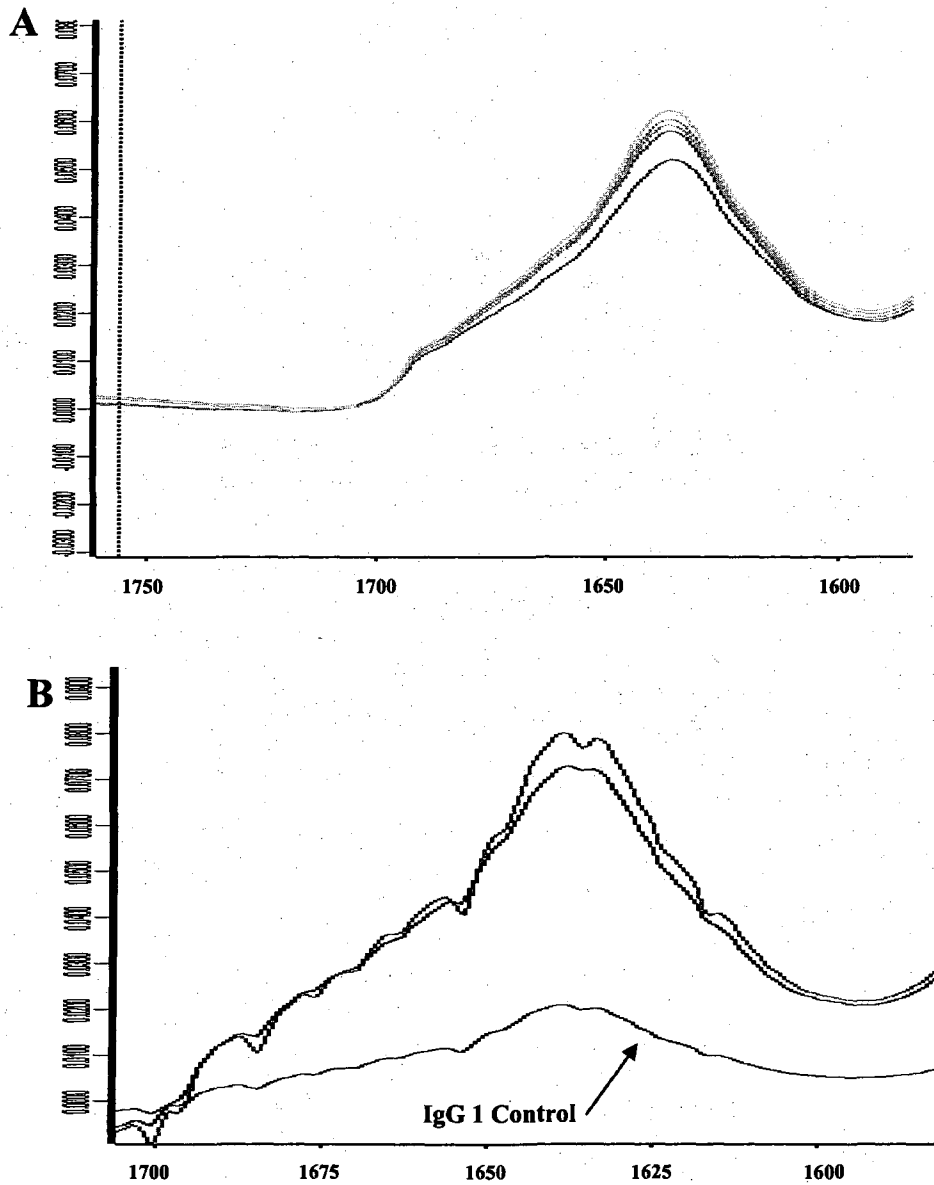


Figure 3.37: (A) The IR spectra of Mab 1 in a buffer containing 10 mM Histidine, pH 6 (2 green traces), 10 mM Histidine, 100 mM NaCl, pH 6 (yellow trace), Mab 2 (purple trace) and Mab 3 (red trace) in a buffer containing 10 mM Histidine, 100 mM NaCl, pH 6 at 4 °C. (B) The IR spectra of Mab 1 in a buffer containing 10 mM Histidine, pH 6 (blue trace) and 10 mM Histidine, 100 mM NaCl, pH 6 (black trace) along with an IgG 1 control in a buffer containing 10 mM Histidine, pH 6 at 20 °C.

proteins, the amide I band, which occurs in the region $1600\text{-}1700\text{ cm}^{-1}$. In Figure 3.37 (Figure 3.37 A), at $4\text{ }^{\circ}\text{C}$, in a buffer containing 10 mM Histidine, $\text{pH } 6 \pm 100\text{ mM NaCl}$, the three antibodies all show an asymmetrically shaped amide I band centered at a maximum of $\sim 1635\text{ cm}^{-1}$. This IR spectroscopic maximum is characteristically indicative of secondary structure which is predominantly antiparallel β -sheet (Krimm, 1986). In Figure 3.37 B, Mab 1 is further analyzed at $20\text{ }^{\circ}\text{C}$, in a buffer containing 10 mM Histidine, $\text{pH } 6 \pm 100\text{ mM NaCl}$, and the results also show an IR spectroscopic maximum at 1635 cm^{-1} . The IgG 1 control overlaid with Mab 1 in Figure 3.37 (B) was actually Mab 2 in a buffer containing 10 mM Histidine, $\text{pH } 6$. It should be noted that the poor sensitivity and low signal to noise ratio of Figure 3.37 (B) was due to an improper alignment of the instrument which was corrected prior to the extensive analysis displayed in Figure 3.37 (A).

Capillary Electrophoresis Studies

Capillary electrophoresis (CE) was employed as a technique to determine the protein valence of the three IgG 1 antibodies and to relate this valence to the observed solubility and apparent aggregation states. This approach measures the electrophoretic mobility of the protein (μ) with respect to that of a neutral marker that moves only with the electroosmotic flow of CE. From the electrophoretic mobility, the effective or apparent valence (Z^*) is directly determined. The final Debye-Henry-Hückel Z (which is independent of the counter-ion shielding, coupling of ionic flows and deformation of the electric field in the vicinity of the protein) of the three IgG 1 samples was then calculated using the software program ZUtilities, in order to examine the effects from incremental

changes in the number of charged groups present on the surface of the proteins. It is important to note that all subsequent references to protein valence will refer to the Debye-Henry-Hückel Z. **Figure 3.38** shows the results of the CE analysis of the three digested IgG 1 antibody F(ab')₂ fragments in the buffer containing 100 mM MES, pH 6 (**Figure 3.38 A**) and 100 mM MES, 100 mM NaCl, pH 6 (**Figure 3.38 B**). The elution positions for run A were, EOF: 4.388; Mab 1: 4.383; Mab 2: 4.396; Mab 3: 4.404, while the elution positions for run B were, EOF: 22.587; Mab 1: 23.096; Mab 2: 24.621; Mab 3: 26.163. These elution positions were then used to generate a protein valence for each F(ab')₂ fragment with the results listed in **Table 3.3**. Along with the F(ab')₂ fragments, the protein valence was also measured by CE for the three intact IgG 1 antibodies in 100 mM MES buffer, pH 6 ± 100 mM NaCl and ± 0.1 mM urea, with the results also listed in **Table 3.3**. From the results listed for the F(ab')₂ fragments, the protein valence is negligible in the buffer without NaCl, then increases to 1.14 for Mab 1, 6.14 for Mab 2 and 9.38 for Mab 3 in the presence of 100 mM NaCl. Although the calculated valence increased in the presence of NaCl, it was still lower than the expected charge based on the amino acid sequence as calculated by Sednterp (Mab 1: 9, Mab 2: 18, Mab 3: 32). For the intact IgG 1 antibodies, there was also a change in the protein valence when 100 mM NaCl was added to the buffer. For Mab 1, the protein valence decreased from 5.4 to 4.61 when NaCl was added while the protein valence for Mab 2 and Mab 3 increased in the presence of NaCl from 8.9 to 9.77 and 11.38 to 13.04 respectively. As with the F(ab')₂ fragments, the calculated valence for the intact protein was lower than the expected charge based on the amino acid sequence as calculated by Sednterp (Mab 1: 22, Mab 2: 28, Mab 3: 42). Finally, the protein valence was determined for the three intact

Figure 3.38: Capillary Electrophoresis Analysis of the IgG Antibody F(ab')₂ Fragments

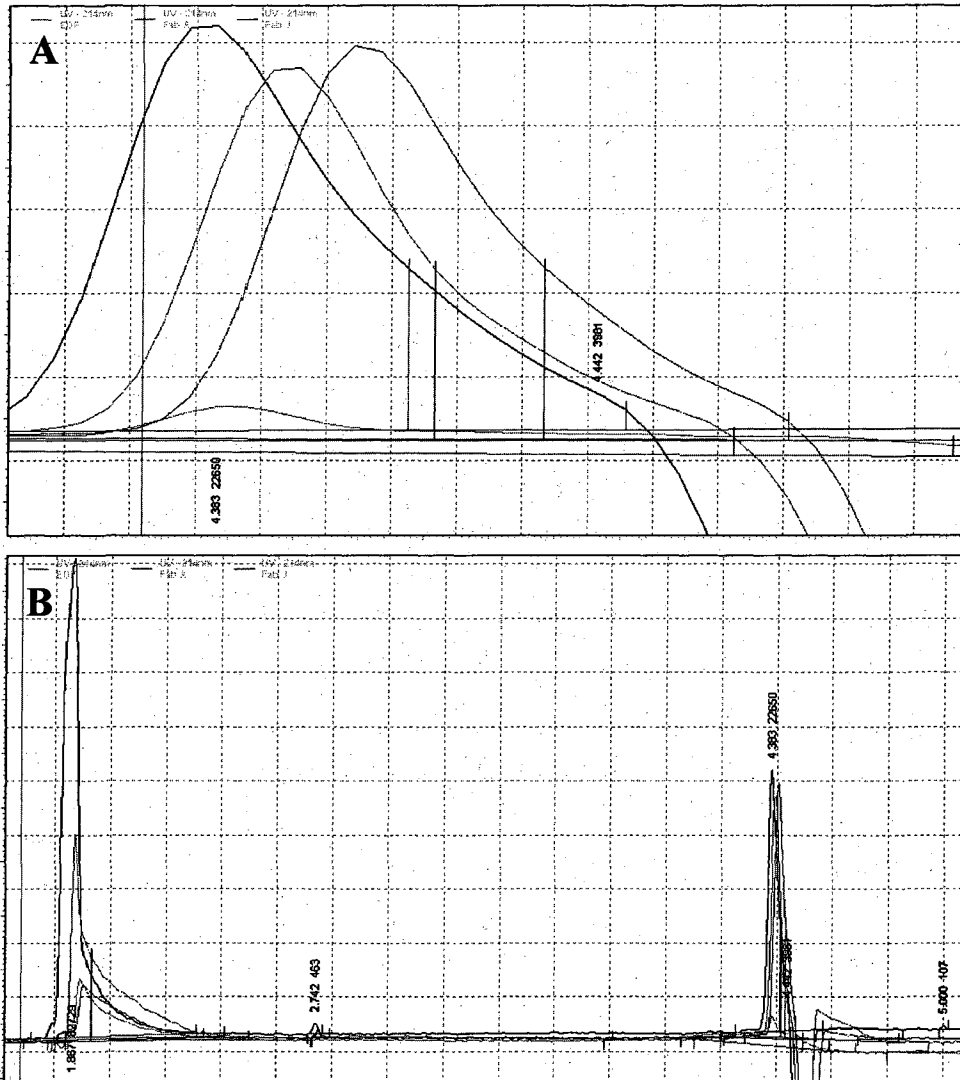


Figure 3.38: The digested F(ab')₂ fragments were analyzed by CE in a buffer containing 100 mM MES, pH 6 (A) and 100 mM MES, 100 mM NaCl, pH 6 (B). The sample concentrations were 0.569 mg/mL (Mab 1), 0.631 mg/mL (Mab 2) and 0.781 (Mab 3) and were run along with an EOF marker with the elution profile monitored at 214 nm. The run voltage for run A was 30 kV while the voltage for run B was 10 kV. The elution positions for run A were EOF: 4.388; Mab 1: 4.383; Mab 2: 4.396; Mab 3: 4.404, while the elution positions for run B were EOF: 22.587; Mab 1: 23.096; Mab 2: 24.621; Mab 3: 26.163.

Table 3.3: Capillary Electrophoresis Results of Intact IgG 1 Antibodies and F(ab')₂ Fragments

	Molecular Weight (Daltons)	Hydrodynamic Radius	Calculated Charge (based on AA seq)	Z
Mab 1 F(ab') ₂	89,637	4.6	9	-0.02
Mab 1 F(ab') ₂ + NaCl				0.22
Mab 1	142,778	5.1	22	2.07
Mab 1 + Urea				2.32
Mab 1 + NaCl				0.83
Mab 1 + NaCl + Urea				0.84
Mab 2 F(ab') ₂	92,347	4.6	18	0.04
Mab 2 F(ab') ₂ + NaCl				1.19
Mab 2	145,838	5.1	28	3.41
Mab 2 + Urea				3.68
Mab 2 + NaCl				1.76
Mab 2 + NaCl + Urea				1.76
Mab 3 F(ab') ₂	92,583	4.7	32	0.08
Mab 3 F(ab') ₂ + NaCl				1.79
Mab 3	143,900	5.1	42	4.36
Mab 3 + Urea				4.61
Mab 3 + NaCl				2.35
Mab 3 + NaCl + Urea				2.34

Table 3.3: The results of capillary electrophoresis for Mab 1, Mab 2 and Mab 3 (fragments and whole IgG 1) in two buffers: Buffer A contained 100 mM MES buffer, 100 mM NaCl, pH 6. Buffer B contained 100 mM MES buffer, 10 mM NaCl, pH 6. Additionally, 0.1 mM urea was also added into the two buffers.

IgG 1 antibodies in a buffer containing 100 mM MES, 0.1 mM urea, pH 6 and 100 mM MES, 100 mM NaCl, 0.1 mM urea pH 6. The results of Mab 1 show that when urea was added, there was a slight increase in the protein valence, from 5.4 to 6.05, in the buffer without NaCl and 4.61 to 4.66, in the buffer containing 100 mM NaCl. The results for Mab 2 show that when urea was added there was also a slight increase in the protein valence, from 8.9 to 9.6, in the buffer without NaCl, but no appreciable change in the protein valence of 9.77 in the buffer containing 100 mM NaCl. Lastly, for Mab 3, the results show that when urea was added there also was an insignificant increase in the protein valence, from 11.38 to 12.03, in the buffer without NaCl, but there was a slight decrease in the protein valence, from 13.04 to 12.99, in the buffer containing 100 mM NaCl.

The effects on the protein valence for the three antibodies upon the addition of urea was somewhat expected due to the changes observed in the overall self-association of Mab 1 in Table 3.2 and the change in viscosity as seen in Figure 3.36. These results suggest that if urea can increase the overall charge on the IgG 1 antibody, the results may lead to an increase in the overall charge-charge repulsion effects and could then alter the observed protein opalescence phenomenon.

CHAPTER VI

DISCUSSION

Electrostatic Forces Driving Protein Aggregation

In order to properly discuss protein aggregation, and specifically antibody aggregation, it is important to first define and then to understand the fundamental forces that drive these noncovalent, relatively weak intermolecular interactions. Intermolecular attractions are attractions between one molecule and a neighboring molecule¹. These interactions take place as molecules approach each other with the strength of the interactions varying with powers of the inverse of the distance. Each individually is very weak, but all of these intermolecular interactions form networks whose energies are additive and thus can make a significant contribution to binding when they are summed over a molecule. These weak interactions are all essentially electrostatic in origin and consist of point charges and permanent dipoles and non-polar, short-range interactions encompassing van der Waals interactions and hydrophobic effects. Hydrogen bonds, whose collective energy is considerably higher than most other noncovalent bonds, are another important bond interaction between a hydrogen atom covalently bonded to an

¹ The forces of attraction which hold an individual molecule together (for example, the covalent bonds) are known as *intramolecular* attractions.

electronegative atom and an adjacent electronegative acceptor group². A list of these electrostatic forces is summarized in **Figure 4.1**. In addition to contributing to protein aggregation, it is also important to mention that these interactions are critical in biological systems as they are responsible for all molecular recognition and for determining and maintaining the three-dimensional structure of proteins.

The most fundamental electrostatic interaction occurs between molecules which each contain a net electrostatic charge. The energy of this polar interaction is described by Coulomb's law as proportional to the product of the two charges divided by the dielectric constant of the medium and the distance between them. If the two charges are of opposite sign, the energy decreases as the molecules approach each other and is a favorable interaction. If the charges are of the same sign, it is a repulsive effect and there is an unfavorable interaction. As the interaction energy varies inversely with only the first power of the distance, it is effective over relatively large distances.

The next fundamental electrostatic interaction is the dipole which occurs between molecules that may not contain a net electrostatic charge but do have variations in their net charge densities. Dipoles interact with point charges and other dipoles (and more complex charge separations) with the orientation of each interaction determined by the relative charge densities on each group. The energy of these polar interactions can be determined by considering the individual charges of each molecule and calculating the coulombic interactions among all of them. Dipole interactions are generally weaker than

² The hydrogen bond is unique from other noncovalent interactions because the dependence of the bonds energy on distance is fixed.

Figure 4.1: Weak Forces Between Molecules

Type of Interaction	Model	Example	Dependence of Energy on Distance
(a) Charge-charge Longest-range force; nondirectional		Na^+ Cl^-	$1/r$
(b) Charge-dipole Depends on orientation of dipole		Na^+ H_2O	$1/r^2$
(c) Dipole-dipole Depends on mutual orientation of dipoles		C_6H_6 C_6H_6	$1/r^3$
(d) Charge-induced dipole Depends on polarizability of molecule in which dipole is induced		Na^+ C_6H_6	$1/r^4$
(e) Dipole-induced dipole Depends on polarizability of molecule in which dipole is induced		H_2O C_6H_6	$1/r^5$
(f) Dispersion Involves mutual synchronization of fluctuating charges		C_6H_6 C_6H_6	$1/r^6$
(g) van der Waals repulsion Occurs when outer electron orbitals overlap			$1/r^{12}$
(h) Hydrogen bond Charge attraction + partial covalent bond		$\text{N}-\text{H} \cdots \text{O}-\text{C}$ Donor Acceptor Hydrogen bond length	Length of bond fixed

From Mathews and van Holde: Biochemistry 2nd Ed. © The Benjamin/Cummings Publishing Company, Inc.

Figure 4.1: The noncovalent interactions that occur with molecules and ions are listed. All of these interactions are fundamentally electrostatic in nature and therefore depend on the forces that electric charges exert on one another.

point charge interactions because both attractions and repulsions occur between the two separated charges of each of the dipoles. Due to this combination of attraction and repulsion, the energy of interactions depend inversely on the second to third power of the distance between interacting molecules when they are in a fixed orientation and on the sixth power when they are free to rotate in response to the interaction (Creighton, 1993). Consequently, the electrostatic interactions between dipoles fall off much more rapidly as the distance between them increases as compared to point charge interactions.

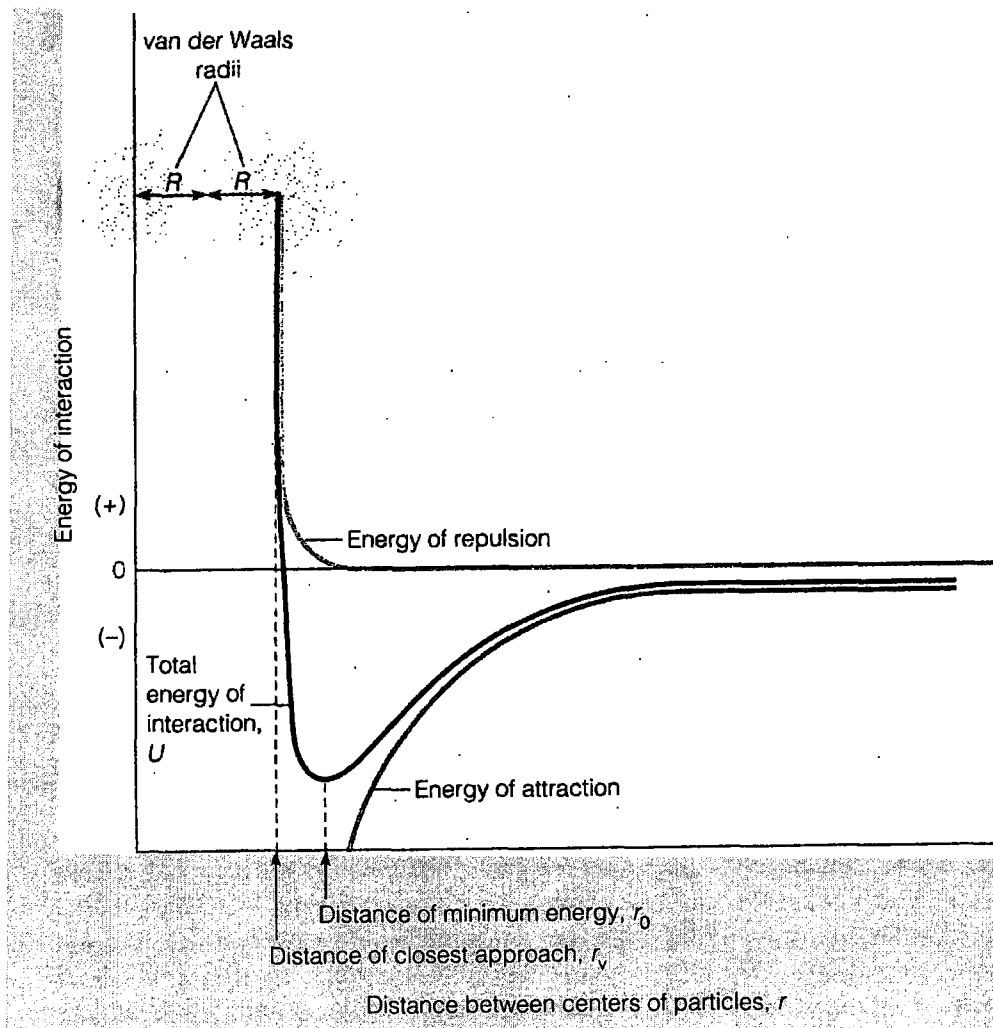
When molecules do not contain a point charge or a dipole, the resulting interactions that occur are known as van der Waals interactions. They arise as a result of an induced polarization effect on the molecule and can consist of three additional types of interactions; those between two permanent dipoles (as previously discussed), a permanent dipole and induced dipole and two dipoles of stochastic origin (also known as dispersion forces). These ubiquitous non-polar interactions are close range and weak as the energy of interactions depend inversely on the sixth power of the distance between interacting molecules.

The most unique and perhaps most import of the noncovalent bonds in biochemistry is the hydrogen bond. It is important because the structure and properties of many biological molecules, and of water, are determined by the strength and directionality of this bond. Although the energy of the individual hydrogen bond is weak, the energy of a network of hydrogen bonds is considerably higher than that of most other noncovalent bonds (Mathews and van Holde, 1996). The main component of the

hydrogen bond is an electrostatic interaction which occurs between the dipole of a covalently bonded hydrogen atom, in which the hydrogen atom has a partial positive charge, and a partial negative charge on another electronegative atom (Creighton, 1993). Unlike the previously described electrostatic interactions, the energy of the hydrogen bond is defined as the center-center distance between the donor and acceptor atoms and varies with distance as $1/r^4$ (Mathews and van Holde, 1996). Also, unlike other noncovalent bonds, hydrogen bonds are highly directional where the bond tends to point directly at the acceptor electron pair. This directionality of the hydrogen bond is important to maintain an organized, regular biochemical structure in proteins and large molecules (Mathews and van Holde, 1996).

In addition to the electrostatic interactions that were described, it is important to note that there are also short range repulsions that eventually take place as molecules approach each other. As molecules come near enough so that their non-bonding electron orbitals overlap, the repulsion increases enormously because the electrons on the different molecules cannot occupy the same part of space at the same time as another molecule as stated by the Pauli Exclusion Principle. This repulsive energy is often said to increase with the inverse of the 12th power of the distance between the centers of the two atoms (Creighton, 1993). Because the repulsive energies rise so sharply, it is then possible to describe molecules as having defined dimensions and occupying volumes that are not able to be occupied by other molecules (Creighton, 1993). Individual molecules are typically defined as spheres and the impenetrable volumes they occupy are known as van der Waals radii. A visual depiction of this principle is illustrated in **Figure 4.2**.

Figure 4.2: Noncovalent Interaction Energy Between two Approaching Molecules



From Mathews and van Holde: Biochemistry 2nd Ed. © The Benjamin/Cummings Publishing Company, Inc.

Figure 4.2: The interaction energy between two approaching molecules is listed as a function of distance from their centers, r . The sum of the energy of attraction and the energy of repulsion is seen as the total energy of interaction, U . As the particles approach one another, the energy of attraction increases along with the energy of repulsion, however, this occurs at different rates. The result is an overall energy of interaction that is first dominated by long range electrostatic interactions until the distances approach the van der Waals radii where the energy of repulsion increases rapidly.

When attempting to lower electrostatic interactions between proteins, and the subsequent aggregation states that can be formed, it is necessary to alter the free energy of association. It has been shown that electrostatic shielding is increased by increasing the ionic strength of the buffer system, or by decreasing the cation size (Coleman, 1999). For protein oligomerization involving “like” molecules, increasing the ionic strength can drive dimerization (and higher order oligomerization) as it may mask the charge-charge repulsion (the molecules repel since they have the same sign charge). On the other hand, lowering the ionic strength of a buffer will decrease the dimerization caused by protein self-association. For protein oligomerization involving charge-dipole and dipole-dipole interactions (and other charge related forces), increasing the ionic strength will generally decrease the strength of association by masking the favorable electrostatic interactions. Any effects of the ionic strength involving hydrophobic interactions between proteins tend to be indirect (e.g. a salt-induced change in structure that either exposes or hides a hydrophobic patch) as water preferentially excludes any non-polar groups. Because hydrophobic interactions are often not very strong, and are also energetically unfavorable due to the loss of entropy, low concentrations of an amphiphile (such as Tween) can be utilized to minimize the degree of interaction.

The unique self-association of Mab 1 has been examined in a variety of solvent conditions and the results compared with two other homologous IgG 1 antibodies (Mab 2 and Mab 3). The self-association of Mab 1 resulted in an alteration of the overall appearance of the protein solution and was described as being visually opalescent. The degree of self-association was as a direct result of the ionic strength of the buffer solution and the relative position of the buffer’s anions and cations on the Hoffmeister series.

Furthermore, the addition of Tween to the buffer system did not result in any changes in the visual appearance of the Mab 1 solution as measured by the EP standards. The resulting opalescence of the Mab 1 antibody was therefore satisfactorily described as being electrostatic in origin through a combination of charge-dipole (minor) and dipole-dipole (predominant) interaction, ultimately consisting of a non-mass-action driven self-association, which is freely reversible, involving mainly the CDR portion of the Fab region.

Comparability of Mab 1, 2 and 3

IgG 1 monoclonal antibodies are capable of extremely prodigious physiological diversity while maintaining structures which are virtually identical. The common structural features of an intact IgG 1 antibody include a Y-shaped molecular structure composed of two "Heavy" and two "Light" chains. The base of the molecule is known as the Fc region while the two arms of the molecule are known as the Fab region. The Fab region consists of several domains including the V_L , C_L , V_H and C_{H1} domains, while the Fc region contains two copies each of the C_{H2} and C_{H3} domains. All of these domains consist of about 100 residues, are homologous in their primary structure and are independently folding structural units.

The region of the IgG 1 which is involved in the specific recognition of antigens is located at the tips of the two Fab arms and is referred to as the complementarity determining regions or CDRs. Different binding sites are generated with different amino acid side chains in this region which consist of three irregular loops between the β -strands of both the Light and Heavy chains. While these six CDR loops are involved in the

complex interaction with the antigen, it is generally recognized that the Heavy chain CDR provides the majority of binding specificity and energy. So based on the amino acid differences that occur in the CDR region, it is important to know how structurally comparable are the three IgG 1 monoclonal antibodies used in this study.

To assess the initial protein purity and overall comparability of Mab 1, 2 and 3, several characterization techniques were employed including SDS-PAGE, SEC-HPLC, CEX-HPLC, peptide mapping and oligosaccharide analysis. Due to the impurities that are formed during the CHO cellular expression system, and the fact that the newly purified antibodies were at an initial concentration of ~75 mg/mL, it was imperative to fully characterize the purity and the initial association state of the antibodies prior to any subsequent opalescence examination. Although this discussion will focus on the results of the Mab 1 purity characterization, it should be noted that all three of the IgG 1 antibodies in this study displayed similar results and therefore it was concluded that they were appropriate for further opalescence comparability studies.

SDS-PAGE: After the initial protein expression and purification, a gradient SDS-PAGE was performed utilizing broad range SDS-PAGE markers. The two major migrating species of Mab 1 in each of the reducing lanes of the gel were consistent with that of an antibody light chain (~25 kDa) and heavy chain (~48 kDa), and each of the five identically loaded lanes appear comparable to each other. As with the reducing gel, each of the five identically loaded lanes in the non-reducing gel appeared to be comparable to each other. The most prominent species on the gel is consistent with that of an IgG 1 monomer (~150 kDa) with minor bands appearing at ~140, ~120, ~90 and ~30 kDa. Although still uncharacterized, it is believed that these other minor bands, present in the

majority of all CHO expressed IgG 1 antibodies, are a combination of antibody fragments and other low Mw species as well as a small amount of de-amidated protein.

SEC-HPLC: Size exclusion chromatography was employed to assess the overall purity and comparability of the IgG 1 monoclonal antibodies in this study. As is evident in the results, the profile of the chromatogram indicates that the majority of the material (~98%) elutes as a single "monomer" peak for each of five purified Mab 1 samples analyzed. The small amount of low Mw and high Mw species seen, were also present in the Mab 2 and Mab 3 SEC chromatograms (data not shown). These results, along with the subtle run to run variations seen in Figure 3.2 are considered normal and indicate that the purity of the IgG 1 samples were comparable enough to allow for further opalescence characterization.

CEX-HPLC: The IgG 1 monoclonal antibodies in this study were also assessed by CEX-HPLC to determine the degree of basic and acidic species present after the final cHA purification step. As previously stated in the results section, the relatively small amount of basic and acidic species present in the chromatograms in Figure 3.3 is considered typical for this degree of purification. Also, the variations that occurred from each of the batches tested could be due, in part, to variations in the time required to complete each of the numerous purification steps or variations of the analysis technique itself. It should also be noted that similar results were seen during the CEX-HPLC analysis of Mab 2 and Mab 3.

The two final steps used to assess the protein purity of the three IgG 1 antibodies were achro-k peptide mapping and n-linked oligosaccharide analysis. The results of the peptide mapping for Mab 1 indicated that the amino acid composition of the antibody

was comparable for the three batches used in this characterization, in terms of peak presence and peak height. Measuring the glycosylation levels are important because all antibodies are glycosylated at conserved positions in their CDR regions, the presence of specific carbohydrate groups can be critical for antigen clearance functions, and for overall solubility. As the results indicated, the three Mab 1 samples did not appear to have identical glycoform levels. The IgG 1 tested in batch two does have a lower glycosylation level of the G0 glycoform and a higher level of the G1 glycoform when compared to the other two batches, but this difference is not typically considered significant (Wright, 1997). Overall, the three Mab 1 batches that were tested, as well as batches from Mab 2 and Mab 3, were comparable in terms of peak presence and percent of total area for each peak.

DIFFERENTIAL SCANNING CALORIMETRY: Thermal denaturation of Mab 1, Mab 2 and Mab 3 was studied by differential scanning calorimetry in 10 mM Histidine, pH 6 (Figure 3.27). The thermal profiles for each IgG 1 antibody shows three transitions which indicate the presence of at least three domains (or groups of domains) that exist under these conditions. These results are consistent with the known morphology of an IgG 1 antibody which consists of a C_{H1} domain in the Fab region and two domains (C_{H2} and C_{H3}) in the Fc region. Any differences in the thermograms seen between the three IgG 1 antibodies may be due to differences in the flexibility of hinge region for each (Vermeer, 2000). When the $F(ab')_2$ and Fc fragments were isolated from the pepsin digestion for Mab 1, the $F(ab')_2$ fragment showed two distinct thermal transitions at 66 °C and 77 °C and two distinct thermal transitions for the Fc fragment at 72 °C and 85 °C (Figure 3.30, pH 7.2). When the $F(ab')_2$ and Fc fragments were isolated

from the pepsin digestion for Mab 2, the F(ab')₂ fragment showed only one thermal transition at 77 °C and two distinct thermal transitions for the Fc fragment at 68 °C and 84 °C (data not shown). The pepsin digest of Mab 3 was not further characterized by DSC. The DSC results show that the thermal transitions of the fragments were comparable to the overall thermal transition profile of the intact IgG 1 for Mab 2 but not for Mab 1. The thermal transitions for the Mab 1 fragments did not match the overall thermal transition profile for the intact IgG 1 until characterized in the buffer containing 10 mM Histidine, 150 mM NaCl, pH 6 (Figure 3.28). The stability of the Fc region appeared to be altered by the NaCl as there was only one visible thermal transition when NaCl was not present and two distinct thermal transitions in the buffer containing 150 mM NaCl. Also, the results of the two thermal transitions for the Fab region of Mab 1 indicate that there is an independent folding domain present in Mab 1 that may not be present in the Fab region of Mab 2. This independent folding domain may also benefit from the enhanced flexibility of the hinge region (encompassing amino acids 216-231), as is typically seen in the IgG 1 subclass, and could lead to increased interaction between the two carboxy-terminal domains C_H2 and C_H3 in the Fc region. This interaction may slightly destabilize one of the folding domains of the Fc region and account for the apparent loss of the thermal transition when NaCl was not present. However, when NaCl is present, the initial independent folding domain of the Fc region reappears at 72 °C as a result of decreased interaction with the Fab region. This decreased Fab-Fc interaction may then facilitate the electrostatic interactions of the Fab region of Mab 1 that occur during the opalescence phenomenon.

The effects of pH on Mab 1 were also analyzed by differential scanning calorimetry at pH 7.2 and 4 on the intact antibody and the F(ab')₂ and Fc fragments. Although the samples were run in PBS-CMF (as previously described) the results showed that the stability of Mab 1 was significantly altered at pH 4. At pH 7.2, the thermogram of the intact Mab 1 was comparable to the thermogram seen in Figure 3.27. The thermograms of the F(ab')₂ and Fc fragments were also comparable to the thermogram in Figure 3.28, in the buffer containing 150 mM NaCl. This is understandable as PBS-CMF does contain a comparable NaCl concentration. However, at pH 4, there is a shift of the intact Mab 1 from four thermal transitions to only three distinct thermal transitions at 56 °C, 72 °C and 92 °C. The change in the number of thermal transitions of the intact Mab 1 is evident when the results of the F(ab')₂ and Fc fragments are examined. At pH 4, the F(ab')₂ fragment displays a distinct shift in the thermal profile from two thermal transitions (at 66 °C and 77 °C) to a single thermal transition at 72 °C while the Fc fragment shifts from 72 °C and 84 °C to 56 °C and 75 °C. The results indicate that there is a loss in the overall stability of Mab 1 at pH 4, indicating an overall loss of efficacy. In addition, the loss of the thermal transition in the F(ab')₂ fragment indicates that there is decreased flexibility which would be another indication of decreased efficacy. From these results it is inferred that pH and heat treatment influence the Mab 1 structure in different ways. Temperature induced denaturation initially affects the Fab region, with a thermal transition at 66 °C, whereas the first transition of the Fc domain is at 72 °C. However, at pH 4, the first (and only) thermal transition of F(ab')₂ is at 72 °C, while the first thermal transition of the Fc region shifts dramatically to 56 °C. These results clearly demonstrate that overall stability of the F(ab')₂ fragment is more sensitive to heat

treatment, while the overall stability of the Fc fragment is more sensitive to pH. The results also show that pH (and therefore charge) plays an important role in the aggregation mechanism following the unfolding of an IgG 1 antibody. The F(ab')₂ fragment appears to have lost a thermal transition at pH 4, indicating a significant change in the secondary structure. And while the two thermal transitions for the Fc fragment were lower at pH 4, maintaining the two thermal transitions may indicate that the resulting shift in the thermogram may be a result of a lesser change in the secondary structure. There is also an additional thermal transition at 92 °C for the intact Mab 1 at pH 4. While it has been shown that an IgG 1 is completely denatured at ~75 °C, a fraction of the secondary structure elements remain which may be stabilized at the lower pH (Vermeer, 2000). Overall, the DSC results indicate that the structure of the F(ab')₂ fragment of Mab 1 appears to be more flexible as is indicated by the two thermal transitions. Also, the structural stability is minimally altered with the addition of NaCl as compared to the F(ab')₂ fragment of Mab 2. These results would also indicate that the NaCl induced opalescence phenomenon of Mab 1 is completely reversible since there is little apparent change in the overall stability (and therefore the structure) with the addition of NaCl. These results are also supported by the results of the serial dilution study (Figure 3.20).

Mab 1 Self-Association is Electrostatically Driven

During the initial characterization of the forces driving the self-association of Mab 1, EP standards were used to assign the degree of opalescence after the addition of NaCl and Tween 80. Although subjective, the EP standards were used in Figure 3.8 (A)

to assign a value to the visual appearance of Mab 1 over a NaCl concentration range of 0 to 8 mM. However, it was evident that at the concentration tested (65 mg/mL), the EP value of Mab 1 (in 10 mM Histidine, pH6) was turbid even in the absence of NaCl. The EP values assigned to the opalescence of Mab 1 quickly climbed from a value of <III (at 0 mM NaCl) to a value that was well off the visual scale (>IV) at only 8 mM NaCl. This is a clear indication that the self-association of Mab 1 is, at least partly, influenced by electrostatic interactions as the addition of NaCl is able to mask the charge-charge repulsion. Also, the low concentration of NaCl required to mask the charge-charge repulsion is also an indication that the overall charge on Mab 1 is relatively low.

The EP standards were also used to assess the ability of Tween 80 to prevent the opalescence of the Mab 1 antibody in the absence of NaCl, at a concentration of 65 mg/mL in 10 mM Histidine, pH 6. It was clear from the results in Figure 3.8 (B), that Tween 80 had little or no effect on the prevention of the antibody opalescence throughout the concentrations of Tween 80, or the concentrations of Mab 1 tested. These results indicate that the Mab 1 self-association was not affected by the addition of Tween 80, suggesting that the predominant attractive forces driving opalescence are not hydrophobic (non-polar) in nature.

EP standards also were used to assign the degree of opalescence of Mab 1 at a concentration of 10 mg/mL and over a range of varying NaCl and pH conditions. From the results seen in Figure 3.9, it can be concluded that the antibody opalescence increased as the pH of the buffer approached that of the calculated isoelectric point (~7.8), across all NaCl concentrations. These results are consistent with a charge dependent aggregation, as the charge on the antibody at the isoelectric point would be theoretically

neutral. In addition, the antibody displayed less opalescence at pH 4 and pH 6 at NaCl concentrations of 0 and 2 mM. This is consistent with the antibody having a greater overall charge at a pH further away from the isoelectric point, leading to charge-charge repulsion. However, it also is observed that the effect of the pH on the antibody opalescence appears to be lost at NaCl concentrations ≥ 10 mM NaCl. These results indicate that the overall charge on the antibody is relatively low and the 10 mM NaCl can sufficiently and adequately mask the molecular charge. It should be noted that at pH 8, the sample immediately precipitated out of solution upon the addition of 150 mM NaCl. It was decided on the basis of these results, to conduct the remainder of the opalescence studies in a buffer containing 10 mM Histidine, pH 6. These conditions were chosen on the basis of published results showing that Histidine enhances the stability of humanized IgG 1 antibodies in both aqueous and solid forms over a pH range of 5.5 to 6.5 (Chen B, 2003).

Although the EP standards were initially useful for assigning opalescence values, it was concluded from the arbitrary and subjective nature of these early visual studies that a more quantitative method for assessing opalescence would be useful. To this end, the turbidity, as determined by the relative optical density of the protein solutions, was measured against purified water at OD₄₀₀. These OD₄₀₀ values were then compared to the OD₄₀₀ values obtained from the EP reference suspensions to allow proper categorization. Ultimately, the assignment of the degree of opalescence became less important as the focus of this work shifted from measuring the changes in the visual opalescent appearance of the antibodies under varying conditions, to exploring the fundamental basis for this phenomenon.

ELECTRO-SEPARATION: In order to fully characterize the phenomenon of antibody opalescence, it was initially deemed necessary to induce the opalescence in a controllable manner, and if possible, to fractionate and collect the subsequent species. The technique of electro-separation was devised after it was hypothesized that charge may be the predominant factor driving the opalescence phenomenon in antibodies (Whitesides, 2006). As previously described, the idea was to apply an electric field, to which the sample would be introduced, and then to monitor and collect any visually opalescent species that were formed for further characterization. Although the technique was not successful (in the opinion of this researcher) and the results were not used to any great extent, it did present some interesting findings that were worth considering. The results from Figure 3.16 (A) clearly show that in the presence of an electric field, and under the conditions tested³, Mab 1 migrated toward the cathode and produced an opalescent cloud whose protein concentration was ~5 X greater than the initial protein concentration of 10 mg/mL. Migration of Mab 1 towards the cathode means that it carries a net positive charge under these conditions. When the pH was measured at the ends of the sample chamber it appeared as though the protons in the buffer had moved against the electric field and were collecting near the anode. This migration of the protons toward the anode may be explained by the Donnan Equilibrium effect in which the charge of an “artificially concentrated”⁴ macro-ion is compensated for, in part, by a reduced concentration of “like charged” ions and an increase in the concentration of ions of opposite charge (Donnan, 1911). This explanation would also account for the severe

³ The sample was at a starting concentration of 10 mg/mL in a buffer containing 10 mM Histidine, pH 6. Although there was no NaCl added to the buffer, there were counter-ions present in solution due to previous filtration and titration steps.

⁴ In the complete explanation of the Donnan's Equilibrium phenomenon, the “artificial concentration” of the macro-ion is achieved through the use of a semi-permeable membrane.

imbalance of the ions discovered when measuring the conductivity at each end of the chamber. The drop in the conductivity to 0.185 mS/cm at the cathode, as compared to the measured conductivity at the anode of 0.86 mS/cm is consistent with the theory that the high protein concentration at the cathode reduced the number or mobility of the available anions in solution leading to a local minimally charged region where the concentration of ions and their overall mobility is highly reduced⁵. This region of high protein concentration then caused the migration of available ions toward the anode, independent of charge, leading to a phenomenon described by Faraday as the conductance per equivalent of electrolyte (Edsall, 1958). Simply stated, the loss of ions in the region of the cathode lowered the equivalent conductivity. In addition, the high protein concentration in the region of the cathode also led to an increase in the solution viscosity which would resist the movement of ions in the electric field and contribute to lower the conductivity (Edsall, 1958). This high protein concentration would also bind any available counter-ions in solution further, thus decreasing their overall mobility. When the same sample was run in a buffer containing 500 mM NaCl, but all other conditions being the same, the results were very different. Figure 3.16 (B) shows that the Mab 1 antibody produced an opalescent cloud that extended across the length of the channel. And unlike the previous results, the pH measured at each end of the channel reflect the expected migration pattern of ions in the buffer with the pH being more acidic (pH 3) at the cathode and basic (pH 8.5) at the anode. The measured conductivity also suggested that there was a balanced distribution of counter-ions in the electric field with a measured value of 44.9 mS/cm at the cathode and 46.2 mS/cm at the anode. Although

⁵ It is important to note that the electrical current has to be the same throughout the entire length of the device and therefore does not contribute to any localized alteration of the mobility.

these results were not initially understood, it appears as though the Mab 1 antibody had bound enough counter-ions to initialize the opalescence phenomenon and, due to the excess number of unbound ions in solution, the remaining ions migrated as expected in the electric field. Although any subsequent experimentation avoided the further utilization of this technique, it was fairly evident from the results that more emphasis had to be placed on the role of charge in the characterization of the antibody opalescence phenomenon.

SALT INDUCED OPALESCENCE STUDY: To better understand the role of salt in the induction of antibody opalescence, a series of experiments were performed to explore the protein-salt and protein-protein interactions in buffers containing various electrolytes and over a range of concentration. In general, it is understood that the effect of salt on the solubility of proteins is a result of favorable electrostatic interactions between the salt ions and the charged residues on the protein (Tanford, 1955). However, in the case of antibody opalescence, it appears as though certain protein-salt interactions are less favorable to protein solubility and more favorable to protein-protein interactions. These protein-protein interactions then appear to lead to a state of self association that resembles a liquid-liquid phase separation which manifested by an opalescent appearance (Muschol, 1997).

When describing protein solubility as a function of the salt ions in solution, it is also important to discuss the resulting charge on the molecule as a function of pH. Protein solubility is generally a strong function of pH and the solubility is a minimum at the isoelectric point of the protein as the net charge is zero (Tanford, 1955). However, in concentrated salt solutions, the electrostatic interactions between the proteins are

minimized and the subsequent protein-protein interaction does not depend on the net charge, and therefore, does not depend on pH (Curtis, 1998). In considering the pH dependence on protein-protein interaction, it is not immediately clear as to whether the short range electrostatic interactions are the driving force or whether the protein-salt interactions need to be modeled independently (Curtis, 1998). The dependence of protein solubility on the salt type has been described by the Hofmeister series, but this dependence cannot be explained fully by considering the effect of the salt ions alone. It is known that the salting out effectiveness is also due to the ability of the salt to either assist or disrupt the structure making ability of water (Collins, 2006). Therefore, to adequately predict protein solubility, both of these factors must be considered when deriving a model of the salt effect on protein solubility and opalescence.

In the results of the visual opalescence studies, a series of salts were used on Mab 1, in a buffer containing 10 mM Histidine, pH 6 at a protein concentration of 63 mg/mL. It is important to note that this concentration was chosen because it represents the typical storage concentration of Mab 1 after final purification⁶. The vials in Figure 3.17 (A) suggest that although all of the salts used in this study appear to produce an opalescent effect to some degree, including the control, NaCl produced the most opalescence after 1 hour at room temperature. While 100 mM Na₂HPO₄ and 100 mM CaCl₂ were specifically chosen as alternative salts to determine whether it was the sodium ion or chloride ion that had a greater effect on the antibody opalescence, the results were somewhat inconclusive. It is apparent from the results in Figure 3.17 (A) that Mab 1 will preferentially bind anions in solution, leading to opalescence formation. However, a

⁶ The Mab 1 antibody was obtained through an industrial collaboration where it is produced for use as a biological therapeutic.

more detailed understanding of the anions involved would be needed to explain why this was not observed when Mab 1 was exposed to Na_2HPO_4 and CaCl_2 .

One explanation as to why Na_2HPO_4 and CaCl_2 did not contribute to the opalescence as strongly as NaCl could be provided by the Hofmeister series. Although the exact mechanism of this effect is not known, it most likely depends on the interaction of the ions with the surrounding water molecules (Collins, 1997). High-lyotropic-series salts (kosmotropes) are higher up in the Hofmeister series and are thought to alter the relatively ordered structure of liquid water and subsequently lead to changes in its surface tension when present in the concentration range of 0.01 to 1 M (Hofmeister, 1888) (Creighton, 1993) (Curtis, 1998). Low-lyotropic-series salts (chaotropes) are thought to break the structure of the surrounding water molecules (relative to bulk water) as a result of the large size of the ion and its weak interaction with water (Curtis, 1998). The Hofmeister series for cations and anions are;

Lyotropic → Chaotropic

CATIONS: NH_4^+ > K^+ > Na^+ > Li^+ > Mg^+ > Ca^{2+} > guanidinium

ANIONS: SO_4^{2-} > HPO_4^{2-} > acetate > citrate > tartrate > Cl^- > NO_3^- > ClO_3^- > I^- > ClO_4^- > SCN^-

The effectiveness of cations and anions are usually independent and additive, with the anion having the larger effect (Creighton, 1993). It is generally accepted that the ions in the series which balance the two effects are Na^+ and Cl^- , so NaCl is considered to be neutral in this respect. Following this explanation, it can be theorized that for CaCl_2 , the Cl^- anion bound to the antibody, but was potentially offset by the highly chaotropic nature of the Ca^{2+} cation, leading to decreased opalescence. Consequently, with the

Na_2HPO_4 salt, the HPO_4^{2-} anion bound to the antibody and was not offset by the effects of the Na^+ cation. In the case of the Na_2HPO_4 salt, the HPO_4^{2-} anion may have had a less favorable electrostatic interaction to the antibody as compared to Cl^- , possibly due to its larger size altering the surface charge density, leading to the delay in opalescence and the eventual gel formation (Figure 3.17 B) (Tanford, 1955) (Collins, 2006).

A further examination to measure the degree of Mab 1 opalescence as a function of NaCl concentration was performed and the results presented in Figure 3.18. In the initial study (Figure 3.18 A) the seemingly linear increase in the apparent OD_{400} from 0 to 20 mM NaCl, while the concentration of Mab 1 remained at 30 mg/mL, strongly indicates the presence of a polydisperse, Mie scattering system (Nassau, 1983). In Figure 3.18 (B), the linear increase in the apparent OD_{400} did not appear to continue past 20 mM, and ultimately began to decrease after a NaCl concentration of 50 mM. Initially, the results were somewhat puzzling considering the results seen in the earlier NaCl induced opalescence studies, however, it was eventually realized that the Mab 1 antibody exposed to NaCl concentrations above 20 mM, formed two distinct phases at the top and bottom of the tube. Since the tubes were opaque in color, it was not initially evident that the top phase was clear and the bottom phase was highly opalescent. From the electro-separation studies, it is understood that the region of protein opalescence contains a higher overall concentration. It is for this reason that the OD_{400} appeared to drop for Mab 1 above 20 mM NaCl as the sample was removed for testing from the top of the tube. However, even with the inaccuracies of the initial NaCl opalescence study, it can clearly be seen from the comparative results with CaCl_2 that the opalescence of Mab 1 was driven to a much greater extent with NaCl. These conclusions are consistent with the position of

NaCl on the Hofmeister series where the overall effect of either Na^+ or Cl^- is not offset by their individual nature.

To further explore the phase differences of the NaCl driven opalescence of Mab 1, a study was performed under conditions similar to the previous experiment, except this time in clear 15 mL conical tubes, with Mab 2 as the control. The results seen in Figure 3.19 (A) clearly display the distinct phases of Mab 1 in 25 and 50 mM NaCl, and to a lesser extent, with the 100 mM NaCl. The tube containing Mab 1 in 150 mM NaCl formed a highly opalescent, homogenous phase that resembled a state of initial gel formation (Champagne, 2000). It can also be seen from Figure 3.19 (B) that the Mab 2 control remained clear throughout all of the NaCl concentrations.

Following the results of the electro-separation experiment, similar studies were then performed on the distinct phases formed in the Mab 1 NaCl induced opalescence experiment. Concentration, chloride ion content, conductivity and pH were measured for each phase (if applicable) and the results listed in Table 3.1. The results for Mab 1 in 0 mM NaCl were nearly as expected due to the fact that there was no apparent phase separation. While the results of the conductivity, pH and even the chloride ion content were expected, the concentration taken at the bottom of the conical tube was higher than expected from the initial 30 mg/mL starting concentration. An explanation is that this may be caused by the low concentration of chloride ions in solution from the initial titration of the Histidine buffer, driving the beginning of a slight phase separation. These results suggest that Mab 1 is very susceptible to opalescence formation even in the presence of very low NaCl concentrations. The same concentration, chloride ion content, conductivity and pH measurements taken for Mab 1 in 25, 50 and 100 mM NaCl show an

even more interesting trend. Although it was expected that the concentration and chloride ion content would be greater in the opalescent region at the bottom of the tube, it was not anticipated that the results of the conductivity and pH would closely mimic the trends seen in the electro-separation experiment. In all three cases, the conductivity was lower and the pH was slightly higher in the opalescent phase. These results were similar to the results encountered in the electro-separation experiment, even though there was no external electric field to drive the opalescence phenomenon. This suggests that although the external electric field greatly enhanced the rate of opalescence formation of Mab 1, it did not artificially induce the phase separation, or the resulting concentration of anions in the opalescent phase and protons in the non-opalescent (or clear) phase. It also appears evident that the conductivity of the Mab 1 solution was altered to a similar extent in the naturally occurring phase separation as it was in the electro-separation induced opalescence. The results of the Mab 1 sample at 150 mM NaCl were also similar to the results of the electro-separation experiment at 500 mM NaCl. There was no apparent phase separation but rather, a single homogenous and highly opalescent phase which appeared to be mimicking the turbidity produced at the early onset of thermally induced gel formation (Champagne, 2000).

In an attempt to compare the concentration and NaCl dependence of Mab 1, Mab 2 and Mab 3, the effective turbidity profile was measured for each using the apparent OD_{400} . The results seen in Figure 3.20 indicate that OD_{400} for Mab 2 and Mab 3 remained linear with an increase in concentration and in the presence of 0 and 50 mM NaCl. In general, a linear increase in the turbidity with an increase in concentration indicates that there is minimal protein-protein self assembly (Timasheff, 1986). In addition, a graph of

OD₄₀₀/concentration vs. concentration for Mab 2 and Mab 3 produced a straight line (data not shown). As a result, it can be concluded that increase in the apparent OD₄₀₀ for Mab 2 and Mab 3 can be attributed solely to the increase in concentrations of the individual solution components, where essentially all of the components exist in monomeric subunit form (Stockmayer, 1950) (Eckhardt, 1994) (Paliwal, 2005). The results of the apparent OD₄₀₀ for Mab 1 were clearly non-linear as compared to Mab 2 and Mab 3. It has been described by Berne that the non-linear measure of turbidity is a direct result of randomly oriented protein polymerization (Berne, 1974). Furthermore, it was described that a linear increase in the turbidity due to protein polymerization follows the Rayleigh-Gans approximation only if it satisfies four criteria. These criteria are (1) the assembled structure must have the geometry of rigid rods composed of optically isotropic monomeric subunits, (2) the rods must be randomly oriented in solution (thermodynamically ideal), (3) they must be monodisperse, and (4) their thickness must be small relative to the wavelength of light, and the length of the rod. Following these criteria, it can be concluded that the measured non-linearity of the apparent OD₄₀₀ for Mab 1 as a result of the increase in concentration, in a buffer containing 50 mM NaCl (and to a lesser extent in the buffer containing 0 mM NaCl) can be attributed to a cooperative self-association (thermodynamically non-ideal) that is not rod shaped and overall, non-linear. Also, because it has been shown that the degree of opalescence is dependent on the concentrations of chloride ions in contact with Mab 1, it stands to reason that the sample disrupted by continuous gentle mixing had a greater degree of non-linearity in the apparent OD₄₀₀ as compared to the undisturbed, phase separated sample measured from the bottom of the tube. It should also be noted that the Mab 1

sample in 50 mM NaCl that was continuously mixed, formed a homogeneous, highly viscous, highly opalescent phase at concentrations above ~30 mg/mL. Finally, the results also indicate that the non-linear self-association of Mab 1 is fully reversible as all of the apparent OD₄₀₀ measurements were performed as dilutions from a stock solution of 80 mg/mL for the phase separated sample and ~30 mg/mL for the continuously mixed sample.

NON-IDEALITY ANALYSIS: One of the few techniques capable of providing an experimental measure of weak protein-protein interactions or chemical potential differences between the solvent and the solute is the second virial coefficient. This technique was used to explore how the IgG 1 monoclonal antibodies deviated from ideal behavior with the addition of NaCl, in order to better interpret what type of electrostatic interaction was occurring. As previously stated, for protein oligomerization involving “like” molecules, increasing the ionic strength can drive dimerization (and higher order oligomerization) as it may mask the charge-charge repulsion (the molecules repel since they have the same sign charge). Simply stated, the measured second virial coefficient for this type of interaction would involve an initial net repulsive effect (or positive second virial coefficient) at low NaCl concentration and would be expected to decrease as NaCl was added. On the other hand, for protein oligomerization involving charge-dipole and dipole-dipole interactions (and other charge related forces), increasing the ionic strength will generally decrease the strength of association by masking the favorable electrostatic interactions. Again, simply stated, the measured second virial coefficient for this type of interaction would involve an initial net attractive effect (or negative second virial coefficient) at low NaCl concentration and would be expected to increase as NaCl was

added. The results of the non-ideality measured as a function of NaCl concentration is seen in Figure 3.31. Mab 1 has an initial negative second virial coefficient at 0 mM NaCl and appears to display a slight increase until 50 mM NaCl. This measured behavior would directly support protein oligomerization involving charge-dipole and dipole-dipole interactions. At 100 mM NaCl, there is a precipitous drop in the second virial coefficient. A description of this behavior has been given by Scatchard who has shown that salts bind to proteins and upon binding, lowers the net charge and the electric double-layer repulsion (Scatchard, 1950). Subsequently, this net attractive protein-protein interaction at higher salt concentrations can be attributed to a drop in the distance between molecules, resulting in more collisions and a lowering of the interaction energy. It should be noted that for protein solutions where the second virial coefficient is less than -8×10^{-4} mL \cdot mol/g², amorphous precipitation occurs because the protein-protein attractions are sufficiently strong that they do not allow for adequate time for molecules to orient themselves to form crystals before forming an amorphous agglomerate (Curtis, 1998). Mab 2 and Mab 3 both have an initial positive second virial coefficient at 0 mM NaCl and continue to have a positive second virial coefficient until reaching 150 mM NaCl. These results are consistent with there being an overall charge-charge repulsion rather than a charge-dipole or dipole-dipole interaction as seen with Mab 1.

Opalescence as a HMW Phase Separation

In the classical works of Willard Gibbs, a phase was described as any part of a system which is homogeneous in all respects. Alternatively stated, a phase is not necessarily a large region visually distinguishable from its neighbor (Tanford, 1961).

This discussion so far has largely presented the opalescence phenomenon as being confined to a single homogeneous liquid phase. However, the phenomenon is believed to be a result of a liquid-liquid phase separation in which the antibody is in equilibrium between two contiguous phases. This section describes the conventional methods employed to isolate and characterize each of the two phases.

In order to correctly describe antibody opalescence as a phase separation, it is important to first understand that the chemical potential of the Mab 1 monomer (along with each of the components of the system) must *individually* have the same value in every phase of the system. In addition, it is important to point out that this condition can apply only to the components and not to species which cannot be transferred independently from one phase to another (Tanford, 1961). Once an opalescent phase separation has occurred and the components have achieved chemical equilibrium (a state in which the free energy reaches a minimum value) the system can be studied in a variety of ways. As it is important to first isolate each phase prior to characterization, size exclusion chromatography was employed. Also, as antibody opalescence is an optical phenomenon, multi-angle light scattering was used for characterization after the SEC separation. However, size exclusion chromatography did not adequately allow for the isolation of each phase so batch multi-angle light scattering was employed along with a free solution separation technique known as field flow fractionation. Sedimentation velocity was used as an alternative free solution separation technique for separation and to have an orthogonal technique to FFF-MALS characterization. Finally, dynamic light scattering was employed in an attempt to characterize each of the phase components without employing a “conventional” method of separation.

SIZE EXCLUSION CHROMATOGRAPHY-MALS: The results of the SEC-MALS experiment measuring the effect of NaCl on the self association state of Mab 1 is seen in Figure 3.10. It is evident that at 10 mM Histidine, pH 6, the Mw distribution of the Mab 1 antibody (at ~57 minutes) consists of approximately 98% monomer with a second peak (at ~47 minutes) containing 2% dimer. A third peak (~32 minutes) was attributed to shedding of the column's silica matrix caused by pressure from the HPLC injection. Results for the Mab 2 and Mab 3 antibodies were consistent under all NaCl concentration tested by SEC-MALS. However, Mab 1 did differ from both Mab 2 and Mab 3 in that the pressure of the HPLC gradually increased after each injection, regardless of the initial NaCl concentration, ultimately limiting the total number of injections to ~25 before reaching the upper pressure limit of the SEC column. These results indicate that some of the Mab 1 antibody was retained on the guard column or the SEC column itself. It is important to note that although the Mab 1 antibody was initially in a buffer containing 10 mM Histidine, pH 6, the mobile phase of the SEC-MALS analysis was in a buffer containing 10 mM Na₂HPO₄, 100 mM NaCl, pH 7.15. This higher ionic strength mobile phase was used to limit non-specific interactions and to follow the protocol established for separations performed with this type of SEC column. Therefore the Mab 1 antibody was inadvertently exposed to a buffer containing 100 mM NaCl for the entire 75 minute HPLC separation regardless of the initial formulation/storage buffer condition. And although the % mass recovery calculated after each 100 ug injection was close to 100% (data not shown), the gradual pressure increase of the HPLC system clearly indicated that some material was retained on the column. The results also indicate that Mab 1 is more sensitive to NaCl induced aggregation than

Mab 2 and 3 and that the opalescent phase may consist of a high Mw species at a very low concentration. The results also indicate that a typical SEC-MALS analysis was not adequate to fully separate and characterize the effect of NaCl on the antibody opalescence phenomenon. Therefore, a “batch” characterization technique was explored to further analyze the opalescence phenomenon and the resulting HMW species in solution.

BATCH-MALS: The technique chosen to characterize the higher order associated species present in the Mab 1 sample was batch-MALS. This technique utilizes the MALS detector, the same as with the SEC-MALS technique, but does not employ SEC column to fractionate the sample. The Mab 1 samples are simply injected into the MALS instrument as a sample “plug” and weight averaged molecular weight (Mw) is determined (Wyatt, 1993).

The results of the Mab 1 sample in a buffer containing 10 mM Histidine buffer, pH 6, and over a concentration range of 0.1 to 1 mg/mL (Figure 3.11) show that the Mw calculated for each of the five concentrations is higher than that of an antibody monomer (~150 kDa) but less than that expected for a dimer (~300 kDa). Also, the Rg for each of the five concentrations examined was between 11 and 14 nm. These results are peculiar because, assuming a globular model, there should not be any angular dependence for an IgG 1 antibody with a radius of ~5.1 for a monomer and ~6.8 for a dimer, at the wavelength of light used (Wyatt, 1993). These results are consistent with there being a very small quantity of a HMW species in solution. The concentration of this additional species has to be very low given the observed angular dependence is small, and the measured Mw is not much greater than the monomer. The lack of any concentration

dependence (Figure 3.11) suggests that the aggregate is irreversible over the time scale of these experiments. These batch-MALS results are consistent with the previous observations that Mab 1 contains a small quantity of large, irreversible aggregate. Although the results of the batch-MALS were not shown for Mab 2 and Mab 3, there was no evidence of HMW species present in any of the conditions tested.

The results of the Mab 1 sample in a buffer containing 10 mM Histidine buffer, 150 mM NaCl, pH 6, and over a concentration range of 0.1 to 1 mg/mL are seen in Figure 3.12. As with the previous analysis, these results show that the M_w calculated for each of the five concentrations is higher than that of an antibody monomer but less than that expected for an antibody dimer. However, unlike the previous analysis the resulting R_g for each of the five concentrations examined was significantly higher, between 50 and 64 nm. These results can also be interpreted as there may be an additional HMW species in solution but the concentration of this additional species may be slightly higher due to the increased effect on the final angular dependence of the light scattering. In theory, the HMW species formed in the low ionic strength buffer may have a similar R_g but these species did not influence the overall results as strongly due to their lower concentration and the sensitivity of the technique. As with the previous analysis, there does not appear to be any concentration dependence on the formation of the HMW species over the concentrations examined as the R_g and M_w do not change with an increase in concentration, and the resulting M_w is consistent with that expected of an antibody monomer with a small amount of dimer present. This apparent lack of very large aggregates at the concentrations tested indicate that low order associations are not significant contributors to the opalescence and that there is a higher order, possibly more

cooperative process. Overall, it can be concluded that the HMW material measured by batch-MALS is irreversible over the time scale of these measurements, the M_w does not change with an increase in the ionic strength and the R_g appears to increase with the addition of NaCl. Unfortunately, due to the sensitivity of this technique and the lack of resolution, it is impossible to quantify the HMW material or to assign a conformation. Therefore a free solution separation technique was employed in an attempt to quantify the HMW material present in solution.

FIELD FLOW FRACTIONATION-MALS: Previous analysis of the higher order associated Mab 1 antibody species was limited due to the potential interaction with the matrix of the SEC column or the lack of resolution in the batch-MALS technique. Field flow fractionation was therefore employed along with MALS to examine the apparent HMW material formed by Mab 1 in the presence of NaCl, in the absence of any “stationary phase”. Figure 3.13 shows the results of the separation of Mab 1 in a mobile phase containing 10 mM Histidine, 100 mM NaCl, pH 6 with a 50 ug injection. The results indicate that in addition to the antibody monomer peak, there is a very broad peak consisting of HMW material (10^6 to over 10^8 Daltons) with a large R_g (20 to 200 nm) and that the concentration of the HMW material was almost non-existent as compared with that of the monomer peak. Due to the resolution of the field flow fractionation, the HMW species that were initially discovered using batch-MALS, were able to be separated from the antibody monomer peak and subsequently characterized. These results indicate that the HMW species that are formed are somewhat discrete in size as the results were reproducible through several injections. In addition, the results also support the theory that antibody opalescence is a high order process that can involve a

very small amount of the total protein concentration. When a similar study was performed for Mab 2 and Mab 3, the elution profile consisted only of the monomer/dimer peaks with no HMW material present.

SEDIMENTATION VELOCITY STUDIES: Sedimentation velocity analysis was performed on the Mab 1 antibody in order to examine the concentration or NaCl dependence. As an orthogonal technique to FFF-MALS, sedimentation velocity does not utilize a “stationary phase” and therefore would not limit the characterization to molecules that would be compatible to the specific matrix utilized, as with size exclusion chromatography. The Mab 1 antibody was analyzed at three concentrations (0.1, 0.5 and 1mg/mL) in a buffer containing 10 mM Histidine, pH 6, ± 150 mM NaCl. These concentrations were chosen to span the linear range of the absorption optics in the XL-A ultracentrifuge and the NaCl concentrations were chosen to closely mimic the effects seen in the FFF-MALS analysis. The results in Figure 3.14 (0 mM NaCl) and Figure 3.15 (150 mM NaCl) both show that the majority of the species present in solution had a Mw consistent with that of an antibody monomer. Also, throughout all of the conditions tested, the only other species present in solution had a Mw that was consistent with that of a dimer and was less than 1% of the total peak area. Although the upper concentration range was limited with this technique, the results appeared to indicate that the only species in solution besides the monomer was a dimer, and that the percent of the dimer did not change with an increase in concentration or the addition of NaCl. It should also be noted that there was nearly 100% mass recovery based on the total peak area calculated after each run. Similar results were seen in all of the sedimentation velocity runs performed on Mab 2 and Mab 3 under the same conditions. Again, these results are

consistent with the batch-MALS technique that the antibody opalescence phenomenon consists of a higher order, possibly cooperative process.

DYNAMIC LIGHT SCATTERING: Dynamic light scattering was employed to study the free solution, association state of the antibodies when NaCl is added. As a result, the polydispersity of each measured association state was calculated and quantified as a function of peak area, and the molecular weight was determined for each as a function of the Mw to Rh model for a globular association. The results for Mab 1 are seen in Figure 3.21 and indicate that the association state is highly dependent on the NaCl concentration. In the buffer containing 10 mM Histidine, pH 6, 0 mM NaCl, Mab 1 appears to consist of nearly 100% monomer as indicated by the Mw determination of 147 KDa and the low polydispersity (as seen by the width of the histogram peak). There is also an additional peak in the histogram but due to the low concentration (less than 0.1%) the software algorithm identified this peak as negligible. In the buffer containing 10 mM Histidine, pH 6 with 100 mM NaCl, it can clearly be seen that Mab 1 shifts from a purely monodisperse, monomer state, to that of polydisperse, largely monomer-dimer state (~95.8%). This monomer-dimer state is indicated by the resulting Mw determination of 229 KDa, which is a weighted average of the monomer Mw (~147 KDa) and the dimer Mw (294 KDa). It is difficult to determine the percentage of monomer and dimer from these results, however, since the final Mw determination is a weighted average, and the Mw of 229 KDa is roughly between the two association states, it can be concluded that there is likely less than 50% dimerization. There are also two other polydisperse, higher order associated states in solution at a Mw of $\sim 1.6 \times 10^7$ KDa (0.2%) and 0.1×10^{12} KDa (4.0%) which may correspond to those species first identified by the batch-MALS results.

When dynamic light scattering was used to measure the NaCl dependence of Mab 2 and Mab 3, the results indicate that both antibodies maintained a relatively monodisperse, monomeric association state (Figure 3.22 and 3.23). There was a small degree of polydispersity associated with the Mab 3 monomer in the buffer containing 10 mM Histidine, 100 mM NaCl, pH 6, however, the Mw of 141 KDa closely matched the monomer Mw of 131 KDa in the buffer containing no NaCl, indicating a relatively small degree of any higher order association. It is important to note that there was an additional peak seen in some of the histograms but as described for the Mab 1 results, the software identified the concentration of the peaks as negligible.

Dynamic light scattering also was used to determine the temperature dependence of Mab 1 association as a function of NaCl concentration. The results in Figure 3.24 indicate that at each of the concentration tested, the addition of 150 mM NaCl lowered the apparent thermal stability of the antibody by ~ 5 °C as indicated by an increase in the Rh. For both concentrations, there was also a decrease in the apparent Rh with an increase in temperature, by approximately 2 nm. It is important to note that the Rh measurements compared in this dynamic light scattering analysis were systematically higher than the 5.1 nm expected for that of a monomeric IgG 1 antibody using a globular Mw to radius model. This can be explained by the fact that the solvent viscosity was corrected for based on the temperature dependence but was not corrected for due to changes in the ionic strength⁷ and protein concentration. As previously described, the results of the temperature dependence of Mab 1 as a function of NaCl concentration can be explained as an apparent lowering of the overall free energy of the system that

⁷ It has been shown that the extent of expansion of Rg and Rh for proteins is inversely proportional to the ionic strength of the buffer (Tanford, 1955).

accompanies the mixing of a solution from its components in their pure state (Tanford, 1961). These theories of the transfer of free energies were also described in detail by Timasheff's preferential interaction model that provides a thermodynamic treatment of protein stability as a function of solvent-solute interactions (Timasheff, 1992). However, since the effect of NaCl on the protein stability as a function of solvent-solute interaction is considered to be neutral, it can be theorized that the overall lowering of the free energy of the system can be attributed to the formation of components other than that of the "pure" monomer state.

Mechanism of HMW Phase Separation

To better understand the association state and mechanism of the antibody opalescence phenomenon, a series of non-conventional techniques were utilized. While attempts were made to disrupt the antibody opalescence and to explore possible structural changes in the antibody monomer through the addition of NaCl, it was the direct measure of the protein charge by capillary electrophoresis that provided the most fundamental insight. The measurement of the antibody valence provided a system property that allowed for a direct correlation between charge and protein stability. It was this insight that also allowed a direct measure of the correlation between the solvent conditions and the onset of antibody opalescence.

THERMAL STABILITY: Differential Scanning Calorimetry (DSC) provides information on the thermal stability of a protein under different solvent conditions and in the case of multi-domain proteins such as antibodies, it has the additional advantage of providing information on the behavior of the individual domains. It has been shown that

there is a direct correlation between the stability of an antibody domain in solution and the relative thermal stability as obtained by DSC (Wen, 2007). Differential Scanning Calorimetry (DSC) was used to measure the thermal stability of Mab 1 and Mab 2 fragments as a function of NaCl concentration (Figure 3.29). The DSC scans for the F(ab')₂ fraction of Mab 1 indicated that there was little loss in the thermal stability from 0 to 150 mM NaCl. These results are consistent with there being a stable structural conformation of the F(ab')₂ fraction of Mab 1 even in the presence of 150 mM NaCl. It could be argued that the results for the thermal transition of the F(ab')₂ fractions are consistent with the proposed electrostatic model of a dipole-dipole or charge-dipole interaction within the Fab region of Mab 1. With the addition of NaCl, the electrostatic interactions would be lowered and there would be minimal change in the overall protein stability. The results of the thermal stability of the F(ab')₂ fraction of Mab 2 show a drop in the ΔT_m , indicating that there is a change in the structural stability with the addition of NaCl. These results for the thermal transition of the F(ab')₂ fractions are consistent with a loss in the electrostatic free energy in the presence of a high salt solution. Studies have shown that there is a considerable decrease in the electrostatic free energy if salt ions are allowed to penetrate into the interior of the protein (Tanford, 1955). This effect is greatly enhanced when the fixed charged of the protein are located in the interior as is the case with antibodies (Tanford, 1955). Also, in biological systems, the electrostatic free energy is supplemented by specific ion effects (Whitesides, 2006). Although these effects are incompletely understood, the data suggests that the IgG 1 antibodies specifically bind chloride ions and these interactions may affect the local dielectric constant of the protein further altering its temperature stability. The same studies were performed on the Fc

regions of Mab 1 and Mab 2 and the results show that there is an equivalent loss in the thermal stability with the addition of NaCl. These results were expected as there is a high degree of homology between the two Fc regions.

VISCOSITY AND STRUCTURAL ANALYSIS: The viscosity of Mab 1 was measured as a function of protein concentration, and then along with Mab 2 and Mab 3, measured as a function of NaCl concentration. Viscosity was utilized in the characterization of the antibody opalescence phenomenon due to its unique ability to quickly and accurately measure protein-protein interactions over a range of concentrations and solvent conditions. The viscosity and the apparent optical density (OD_{400}) of Mab 1 was determined over a concentration range of 1 to 60 mg/mL at 4 °C and 25 °C. The samples were prepared in a buffer containing 10 mM Histidine, 50 mM NaCl, pH 6 and the results of the viscosity measured in units of centipoise. The results show that the viscosity of Mab 1 is highly dependent on the protein concentration and increases non-linearly with increasing antibody concentration at both 4 and 25 °C (Figure 3.32 A). The apparent optical density (OD_{400}) of Mab 1 also increases in a non-linear fashion; however, the increase appears to be slightly faster at 4 °C vs. 25 °C. This indicates that Mab 1 under these conditions behaves as a non-Newtonian fluid. Since non-Newtonian fluids often contain several micro structural species that are made of large and elongated aggregates, rather than smaller uniform non-interacting monomers, this result suggests that Mab 1 may undergo self-association (Liu, 2005). However, the non-linearity in the viscosity is predominantly observed at higher protein concentrations suggesting that these micro-structural aggregates are also fully reversible and only form at higher protein concentrations. The results from the measured apparent optical density

also suggest that these micro-structural aggregates are temperature dependent, appearing to form more readily at decreased temperatures. This would indicate that the forces driving the temperature dependent aggregates are entropic rather than enthalpic in origin. The viscosity of Mab 1 is also dependent on the concentration of NaCl. Figure 3.33 shows the result of Mab 1, Mab 2 and Mab 3 at 5 mg/mL in a buffer containing 10 mM Histidine, pH 6 with 0, 50 and 100 mM NaCl. As the concentration of NaCl increased, the viscosity of each antibody appears to increase slightly, and in a non-linear fashion, with Mab 1 increasing the most. Mab 1 also appears to begin to level off at the higher NaCl concentrations. Additionally, NaCl does not appear to have a significant impact on the conformation of Mab 1. Structural characterization using near UV-CD and fluorescence (Figure 3.34) as well as FTIR (Figure 3.37), in the presence of 0 and 100 mM NaCl, indicate that Mab 1 has essentially the same conformation in solution, both at 4 °C and 20 °C⁸. These results suggest that electrostatic interactions play a major role in causing the increase in the viscosity of the Mab 1 solution. These results also suggest that with the addition of NaCl, the viscosity and the resulting opalescence of Mab 1 is as a result of higher order associations which are fully reversible at lower concentrations or through the removal of the NaCl.

CONGO RED: Congo red (CR) has been the subject of many studies due to its ability to bind amyloid fibrils and induce a characteristic shift in the maximal absorbance from ~490 to ~540 nm (Kim, 2003). Although it has not been fully elucidated, the binding mechanism has been proposed to be intercalation of the CR molecules between the antiparallel β -pleated sheets of amyloid fibrils or alignment of the CR molecules

⁸ Temperature dependence on the structure of Mab 1 in 0 and 100 mM NaCl was examined by FTIR alone.

along the fibril axis by electrostatic interactions (Kim, 2003). Because of these findings, and the theory that the possible mechanism of Mab 1 opalescence is as a result of higher order linear association, it was proposed that congo red might be used to support this mechanism of association. However, when congo red was introduced to Mab 1 at concentrations of 1 and 10 mg/mL, in a buffer containing 10 mM Histidine, pH 6 ± 50 mM NaCl, at room temperature and at 4 °C, the results were not initially clear. Even though the Mab 1 samples containing NaCl were visually opalescent, there was not a “red shift” in the absorbance spectra but rather a slight “blue shift” in the OD maximum (Figure 3.35). The observed blue shift would indicate that CR did not successfully bind to Mab 1 even in the presence of the antibody opalescence phenomenon. Initially, the conclusion was that there was not a red shift because of the lack of any fibril structure formation by Mab 1 with the addition of NaCl. However, this did not fully explain the blue shift in all of the Mab 1 buffers containing NaCl. Previous studies have shown that the structural features of CR strongly suggest that electrostatic interactions were primarily responsible for the binding of CR. Furthermore, it was speculated that the negatively charged sulfate groups on the CR were specifically important for binding to proteins (Heegaard, 2000). These insights led to the conclusion that CR was not able to bind to Mab 1 due to the lack of any specific fibril structure and possibly because any available binding sites would already be occupied by chloride ions or another Mab 1 antibody during the opalescence phenomenon. These results also suggest that there are site specific binding site(s) on Mab 1 as there is a red shift due to the binding of the CR when NaCl is not present.

UREA ANALYSIS: The ability of urea to alter the self-association characteristics of Mab 1 were examined over a range of NaCl and urea concentrations. Although the exact mechanism of protein interaction and denaturation by urea is unknown, it was theorized that since urea is a highly polar molecule, and has a dielectric increment of +2.7⁹, it could be used to disrupt the dipole-dipole self-interactions of Mab 1. In homogeneous environments, the energy of the electrostatic interaction (ΔE) between two molecules (A and B) is simply the product of two charges divided by the product of the distance between them (r_{AB}) and the dielectric constant (D):

$$\Delta E = \frac{Z_A Z_B \epsilon^2}{D r_{AB}}$$

where ϵ is the charge on the electron and $Z_{(A,B)}$ is the number of such charges on each atom. The results were measured by DLS and are seen in Table 3.2. The initial results were clear that high concentrations of urea (6000:1) could disrupt the self-association of Mab 1 caused by the addition of 100 mM NaCl. This was determined by the lower average molecular weight in peak 1 and the complete elimination of the high molecular weight material represented by peak 2 and peak 3. At lower urea concentrations (10:1), similar effects were initially seen but the average molecular weight of peak 1 did increase after 24 hours and there was a small amount of high molecular weight material that also had formed. When the urea concentration was lowered to 0.03 mM (1:1), the results indicated that the average molecular weight of peak 1 did not represent a "pure" monomer (similar to the results seen in the 10:1 urea concentration study) however, there was no high molecular weight material formed until after 24 hours. These results are consistent with the theory that there is a site specific protein-urea interaction and that

⁹ From: Cohn & Edsell, *Proteins, Amino Acids and Peptides*, 1943

there is probably more than one binding site on Mab 1 (as the average Mw of peak one was higher than a monomer, indicating some dimer formation). From the results, it is impossible to determine the number of possible binding sites that are available on Mab 1 but because of the well known dimeric structure of IgG 1 antibodies, it can be speculated that there should be two possible sites in the F(ab')₂ region which an electrostatic dipole interaction could occur. This multiple binding sites were apparent by the non-linearity of the OD₄₀₀ when measuring the dilution effect of Mab 1 in Figure 3.20. It is also evident from this study that a low concentration of urea (1:1) is sufficient to alter the free energy of association of Mab 1 by occupying at least one of the binding sites. It should be noted that the mean circulating concentration of urea found in the blood of normal individuals is typically 4 mM. This would indicate that in vivo, antibody self-association would be negligible for Mab 1, and potentially for other similarly behaved IgG 1 antibody therapeutics.

In addition to urea, arginine has also been shown to suppress protein aggregation and protein-protein or protein-surface interactions (Arakawa, 2007). While the mechanism of these effects have not yet been fully elucidated, it was theorized that arginine may also serve to disrupt the NaCl induced opalescence of Mab 1. One explanation for ability of arginine to disrupt the self-association of Mab 1 may be due to its high dielectric increment of +62¹⁰. The effects of urea and arginine on NaCl induced Mab 1 opalescence were measured by viscosity and dynamic light scattering (Figure 3.36). Without the addition of urea or arginine, Mab 1 opalescence was readily induced with the addition of 100 mM NaCl as is evident by the increase in HMW material measured by DLS and the increase in the solution viscosity from 1.2 to ~1.6 centipoise.

¹⁰ From: Cohn & Edsell, *Proteins, Amino Acids and Peptides*, 1943

As previously described, urea was successful in disrupting the antibody opalescence formed when Mab 1 is exposed to buffer containing NaCl as is evident by the loss of any HMW material measured by DLS and the slight lowering of the solution viscosity. The slight loss in viscosity with the addition of NaCl also fits the electrostatic model that Mab 1 interactions are both dipole-dipole and charge-dipole in nature. While urea binds to Mab 1 and blocks the majority of the dipole-dipole interactions, the remaining charge-dipole interactions are further masked with the addition of NaCl, resulting in a slightly lower solution viscosity. Similar effects on Mab 1 are seen with the addition of arginine. However, for the effects to occur, the concentration of arginine was 200 mM which is significantly higher than the 0.3 mM urea concentration. These results indicate that although arginine may disrupt the HMW material formed at the onset of the opalescence phenomenon, the interaction with the antibody is relatively weak and the interactions may be different from that of urea.

CAPILLARY ELECTROPHORESIS: In order to determine the net charge (Q) or valence (Z) on the three IgG1 antibodies, capillary electrophoresis (CE) was employed over a variety of buffer conditions. Understanding the net charge is important because it is a fundamental physical property that contributes to the proteins solubility, stability, and its ability to interact with other proteins (Chase, 2008). The net charge values are also important in the processes that lead to the separation and purification of proteins. In addition, the net charge also influences the electrophoretic mobility of proteins in solution, a fact which will be utilized when measuring the valence of the three antibodies by CE. It is important to note that a protein's valence is a system property and not a property of the molecule. It is for this reason that a direct measure of the actual protein

valence was necessary to make accurate inferences concerning the role of charge in a protein's behavior.

Both experimental and theoretical models suggest that the net charge on a protein can influence the rates of protein-protein association and enzymatic catalysis (Whitesides, 2006). Although not fully understood, it has also been suggested that there is a direct link between net charge and the second virial coefficient (A_2) (Neal, 1998). It is known empirically that if there is a net attractive force between proteins in solution and that if the value of the second virial coefficient is too negative, then proteins will aggregate and precipitate rather than crystallize. However, if the proteins have a net repulsion (a positive second virial coefficient) the solution is stable and crystallization does not occur (Neal, 1998) (Elcock, 2001) (Paliwal, 2005). Since it has been shown that the aggregation state for Mab 1 (and to a lesser extent Mab 2 and Mab 3) is dependent on NaCl, it was suggested that the valence may also be altered in the presence of NaCl, and therefore used as a predictive tool.

The results of the CE experiment are listed in Table 3.3 for the three antibodies in a variety of conditions. For each antibody, the charge was calculated based on the amino acid sequence (for the whole molecule and the $F(ab')_2$ fraction) and then compared to the measured valence. For the $F(ab')_2$ fraction of Mab 1, the valence was -0.05 in the buffer without NaCl and 1.14 when NaCl was present. These values represented a large discrepancy from the calculated charge of 9. Although further conclusions were difficult for the valence of the fractionated species, as the second virial coefficients were not measured, it should be noted that the changes in the valence were appreciably greater for Mab 2 (0.01 to 6.14) and Mab 3 (0.2 to 9.38) with the addition of NaCl. For the intact

Mab 1, the measured valence was 5.4 in the buffer without NaCl and 4.61 when NaCl was present. These values also represented a large discrepancy from the calculated charge of 22 for the intact antibody. It was therefore theorized that there may be a link between large deviations of the measured valence from the calculated charge and the protein's stability. To test this theory, both the intact Mab 2 and Mab 3 as well as the $F(ab')_2$ fractions were similarly tested. It was shown that these values also exhibited large deviations of the measured valence from the calculated charge. Subsequently it was theorized that IgG 1 antibodies may all exhibit an unequal charge distribution within the interior of the molecule in order to remain biologically relevant. Because of this, relative comparisons of the measured valence were then made between each of the three antibodies. Since Mab 2 and Mab 3 did not show strong NaCl dependence, the change in their measured valence in the presence of NaCl was compared to that of Mab 1. It was shown that while Mab 2 and Mab 3 showed an increase in their valence with the addition of NaCl, Mab 1 showed a decrease from 5.4 to 4.61. These results correspond well with the measured second virial coefficients for each in Figure 3.31. Correspondingly, in the presence of urea (which was shown to disrupt the aggregation state of Mab 1) there was an increase in the measured valence from 5.4 to 6.05 without NaCl present. When the same measurements were made with Mab 2 and Mab 3 with the addition of urea, the results showed a lower overall increase in valence for both. When the valence was measured in the presence of urea and NaCl, there was a slight increase of 4.61 to 4.66 for Mab 1, no increase for Mab 2 and a decrease from 13.04 to 12.99 for Mab 3. These results match the loss in the aggregation state for Mab 1 when measured by viscosity (Figure 3.36) and dynamic light scattering (Figure 3.36 and Table 3.2) in the presence of

urea. Corresponding viscosity and dynamic light scattering measurements were not performed for Mab 2 and Mab 3 due to the lack of NaCl dependence on the formation of HMW species as seen in Figure 3.22 (Mab 2) and Figure 3.23 (Mab 3). From the results, it was evident that under the conditions tested, there was good agreement between the measured valence and the measured second virial coefficient, viscosity and dynamic light scattering results for Mab 1. In addition, it should be stated that directly measuring the valence of an IgG 1 antibody is of particular importance as the measured valence does not correspond to the expected valence based on the amino acid composition.

Predicting Behavior of Antibodies to Phase Separate

When attempting to predict the behavior of antibody therapeutics to phase separate, it is essential to utilize techniques that directly measure first principle properties such as mass, charge, shape and size, optical properties and functional properties. In addition, each of the techniques must be capable of relating the measured value to a property of interest such as stability, solubility and ability to interact with other molecules. This study has utilized many techniques to measure the characteristics of phase separation of Mab 1, but only three techniques stand out as wholly predictive tools; differential scanning calorimetry, non-ideality and the direct measure of the protein valence by capillary electrophoresis.

The technique of differential scanning calorimetry was essential for determining the thermal stability for the three IgG 1 samples in different pH and buffer conditions. Understanding the effects of these various conditions on the thermal stability, and what trends they follow, for various antibody candidates will aid in formulation, development

of analytical methods, selection of process conditions and the investigation of incidents, such as the opalescence phenomenon, for these important therapeutics. DSC was an important tool in determining three important factors in the investigation of the opalescence phenomenon of Mab 1. The first was that the Fab region of Mab 1 had two distinct thermal transitions which were not NaCl dependent. Second, the Fab region in Mab 1 was stable in the presence of NaCl (unlike Mab 2 and Mab 3) which gave an insight into the potential reversibility of the opalescence phenomenon when NaCl was removed. The third was that NaCl appeared to alter the stability of the C_{H2} carboxy-terminal domain located near the hinge region on the Fc which led to the theory that this alteration may have increased the overall flexibility of the Fab region.

The electrostatic interactions between antibody therapeutics are often sufficiently weak that their study through the use of conventional structural techniques becomes problematic. Of the few techniques capable of providing experimental measures of weak protein-protein interactions, perhaps the most useful is the measure of the non-ideality or second virial coefficient. Throughout this study, measuring the second virial coefficient provided a predictive tool which was used to determine the NaCl and concentration dependence of the three antibodies. These measurements were also crucial in the determination the type of electrostatic interactions of Mab 1 that were responsible for the opalescence phenomenon. In addition, the second virial coefficients provided an insight as to the structural characteristics of the Mab 1 self-association. It has been shown that protein solutions with a second virial coefficient less than $-8 \times 10^{-4} \text{ mL-mol/g}^2$ will not have time to orient themselves but will form an amorphous agglomerate (Curtis, 1998). This phenomenon was readily observed with Mab 1 and the second virial coefficient

measurements allowed a good prediction of the antibody to form a clear liquid-liquid, liquid-solid or visually opalescent phase transition.

Of the three techniques used to predict the behavior of antibodies to phase separate, perhaps the antibody valence measurement by capillary electrophoresis proved to be the most sensitive. The most noticeable feature of the three antibodies, when measured by capillary electrophoresis, was the discrepancy between the measured valence and the calculated valence based on the amino acid sequence. Because of this discrepancy, it was necessary to make relative comparisons between the valence measured for Mab 1 and those measured for Mab 2 and Mab 3 when relating charge to solution behavior. Experimental evidence suggests that the extent of deviation of the measured valence from the calculated valence corresponds well with the measured second virial coefficients when determining an antibodies deviation from ideal behavior. Finally, a plot was constructed for each to compare the activation energy of approach for Mab 1 using the calculated valence (based on the AA sequence) and the measured valence by CE (**Figure 4.3**)¹¹. The plots depict the electrostatic interaction energy between two molecules as a function of distance and could be used to predict the energy of attraction depending on the measured valence of a molecule and the resulting influence from added excipients that may change the dielectric increment of the buffer. It is clearly evident from the plots that the activation energy of approach for Mab 1 at a predicted charge of 20 (Figure 4.3 A) is greater than that of Mab 1 at the actual measured valence of 5 (Figure 4.3 B). The decreased activation energy of approach for Mab 1, using the

¹¹ The program ElectroGraph was written by Dr. Thomas Laue and is available through BITC (www.BITC.unh.edu)

Figure 4.3: The Activation Energy of Approach for Mab 1

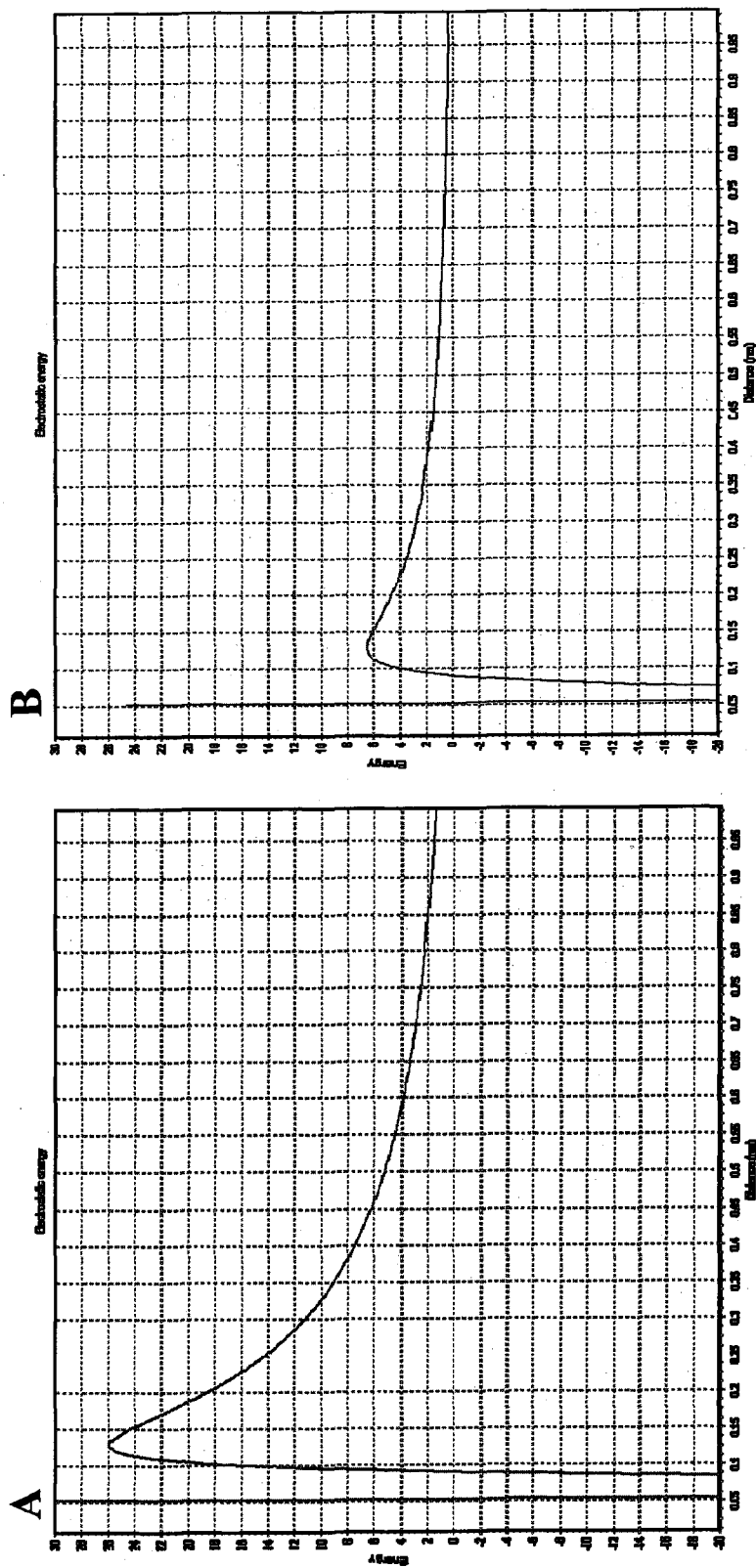


Figure 4.3: The activation energy of approach was theoretically determined for Mab 1 using the calculated valence of ~20 (based on the AA sequence) (A) and using the measured valence by CE of ~5 (B). The graphs depict the interaction energy between two molecules as a function of distance. As the energy values increase, the overall energy of interaction is unfavorable and as the energy values decrease, the overall energy of interaction becomes more favorable.

measured valence, indicates that as the distances between the two molecules decrease, there will be a greater likelihood of intermolecular protein interaction, as was observed. Although it is a relatively new technique, and there are few studies to corroborate these results, as more protein valence measurements are made, the relationship of charge to other physical properties such as solubility and stability will become more apparent.

Conclusion

The results of this study indicate that the opalescence phenomenon observed with Mab 1 is a result of a salt induced, non-mass-action driven self-association which is mainly entropic in origin. Although the opalescence phenomenon has been observed with the addition of other salts, including Na_2HPO_4 and CaCl_2 , it is driven primarily by the presence of NaCl in the buffer. This is thought to be due to the preferential binding of the Cl^- ions by Mab 1 without an excessively kosmotropic influence by the Na^+ ions. The resulting self-association of the Mab 1 antibody is thought to be electrostatic in origin and exists through a combination of long-range polar interactions such as charge-dipole (minor) and dipole-dipole (predominant)¹². The interactions appear to involve mainly the CDR portion of the Fab but may also exist through multiple binding sites throughout the Fab region. These intermolecular interactions appear to be facilitated through the enhanced flexibility of the independent folding domain present in the Fab

¹² It should be noted that the electrostatic free energy of this interaction involves other noncovalent interactions whose individual contributions may be weak, but they are additive and serve to stabilize the interaction through a significant contribution when summed over the antibody.

region of Mab 1. In addition, the flexibility of this Fab folding domain may also benefit from the NaCl induced destabilization of the C_{H2} carboxy-terminal domain located near the hinge region on the Fc. When the self-association occurs, it results in either a liquid-liquid or liquid-solid phase transition and can be clear or cloudy depending on the degree of non-ideality. When the measured second virial coefficient is $\geq -8 \times 10^{-4}$ mL-mol/g², the phase transition is clear indicating an ordered structure, however, when the second virial coefficient is $\leq -8 \times 10^{-4}$ mL-mol/g², the phase transition appears cloudy because the protein-protein interactions are sufficiently strong as they do not allow for adequate time to orient themselves. Although it is typically visually apparent, the resulting opalescence phenomenon appears to exist as only a small fraction of fairly discrete high molecular weight material when analyzed by FFF-MALS. The Mab 1 self-association also appears to be freely reversible upon the removal of NaCl which is thought to be due to the finding that the Fab region of Mab 1 is minimally destabilized with the addition of NaCl as shown by the DSC results. The NaCl induced self-association of Mab 1 also appears to be cooperative in nature as is indicated by the non-linearity of the OD₄₀₀ and viscosity data. Furthermore, the addition of 0.03 mM urea (1:1) is sufficient to disrupt the opalescence phenomenon of Mab 1, indicating that the interaction with urea is site specific and consists of a dipole-dipole interaction. It is important to note that the average circulating levels of urea in the serum of normal individuals is ~4 mM (MacKay, 1927). The urea study also supports the theory that there is more than one urea specific (dipole-dipole) binding site on Mab 1 as the average Mw of peak measured by dynamic light scattering was higher than that of a monomer, indicating some dimer formation. Finally, there was an appreciable discrepancy between the measured valence

by CE and the calculated valence based on the amino acid sequence. Although this discrepancy was seen with all three of the IgG 1 antibodies in the study, the extent of deviation from the calculated valence for Mab 1 was unique in the conditions that are known to drive the opalescence phenomenon. As these deviations appeared to correspond well with the measured second virial coefficient, it has been proposed that the direct measure of the valence may be an important new tool when determining an antibodies deviation from ideal behavior.

Based on the finding of this study, a mechanism of the Mab 1 opalescence phenomenon has been proposed (**Figure 4.4**). As NaCl is added to Mab 1, and if the second virial coefficient is $\geq -8 \times 10^{-4} \text{ mL-mol/g}^2$, the antibody self-associates through a site specific interaction located on the CDR region of the Fab. This self-association occurs slowly so that the molecules have enough time to orient themselves. The result is a clear liquid-liquid phase transition that if left long enough, will form a clear gel. The other path occurs if the second virial coefficient is $\leq -8 \times 10^{-4} \text{ mL-mol/g}^2$ when NaCl is added. This self-association occurs rapidly so that the molecules do not have enough time to orient themselves. The result is a cloudy or opalescent liquid-liquid phase transition. This phase transition differs from the first as it will not go on to form a solid gel but will eventually form an amorphous agglomerate.

Figure 4.4: Proposed Mechanism of the Mab 1 Opalescence Phenomenon

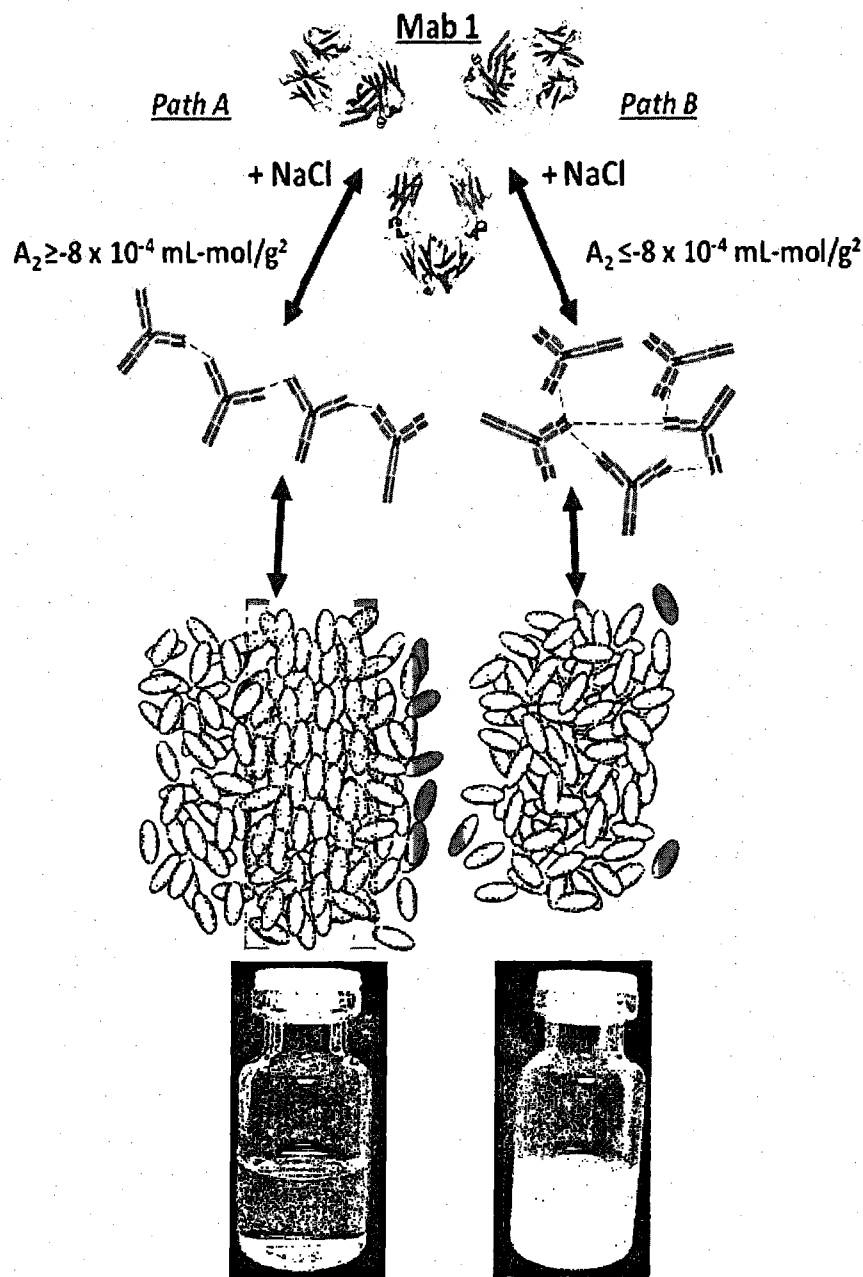


Figure 4.4: When NaCl is added to Mab 1 through Path A, and the second virial coefficient is $\geq -8 \times 10^{-4} \text{ mL-mol/g}^2$, the antibody self-associates via the CDR region with enough time for specific orientation. The result is a clear liquid-liquid phase transition. When NaCl is added to Mab 1 through Path B, and the second virial coefficient is $\leq -8 \times 10^{-4} \text{ mL-mol/g}^2$, the antibody self-associates via the CDR region without enough time for specific orientation. The result is a cloudy or opalescent liquid-liquid phase transition.

APPENDIX A

	<u>EOF</u>	<u>Peak 1</u>	<u>Run Voltage</u>	<u>Teof</u>	<u>Ip</u>	<u>Yeof</u>	<u>Yp</u>	<u>E</u>	<u>U*p</u>	<u>Ueof</u>	<u>Up</u>	<u>Z*</u>	<u>Z</u>
EOF	4.138		30000	248.28	272.76	0.2046077	0.1862443	487.01299	0.0003824	0.0004201			
Mab 1		4.546	30000				0.1862443	487.01299	0.0003824				
Mab 1 + EOF	4.171	4.546	30000	250.26	272.76	0.2029889	0.1862443	487.01299	0.0003824	0.0004168	3.438E-05	2.07	5.4
Mab 2		4.847	30000				0.1746785	487.01299	0.0003587				
Mab 2 + EOF	4.171	4.829	30000	250.26	290.82	0.2029889	0.1746785	487.01299	0.0003587	0.0004168	5.679E-05	3.41	8.9
Mab 3		5.063	30000				0.1672263	487.01299	0.0003434				
Mab 3 + EOF	4.179	5.063	30000	250.74	303.78	0.2026003	0.1672263	487.01299	0.0003434	0.000416	7.263E-05	4.36	11.38
EOF + NaCl	17.608		10000	1056.48			0.0480842	162.33766	0.0002962				
Mab 1 + NaCl + EOF	18.462	19.421	10000	1107.72	1165.26	0.04586	0.0435954	162.33766	0.0002685	0.0002825	1.395E-05	0.83	4.61
Mab 2 + NaCl		19.721	10000				0.0429322	162.33766	0.0002645				
Mab 2 + NaCl + EOF	17.783	19.758	10000	1066.98	1185.48	0.047611	0.0428518	162.33766	0.000264	0.0002933	2.932E-05	1.76	9.77
Mab 3 + NaCl		20.717	10000				0.0408682	162.33766	0.0002517				
Mab 3 + NaCl + EOF	17.879	20.654	10000	1072.74	1239.24	0.0473554	0.0409929	162.33766	0.0002525	0.0002917	3.919E-05	2.35	13.04
Mab 1 + Urea + EOF	4.108	4.521	30000	246.48	271.26	0.2061019	0.1872742	487.01299	0.0003845	0.0004232	3.866E-05	2.32	6.05
Mab 2 + Urea + EOF	4.129	4.833	30000	247.74	289.98	0.2050537	0.1751845	487.01299	0.0003597	0.000421	6.133E-05	3.68	9.6
Mab 3 + Urea + EOF	4.167	5.108	30000	250.02	306.48	0.2031837	0.1657531	487.01299	0.0003403	0.0004172	7.686E-05	4.61	12.03
Mab 1 + NaCl + Urea + EOF	18.554	19.529	10000	1113.24	1171.74	0.0456326	0.0433543	162.33766	0.0002671	0.0002811	1.403E-05	0.84	4.66
Mab 2 + NaCl + Urea		20.192	10000				0.0419308	162.33766	0.0002583				
Mab 2 + NaCl + Urea + EOF	18.279	20.379	10000	1096.74	1222.74	0.0463191	0.041546	162.33766	0.0002559	0.0002853	2.94E-05	1.76	9.77
Mab 3 + NaCl + Urea		21.283	10000				0.0397814	162.33766	0.0002451				
Mab 3 + NaCl + Urea + EOF	18.45	21.4	10000	1107	1284	0.0458898	0.0395639	162.33766	0.0002437	0.0002827	3.897E-05	2.34	12.99
EOF	4.388		30000	263.28			0.1929505	487.01299	0.0003962				
Mab 1 F(ab)2	4.388		30000	263.28			0.1929505	487.01299	0.0003962				
Mab 1 F(ab)2 + EOF	4.388	4.383	30000	263.28	262.98	0.1929505	0.1931706	487.01299	0.0003966	0.0003962	4.52E-07	-0.02	-0.05
Mab 2 F(ab)2	4.388		30000	263.28			0.1929505	487.01299	0.0003962				
Mab 2 F(ab)2 + EOF	4.388	4.396	30000	263.28	263.76	0.1929505	0.1925993	487.01299	0.0003955	0.0003962	7.21E-07	0.04	0.01
Mab 3 F(ab)2	4.388		30000	263.28			0.1929505	487.01299	0.0003962				
Mab 3 F(ab)2 + EOF	4.388	4.404	30000	263.28	264.24	0.1929505	0.1922495	487.01299	0.0003948	0.0003962	1.439E-06	0.08	0.2
EOF + NaCl	22.587		10000	1355.22			0.0374847	162.33766					
Mab 1 F(ab)2 + NaCl	22.525	23.096	10000	1351.5	1385.76	0.0375879	0.0366586	162.33766	0.0002258	0.0002315			
Mab 1 F(ab)2 + NaCl + EOF	22.578	22.983	10000	1354.68	1378.98	0.0374996	0.0368388	162.33766	0.0002269	0.000231	4.071E-06	0.22	1.14
Mab 2 F(ab)2 + NaCl	22.321	24.621	10000	1339.26	1477.26	0.0379314	0.034388	162.33766	0.0002118	0.0002337			
Mab 2 F(ab)2 + NaCl + EOF	22.575	24.938	10000	1354.5	1496.28	0.0375046	0.0339509	162.33766	0.0002091	0.000231	2.189E-05	1.19	6.14
Mab 3 F(ab)2 + NaCl	22.504	26.163	10000	1350.24	1569.78	0.0376229	0.0323612	162.33766	0.0001993	0.0002318			
Mab 3 F(ab)2 + NaCl + EOF	22.563	26.242	10000	1353.78	1574.52	0.0375246	0.0322638	162.33766	0.0001987	0.0002312	3.241E-05	1.79	9.38

APPENDIX B

"Chasing a Ghost"
Addressing the Aggregation/Opalescence
Relationship in an IgG 1 Antibody



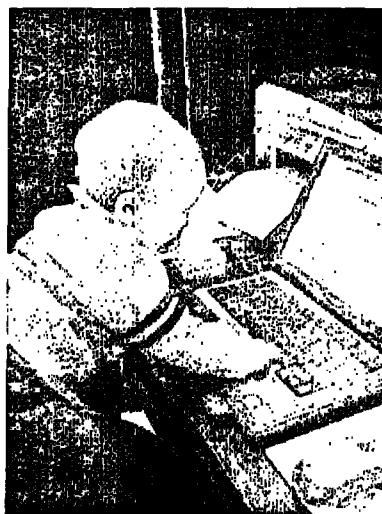
John Champagne

Laue Lab

Acknowledgements

2

- **Laue Lab (all members)**
 - Tom Laue
 - Sue Lucius
 - Sue Chase
 - Jennifer Durant
- **Wyatt Technology Corporation**
 - Philip Wyatt
 - Geof Wyatt
 - Cliff Wyatt
 - Michael Larkin
 - Amy Hanlon
- **Wyeth BioPharma**
 - Pilarin Nichols
 - Steven Raso
 - Donna Luisi
- **My Editor...**



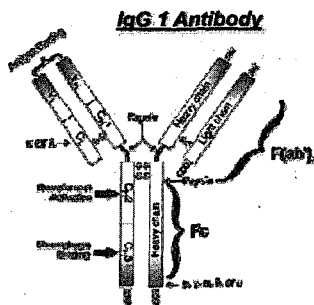
Where the story begins...

3

- It all started innocently enough with "Mab 1"
- The importance of antibody therapeutics (differing perspectives)
- Opalescence vs. aggregation
- Initial characterization
- Hypothesis and Action Plan
- Can we predict the opalescence phenomenon
- Proposed model of assembly
- Conclusions

Antibody Therapeutics: Biological Perspective

4



- There are 4 human IgG sub-classes
- IgG 1 ~43-75% of total IgGs
- Over 90% homologous
- Responds to proteins, polysaccharides and antigens
- Serum conc. 9.5-12.5 mg/mL
- Serum $\frac{1}{2}$ life ~23 days
- Dimer held together by 2 disulfide bonds (hinge region)
- One folding domain in Fab and two in Fc region
- Can be cleaved by Pepsin and Papain

Antibody Therapeutics: Historical Perspective

5

1890: Emil Behring published a paper demonstrating that diphtheria antitoxin serum could protect against a lethal dose of diphtheria toxin

1906: Paul Ehrlich proposed antibodies may be used as "magic bullets" to target diseases

1929: "nothing may be hoped for at present in respect to a successful therapy from this direction"

1974: The first monoclonal antibody made: Sp1, a mouse IgM antibody specific for SRBC, by Kohler and Milstein, published in 1975

1986: ORTHOCONE OKT3, the world's first therapeutic murine monoclonal antibody approved for human use

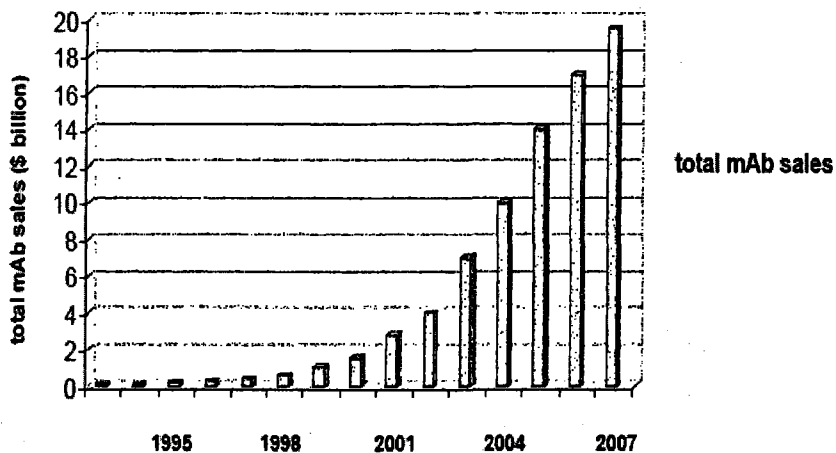
2002: Humira, the world's first fully human therapeutic antibody approved for human use

2003: Antibody products with 125 mg/mL concentration approved for human use (Xolair)

Today: >20 mAb and Fc fusion protein products approved, >>100 development programs, sophisticated delivery devices, 200 mg/mL formulation approaches published

Antibody Therapeutics: Business Perspective

6



IMS Midas, Dec 2002, Data Monitor Apr 2008

2008: \$22 billion

2010: \$30 billion estimated

Antibody Therapeutics: Pharmacological Perspective ⁷

Biologic	Company	Launch	Dose (g/yr)	Avg. Dose
Rituxan	Genentech/Roche	1997	2.3	<2 g/yr
Synagis	MedImmune	1998	0.5	
Remicade	J&J	1998	2	
Entrel	Amgen	1998	2.6	
Herceptin	Genentech/Roche	1998	3	
Humira	Abbott	2002	1	
Raptiva	Genentech	2003	1	>5 g/yr
Xolair	Genentech	2003	6	
Erbix	ImClone/BMS	2004	2.2	
Avastin	Genentech	2004	12	
Orencia	BMS	2005	10	
Tysabri	Biogen Idec	2006	3.9	

*Estimates based on company websites

- Substantial efforts to improve yield (tons per year)
- IV route is preferred as it allows for high concentration and rapid systemic availability
- IV route is not convenient for patients so SC is preferred
- Average patient requires weekly doses of ~130 mg (145 lb patient)
- Max volume for SC is ~1.5 mL
- Increased Mab concentration issues:
 - Stability issues (aggregation)
 - Safety concerns (efficacy and immunogenicity risks)
 - Increase in viscosity (process and delivery concerns)

Antibody Therapeutics: Immunological Perspective ⁸

Effects of Protein Aggregates: An Immunologic Perspective

Submitted: March 3, 2006; Accepted: May 24, 2006; Published: August 4, 2006

Amy S. Rosenberg¹

¹Food and Drug Administration, Center for Drug Evaluation and Research, Bethesda, MD

EVIDENCE FOR THE ROLE OF PRODUCT AGGREGATES IN INDUCTION OF IMMUNE RESPONSES TO THERAPEUTIC PROTEIN PRODUCT: CLINICAL STUDIES

Clinically, evidence that aggregates in therapeutic protein products had profound effects on immunogenicity was apparent from very early studies.

MEASUREMENT OF PRODUCT AGGREGATES/HIGH RISK CHANGES FOR AGGREGATE GENERATION

Protein aggregates in therapeutic protein products are almost exclusively assessed by a size exclusion chromatography (SEC) method. While sensitive, this method has critical flaws, including failure of some high MW species to penetrate the gel. Thus, methods orthogonal to SEC need to be employed to assess product aggregates.



This may refer to

- Analytical Ultracentrifugation
- Field flow fractionation
- Dynamic light scattering
- Static light scattering
- others

The AAPS Journal 2006; 8 (3) Article 59 (<http://www.aapsj.org>)

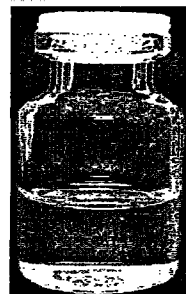
Opalescence vs. Aggregation

9

Definition of aggregate: A mass or body of units or parts somewhat loosely associated with one another*

• **Factors leading to aggregation**

- Genetic mutations
- Glycosylation
- Proteolytic degradation
- Oxidation
- Deamidation
- Excluded volume effects



• **If we have accounted for all of these factors...**

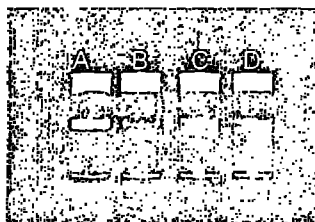
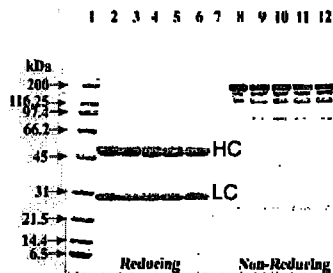
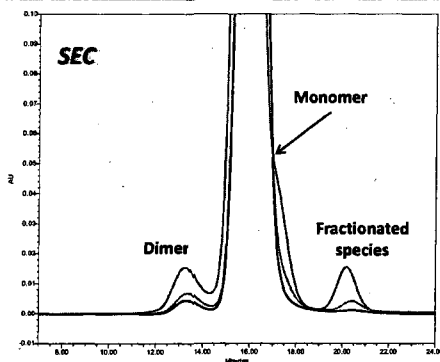
- Why do we still encounter opalescence?

Is opalescence really the same "issue" as aggregation?

*Webster's Revised Unabridged, 1913 Edition.

Initial Characterization: Traditional Techniques

10



- SEC showed only monomer/dimer/fractionated species
- SDS page showed only monomeric protein
- Tyndall beam technique (Ph. Eur, 1980)
 - A = Formulation buffer (10 mM Histidine, pH 6)
 - B = Mab 1 at 60 mg/mL, >99% monomer (EP I)
 - C = EP II standard
 - D = EP III standard

Initial Characterization: Traditional Techniques

NaCl (1M) or Polysorbate 80 (0.5%, 10%) stock solutions spiked into Mab1 at 65 mg/mL protein concentration



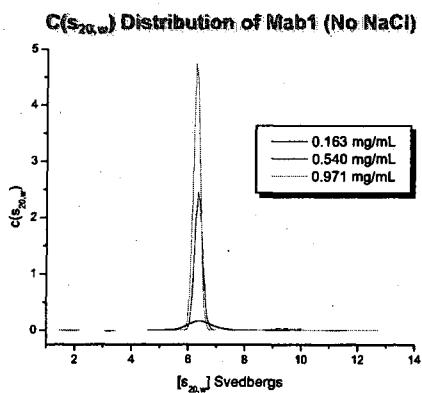
Concentration of NaCl (mM)	Appearance (E.P.2.2.1)
0	< III
1	< III
2	III
3	< IV
4	< IV
5	< IV
6	IV
7	IV
8	> IV

Theoretical % PS 80	Sample Volume (µL)	Theoretical Protein Conc. Based on Increased Vol. (mg)	Appearance (E.P. 2.2.1)
0	3000	65.0	< III
0.0005	3003	64.9	< III
0.001	3006	64.8	< III
0.0015	3009	64.8	< III
0.002	3012	64.7	< III
0.0025	3015	64.7	< III
0.005	3030	64.4	< III
0.01	3060	63.7	< III
0.02	3120	62.5	< III
0.04	3240	60.2	< III
0.08	3480	56.0	< III
0.16	3500	55.7	< III
0.32	3520	55.4	< III

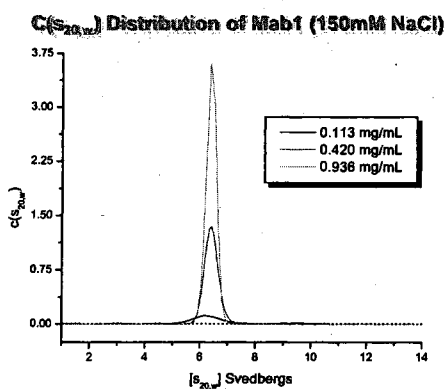
- As little as 2 mM added NaCl increased level of opalescence
- Added Polysorbate 80 had no effect on level of opalescence

Initial Characterization: Non-Traditional Techniques

Analytical Ultracentrifugation



Samples appeared homogeneous with only ~3 % HMW



Samples appeared very homogeneous with only ~1 % HMW

All samples run in 10 mM Histidine buffer pH 6 150 mM NaCl

Are We Chasing a Ghost?

Opalescent Appearance of an IgG1 Antibody at High Concentrations and Its Relationship to Noncovalent Association

Muppalla Sukumar,^{1,2} Brandon L. Doyle,¹ Jessica L. Combs,¹ and Allen H. Pekar¹

Received December 18, 2003; accepted March 15, 2004

Purpose. Therapeutic antibodies are often formulated at a high concentration where they may have an opalescent appearance. The purpose of this study is to understand the origin of this opalescence, especially its relationship to noncovalent association and physical stability.

Methods. The turbidity and the association state of an IgG1 antibody were investigated as a function of concentration and temperature using static and dynamic light scattering, nephelometric turbidity, and analytical ultracentrifugation.

Results. The antibody had increasingly opalescent appearance in the concentration range 5–50 mg/ml. The opalescence was greater at refrigerated temperature but was readily reversible upon warming to room temperature. Turbidity measured at 25°C was linear with concentration, as expected for Rayleigh scatter in the absence of association. In the concentration range 1–50 mg/ml, the weight average molecular weights were close to that expected for a monomer. Zimm

plots of the bulk drug substance or formulated solution (7). In an attempt to understand the origin of the opalescence of antibody solutions at high concentration, especially its relationship to noncovalent association, an IgG1 antibody (148.9 kDa) was investigated over a 100-fold concentration range (0.5–50 mg/ml). Solutions of this antibody had an increasingly opalescent appearance in the concentration range 5–50 mg/

(0.5–50 mg/ml). Solutions of this antibody had an increasingly opalescent appearance in the concentration range 5–50 mg/ml, which persisted even after filtration through a 0.2- μ m sterilizing filter, suggesting that opalescent appearance was not caused by large filterable particles. It was also noted that

large molecules at high concentration (8) or is it a consequence of noncovalent association at high concentrations?

Determination of the association state of the molecule directly at the high concentration is most relevant to assess its impact on the stability and biopharmaceutical properties; yet, it is complicated by the limitations of various instrumental techniques and the potential nonideality effects. For example, the high refractive index or absorbance at these high concentrations makes the application of analytical ultracentrifugation difficult (9–10). Similarly, the use of size exclusion chromatography is limited by the dilution and peak broadening that occurs, and the interaction of the antibody with the col-

Conclusions. The results indicate that opalescent appearance is not due to self-association but is a simple consequence of Rayleigh scatter. Opalescent appearance did not result in physical instability.

KEY WORDS: light scattering; protein aggregation; protein formulation; reversible association; turbidity.

over, one needs to be cautious about potential nonideality effects at high concentrations (8). Viscosity changes as a func-

Pharmaceutical Research, Vol. 21, No. 7, July 2004 (© 2004)

Hypothesis and Action Plan

The observed opalescence seen in IgG 1 molecules is due to a specific alteration in the thermodynamic equilibrium of the system and that this alteration was leading to a discrete higher order associated species...

ACTION PLAN

1. Are there HMW species present
2. Can we induce opalescence "artificially"
3. Can other salts induce opalescence
4. How does opalescence of Mab 1 compare to other Mabs
5. Are the HMW species reversible
6. Is Mab 1 structurally unique
7. Is the non-ideality of Mab 1 opalescence unique
8. Is viscosity enhanced from opalescence
9. Any structural changes to Mab 1 from NaCl
10. Possibility of fibril formation
11. Can we prevent opalescence
12. Does opalescence alter the valence

...can we predict opalescence?

1. Are there HMW species present

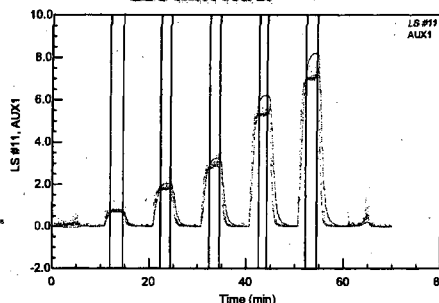
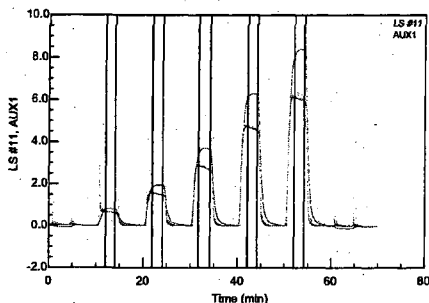
15

Batch Multi-Angle Light Scattering

$I_{\text{scattered}} \propto M_w C$

No NaCl

150 mM NaCl



Conc	Mass	Radius
0.1 mg/mL	195 kDa	14 nm
0.25 mg/mL	182 kDa	11 nm
0.5 mg/mL	176 kDa	11 nm
0.75 mg/mL	172 kDa	12 nm
1.0 mg/mL	169 kDa	12 nm

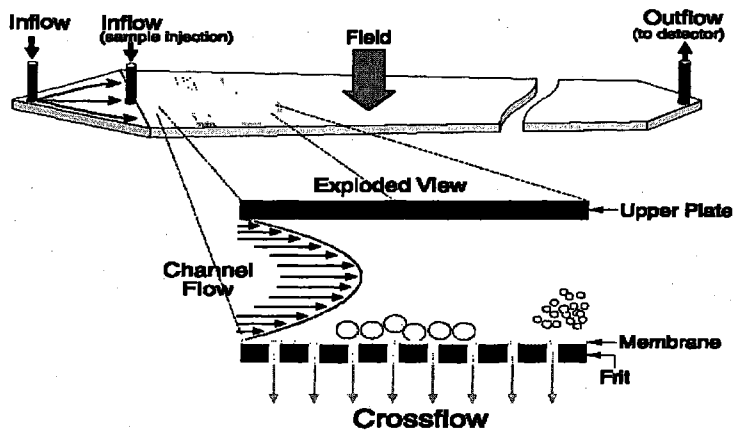
Conc	Mass	Radius
0.1 mg/mL	182 kDa	64 nm
0.25 mg/mL	172 kDa	50 nm
0.5 mg/mL	174 kDa	56 nm
0.75 mg/mL	160 kDa	52 nm
1.0 mg/mL	162 kDa	52 nm

All samples run in 10 mM Histidine buffer pH 6 ± 150 mM NaCl

1. Are there HMW species present

16

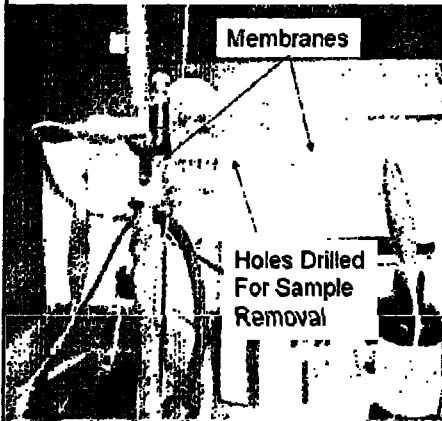
Field Flow Fractionation-MALS



A large aggregate peak was present... ≥ 200 nm and 10 MDa!

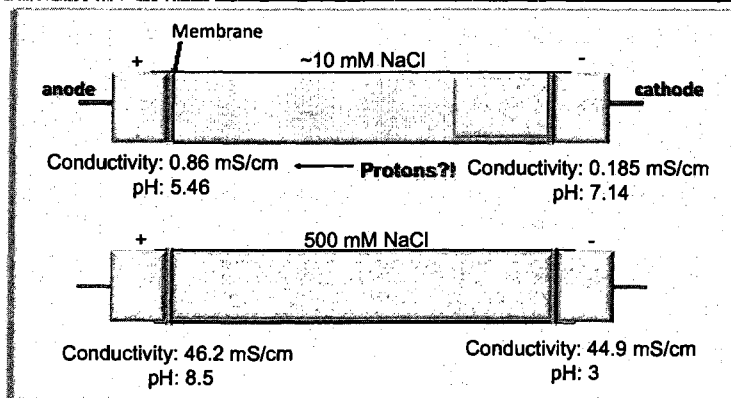
2. Can we induce opalescence "artificially" 17

"Electroseparation"



- 15 mL conical tube modified with #00 stoppers with electrodes
- Mab 1 at 10 mg/mL in Histidine buffer \pm 500 mM NaCl
- Constant voltage (80 volts) was applied until current was steady
- Power turned off and 10 μ L of sample removed at each port
- Samples diluted (1:10) and measured (OD_{400} , pH and conductance)
- Results gave insight into Cl^- ion binding

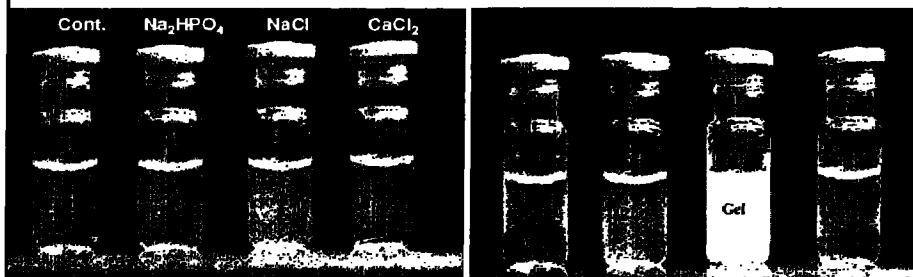
2. Can we induce opalescence "artificially" 18



- An opalescence cloud appeared at the cathode (reformed when field reversed)
- Ion and concentration imbalance (5X greater concentration at cathode)
- Protons moved against the E field due to Donnan effect (suggests that Mab 1 binds Cl^- during opalescence phenomenon)
- Concentration and ions balanced in 500 mM NaCl

3. Can other salts induce opalescence

19



Overnight at 2-8 °C

- Mab 1 concentration was ~60 mg/mL in 10 mM Histidine, pH 6 ± 100 mM salt
- Na₂HPO₄ and CaCl₂ were chosen to determine the effects of Na⁺ and Cl⁻
- Samples prepared and examined after 1 hour and then overnight
- NaCl was most opalescent and formed a solid gel after 24 hours (Na₂HPO₄ also formed a gel after 2 weeks)
- The highly chaotropic nature of Ca²⁺ and large size of HPO₄²⁻ may have interfered with/delayed opalescence (NaCl considered "neutral")

kosmotropic

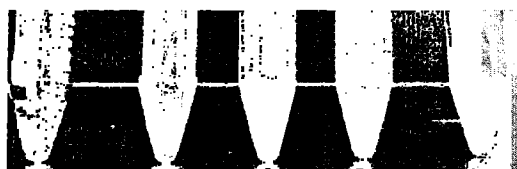
Citrate³⁻ > succinate²⁻ > sulfate²⁻ > acetate > Cl⁻ > Br⁻ > I⁻ > SCN⁻
 N(CH₃)₄⁺ > NH₄⁺ > Na⁺ > Ca²⁺ > Mg²⁺ > Guanidium⁺

chaotropic

4. How does Opalescence of Mab 1 compare

20

Observation 1 : Mab 1 with varying amounts of NaCl



0mM 25mM 50mM 100mM 150mM

Observation 2: Mab 2 with varying amounts of NaCl



0mM 25mM 50mM 100mM 150mM

All samples contained 10mM Histidine, pH 6.0, ~30mg/mL

5. Are the HIVV species reversible

21

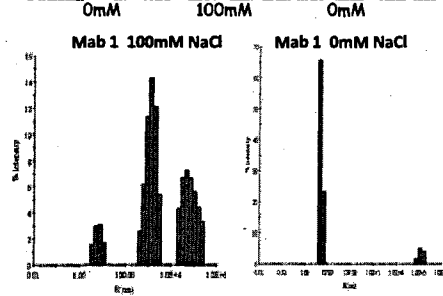
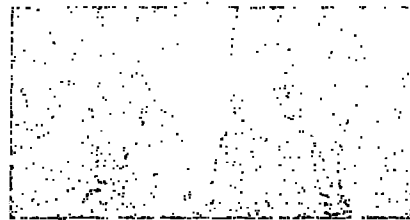
- Sample dialyzed from 0mM to 100mM back to 0mM NaCl, visually opalescence was reduced

DLS Data: Peak 1 64.4% to 99.2%

- This material can also be filtered out using a 0.2um filter (data not shown)

DLS Data: Peak 1 64.4% to 100%

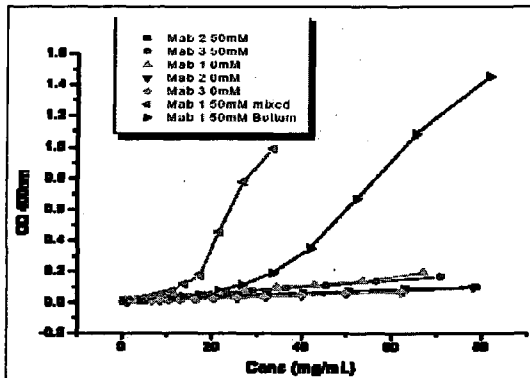
- Opalescence eventually returned!



5 mg/mL, 10mM Histidine, pH 6.0

5. Are the HIVV species reversible

22



- A dilution study was performed on Mab 1, Mab 2 and Mab 3 in a buffer containing 10 mM Histidine, pH 6 ± 50 mM NaCl

• Samples measured OD₄₀₀ to assess degree of association

• Linear profile indicates minimum protein-protein self assembly

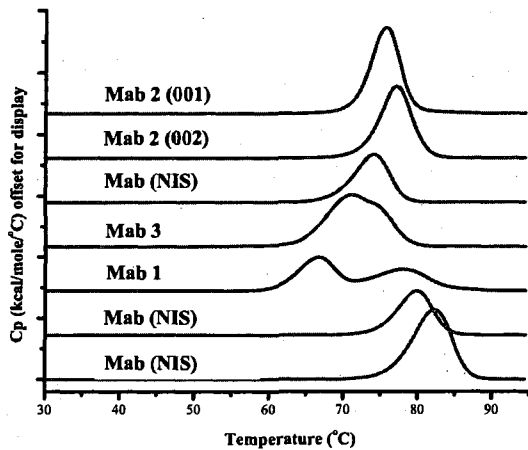


- Mab 1 self-association appeared to be completely reversible
- Dilution profile of Mab 1 (top and bottom) was non-linear indicating cooperativity (non-mass action driven)
- When Mab 1 was mixed, it became highly viscous and opalescent at only 30 mg/mL possibly indicating that the Cf ions were continuously re-introduced

5. Is Mab 1 structurally unique

23

Differential Scanning Calorimetry

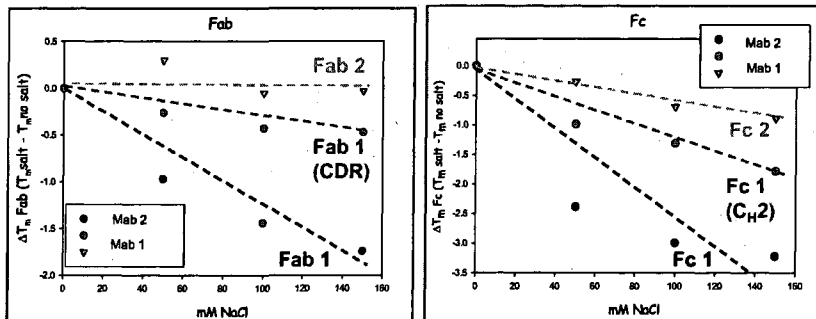


- Pepsin cleaved F(ab')₂ fragments were analyzed for Mab 1, 2, 3 and Mabs not in the study (NIS)
- Mab 1 clearly shows 2 distinct transitions
- Mab 3 appears to also have 2 transitions...less opalescent
- Greater structural flexibility for Fab region of Mab 1 and Mab 3
- Could be used as a predictive tool...

1.5 mg/mL, 10 mM Histidine, pH 6.0

5. Is Mab 1 structurally unique

24



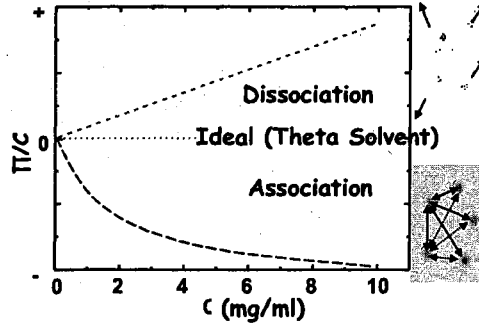
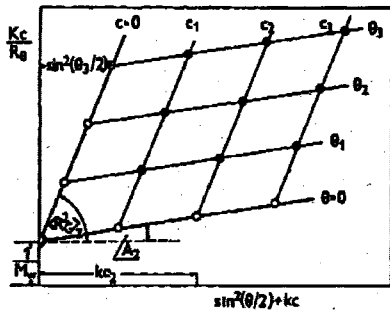
- Little loss in thermal stability for the Fab region of Mab 1 with addition of NaCl
- Stability of Fab region may be responsible for reversibility of opalescence
- There is an equivalent loss in thermal stability for the Fc region
- This altered stability in the C_H2 domain with the addition of NaCl may allow for greater flexibility of the Fab region at the hinge region
- The altered stability of the Fc region and independent folding domain of the Fab region may be responsible for the enhanced protein-protein interactions

1.5 mg/mL, 10 mM Histidine, pH 6.0

7. Is the non-ideality of Mab 1 opalescence unique

25

Second Virial Coefficient

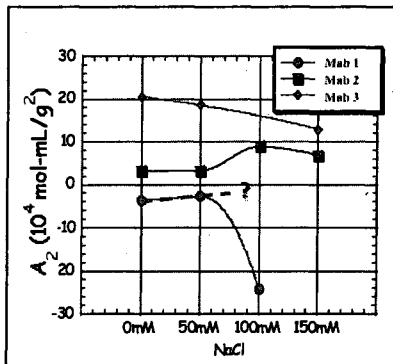


*B. H. Zimm, *Journal of Phys. Chem.* (1946)

*C. Tanford, *Physical Chemistry of Macromolecules* (1961)

7. Is the non-ideality of Mab 1 opalescence unique

26

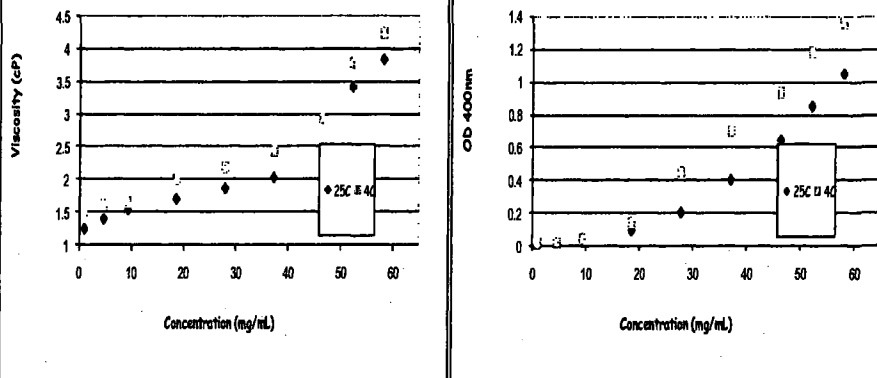


Sample	A ₂ [10 ⁻⁴ mol·mL/g ²]
Mab 1 0mM NaCl	-3.6
Mab 1 50mM NaCl	-2.7
Mab 1 100mM NaCl	-24.1
Mab 2 0mM NaCl	3.3
Mab 2 50mM NaCl	3.1
Mab 2 100mM NaCl	9.0
Mab 2 150mM NaCl	6.8
Mab 3 0mM NaCl	20.5
Mab 3 50mM NaCl	18.5
Mab 3 150mM NaCl	12.9

- Slight increase in A₂ with the addition of NaCl??
(Indicative of charge-dipole and dipole-dipole interaction)
- At 100 mM NaCl, the A₂ dropped precipitously (A₂ < -8 x 10⁻⁴ mL·mol/g²)
- Mab 2 and Mab 3 continued to have a positive A₂ until reaching 150 mM NaCl
(Indicative of an overall charge-charge repulsion)

8. Is viscosity enhanced from opalescence

27



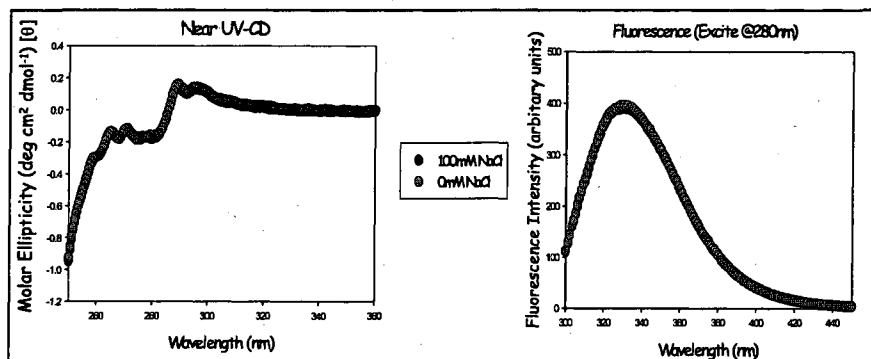
- Viscosity of Mab 1 is predominantly non-linear at higher concentrations (>40 mg/mL)
- Non-linear increase in viscosity is consistent with protein-protein interactions
- Increase in viscosity is faster at 4 °C indicating that the interaction is predominantly entropic in origin

10mM Histidine, 50 mM NaCl, pH 6

9. Any structural changes to Mab 1 from NaCl

28

Circular Dichroism and Fluorescence



There appears to be no significant change in the 2° or 3° structure of Mab 1 with the addition of NaCl

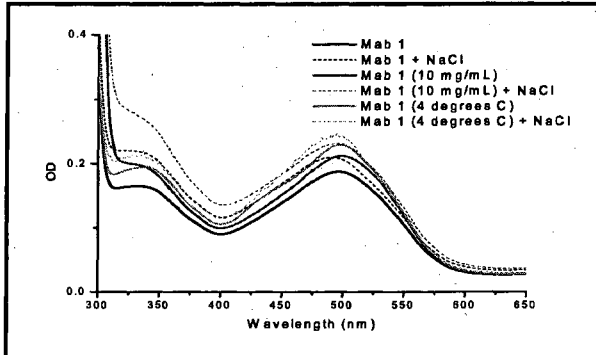
4 mg/mL, 10 mM Histidine, pH 6.0 100 mM NaCl

10. Possibility of fibril formation

29

Congo Red Analysis

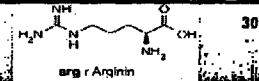
- CR will bind amyloid fibrils and shift OD from ~490nm to ~540nm
- Mab 1 samples were opalescent and giving a "blue shift"?
- Believed that CR binds due to electrostatic interaction of negative charged sulfate group
- Mab 1 may bind CR when NaCl is not present but cannot bind when Cl⁻ ions occupy specific binding sites



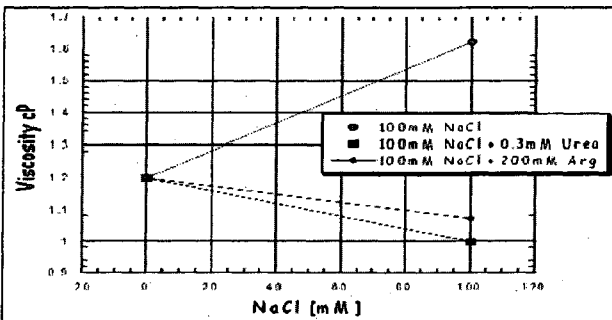
Electron Microscopy
(Genentech 2005)

1 and 10 mg/mL, 10mM Histidine, pH 6.0 50 mM NaCl

11. Can we prevent opalescence



30



$$D = D_0 + \delta C$$

Material*	δ M ⁻¹
NaCl	0
ETOH	-2.6
Glycerol	-2.6
Mannitol	-2.6
Sucrose	-7.6
Dioxane	-8.3
Urea	+2.7
Glycine (anhydride)	-10
Glycine	+22.6
diGlycine	+71
Arginine	+62
Lysylglutamate	+345

Mab 1	Peak 1		Peak 2		Peak 3	
	MW KDa	%Mass	MW KDa	%Mass	MW KDa	%Mass
100mM NaCl	229	95.8%	1.6x10 ⁷	0.2%	1.1x10 ¹¹	4.0%
100mM NaCl + 0.3mM Urea	134	100%	NA	NA	NA	NA
100mM NaCl + 200mM Arginine	143	100%	NA	NA	NA	NA

*Cohn & Edsall, *Proteins, amino acids and Peptides*, 1943

11. Can we prevent opalescence

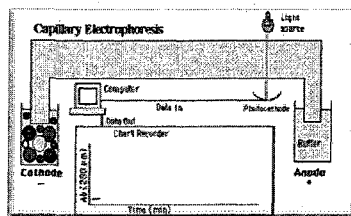
Sample Mab 1 (diluted to 5mg/ml)	Peak 1		Peak 2		Peak 3	
	MW KDa	%Mass	MW KDa	%Mass	MW KDa	%Mass
100mM NaCl	229	95.8%	1.6x10 ⁷	0.2%	1.1x10 ¹¹	4.0%
100mM NaCl + 200mM Urea (5000:1)	135	100%	NA	NA	NA	NA
100mM NaCl + 200mM Urea 24hrs 4C	136	100%	NA	NA	NA	NA
100mM NaCl + 0.3mM Urea (10:1)	134	100%	NA	NA	NA	NA
100mM NaCl + 0.3mM Urea 24hrs 4C	185	99.5%	NA	NA	0.4x10 ¹¹	0.5%
100mM NaCl + 0.03mM Urea (1:1)	160	100%	NA	NA	NA	NA
100mM NaCl + 0.03mM Urea 24hrs 4C	165	99.6%	NA	NA	0.1x10 ¹¹	0.4%

- Urea can block opalescence at a ratio of 1:10 and inhibit opalescence at 1:1
- Urea is highly polar and may bind to dipole(s) on Mab 1
- Mab 1 appears to contain more than 1 dipole as some dimer still forms
- Average circulating levels of urea in blood is ~4mM (IgG 1 conc. is ~10mg/ml)

5 mg/mL, 10mM Histidine, pH 6.0



12. Does opalescence alter the valence



$$z^* = \frac{\mu k_B T}{D_T e}$$

$$z \cong z^* \frac{(1 + \kappa a)}{f(\kappa a)}$$

- z^* is the effective or apparent valence
- μ is the mobility
- k_B is Boltzmann's constant
- T is the absolute temperature.
- D_T is the translational diffusion coefficient
- e is the elementary charge of proton

- κ is the inverse Debye length
- a is the sum of Stokes radii ($R_s + R_i$)
- $f(\kappa a)$ is Henry's function (unitless)

12. Does opalescence alter the valence

33

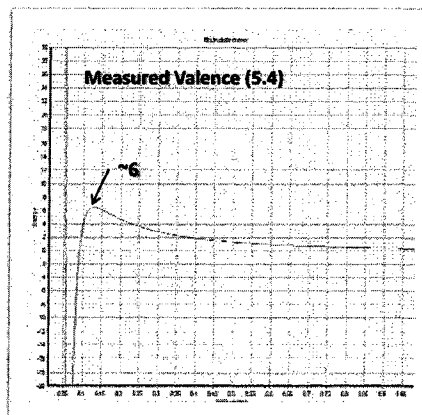
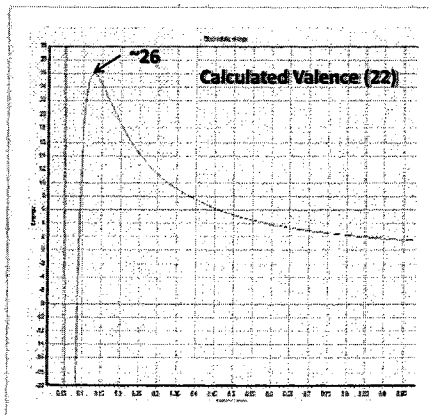
	Molecular Weight (Daltons)	Hydrodynamic Radius	Calculated Charge (based on AA seq)	Z'	Z
Mab 1 F(ab') ₂	89,657	4.6	9	-0.02	-0.05
Mab 1 F(ab') ₂ + NaCl				0.22	1.14
Mab 1	142,778	5.1	22	2.97	5.4
Mab 1 + Urea				2.32	6.05
Mab 1 + NaCl				0.53	1.51
Mab 1 + NaCl + Urea				0.84	4.66
Mab 2 F(ab') ₂	92,147	4.6	15	0.04	0.1
Mab 2 F(ab') ₂ + NaCl				1.19	6.14
Mab 2	145,938	5.1	25	3.41	5.9
Mab 2 + Urea				3.68	9.6
Mab 2 + NaCl				1.76	9.77
Mab 2 + NaCl + Urea				1.76	9.77
Mab 3 F(ab') ₂	92,583	4.7	32	0.08	0.2
Mab 3 F(ab') ₂ + NaCl				1.79	9.38
Mab 3	143,900	5.1	42	4.36	11.38
Mab 3 + Urea				4.61	12.03
Mab 3 + NaCl				2.35	13.04
Mab 3 + NaCl + Urea				2.34	12.99

- The measured charge is far lower than the calculated charge (AA sequence)
- This charge discrepancy may be due to unequal charge distribution in the interior of antibodies to remain "biologically relevant"
- The decrease in valence for Mab 1 containing NaCl matches A₂ measurements
- The addition of urea slightly increases the charge for Mab 1

0.5 mg/mL, 10 mM NaCl, 100 mM MES, pH 6.0 100 mM NaCl 0.1 mM urea

Can we Predict Opalescence Phenomenon

34

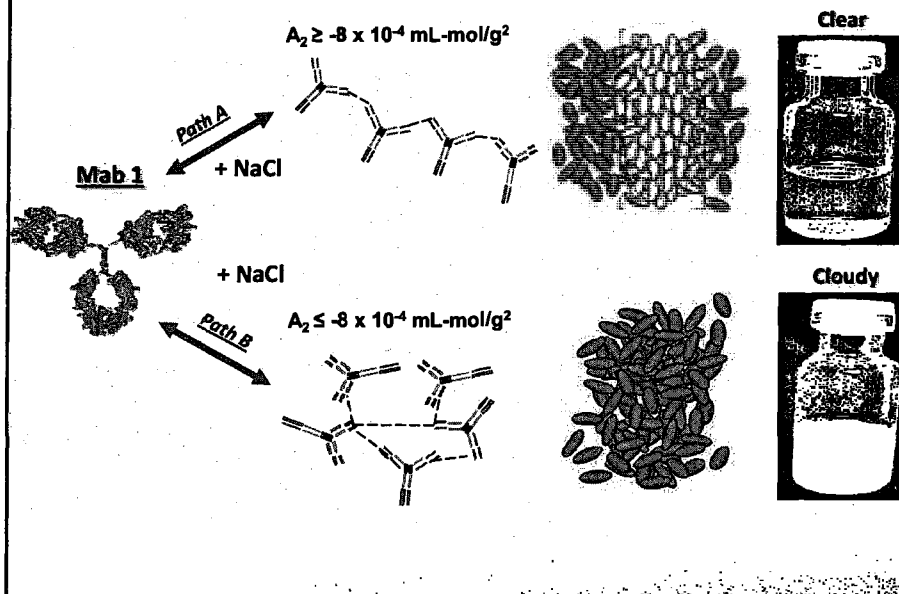


- The activation energy of approach was determined for calculated and measured valence of Mab 1 using ElectroGraph[®] as a function of distance (nm)
- The graphs clearly indicates that the lower measured valence would be more susceptible to non-ideal behavior

The program ElectroGraph was written by Tom Laue and is available through BITC (www.BITC.unh.edu)

Proposed model of Opalescence Phenomenon

35



Conclusions

36

- Opalescence is due to salt induced non-mass-action driven self-association which is mainly entropic in origin
- Opalescence has been induced by other salts including Na_2HPO_4 and CaCl_2 but it is driven predominantly by NaCl
- The self-association is thought to be electrostatic in origin and exist through interactions such as charge-dipole (minor) and dipole-dipole (predominant)
- The interactions involve mainly the CDR region (there may be multiple sites)
- The intermolecular interactions appear to be facilitated by enhanced flexibility of Fc region and the independent Fab folding domain on Mab 1
- Opalescence phenomenon is a liquid-liquid or liquid-solid phase transition and can be clear or cloudy depending on A_2
- The opalescence phenomenon appears to be a relatively small fraction of discrete HMW material which is freely reversible (liquid-liquid phase)
- The reversibility is believed to be due to the findings that the Fab region is not appreciably destabilized with the addition of NaCl
- A ratio of 1:1 urea to protein is adequate to disrupt the opalescence of Mab 1
- There is a discrepancy between the measured and calculated valence of IgG1 antibodies and this may be used as a predictive tool of non-ideal behavior

...we may have finally caught the "ghost"

REFERENCES

REFERENCES

- Arakawa, T. E. (2007). Suppression of protein interactions by arginine: A proposed mechanism of the arginine effects. *Biophysical Chemistry* , Vol. 127, 1-8.
- Attri, A. M. (2004). New Methods from Measuring Macromolecular Interactions in Solution via Light Scattering: Basic Methodology and Application to Non-Associating and Self-Associating Proteins. *Analytical Biochemistry* , 1-22.
- B.L. Neal, D. A. (1998). Molecular Origins of Osmotic Second Virial Coefficient of Proteins . *Biophysical Journal* , Vol. 75, 2469-2477.
- Berne, B. J. (1974). *J. Mol. Biol.* , Vol. 89, 755.
- Caldwell, K. S. (2000). *FFF Handbook*. New York: John Wiley and Sons.
- Camerini-Otero, R. D. (1978). The Wavelength Dependence of the Turbidity of Solutions of Macromolecules. *Biopolymers* , 17: 2241-2249.
- Campbell, P. M. (2003). Monoclonal Antibody Therapy for Lymphoma. *Blood* , 143-152.
- Carpenter, J. R. (2008). Overlooking Subvisible Particles in Therapeutic Protein Products: Gaps That May Compromise Product Quality. *Journal of Pharmaceutical Sciences* , 1-5.
- Champagne, J. C. (2000). *An Analysis of the Gelation Properties of B-Lactoglobulin A and B*. University of New Hampshire: Masters Thesis.
- Chase, S. L. (2008, February Volume 12). The Determination of Protein Valence by Capillary Electrophoresis. *Beckman Coulter Application Note* , pp. 1-5.
- Chen B, B. R. (2003). Influence of Histidine on the Stability and Physical Properties of a Fully Human Antibody in Aqueous and Solid Forms. *Pharmaceutical Research* , Vol. 20, No. 12, 1952-1960.
- Chen, C. S. (1972). *Biochemistry* , 11 (3559-3564).
- Christian Shultz, H. F. Fourier Transform Infrared Spectroscopy in Peptide and Protein Analysis. In *Encyclopedia of Analytical Chemistry* (pp. 1-24). New York: John Wiley and Sons Ltd.

- Coleman, J. E. (1999). Characterization of the Self Association of Avian Sarcoma Virus Integrase by Analytical Ultracentrifugation. *Journal of Biological Chemistry* , Vol. 274, No. 46, 32842-32846.
- Collins. (1997). Charge density-dependent strength of hydration and biological structure. *Biophys. J.* , Vol 72, 65-76.
- Collins, K. (2006). Ion Hydration: Implications for cellular function, polyelectrolytes and protein crystallization. *Biophysical Chemistry* , Vol. 119, 271-281.
- Creighton, T. E. (1993). *Proteins*. New York: W. H. Freeman and Company.
- Curtis, R. P. (1998). Protein-Protein and Protein-Salt Interaction in Aqueous Protein Solutions Containing Concentrated Electrolytes. *Biotechnology and Bioengineering* , Vol. 57, 11-21.
- Debye, P. (1944). *J. Appl. Phys.* , 15: 338.
- Deszczynski, M. H. (2006). Negative second virial coefficients as predictors of protein crystal growth: Evidence from sedimentation equilibrium studies that refutes the designation of those light scattering parameters as osmotic virial coefficients . *Biophysical Chemistry* , 120: 106-113.
- Donnan, F. G. (1911). *Electrochem* , 572.
- Doty, P. S. (1950). Light Scattering and Spectrophotometry of Colloidal Solutions. *The Journal of Chemical Physics* , 18: 1211-1220.
- Durant, J. M. (2003). The experimental determination of protein valence. *Nature* .
- E. D. Lobo, R. J. (2004). Antibody Pharmacokinetics and Pharmacodynamics. *Journal of Pharmaceutical Sciences* , Vol. 93, No. 11, 2645-2668.
- E. P. O'Brien, R. L. (2007). Interactions between Hydrophobic and Ionic Solutes in Aqueous Guanidinium Chloride and Urea Solutions: Lessons for Protein Denaturation Mechanisms . *J. Am. Chem. Soc.* , Vol. 129, 7346-7353.
- Eckhardt, B. O. (1994). A Turbidometric Method to Determine Visual Appearance of Protein Solutions. *Journal of Pharmaceutical Science and Technology* , Vol. 48, No. 2, 64-70.
- Edsall, J. W. (1958). *Biophysical Chemistry*. New York: Academic Press.
- Edsell, C. &. (1943). *Proteins, Amino Acids and Peptides*.

- Elcock, A. M. (2001). Calculation of Weak Protein-Protein Interactions: The pH Dependence of the Second Virial Coefficient. *Bioophysical Journal* , Vol. 80, 613-625.
- Frazer, J. C. (1999). Immunoglobulins: Structure and Function. In: *Fundamental immunology* 4th edn. . Philadelphia: Lippincott-Raven.
- Frei, P. B. (1965). Phagocytosis of the antigen, a crucial step in the introduction of the primary response. *Proc Natl Acad Sci* , Vol 53: 20-23.
- Gelfand, E. (2001). Antibody-directed Therapy: Past, Present, Future. *J. Allergy Clin Immunol* , 111-116.
- Giddings, J. C. (1991). *Unified Separation Science*. New York: John Wiley and Sons.
- Grillo-Lopez, A. (2003). Rituximab (Rituxan/MabThera): The first decade (1993-2003). *Expert Review of Anticancer Therapy* , Vol 3, 403-408.
- Hammes, G. G. (1967). An Investigation of Water-Urea and Water-Urea-Polyethylene Glycol Interactions. *Journal of the American Chemical Society* , Vol. 89, No. 2.
- Harris, L. S. (1998). Crystallography Structure of an Intact IgG 1 Monoclonal Antibody. *J. Mol. Biol.* , Vol 275, 861-872.
- Hayes, D. C. (2003). Direct Measurement of the Apparent Charge on Single and Double Stranded DNA Fragments. *Journal of Biophysics* , 3035-3055.
- Heegaard, N. H. (2000). *J. Chromatography* , A 894, 319-327.
- Henry, D. (1948). The Electrophoresis of Suspended Particles. IV. The Surface Conductivity Effect. *Trans. Faraday Soc.* , Vol. 44, 1021-1026.
- Hofmeister, F. (1888). Zur lehre von der wirkung der salze. *Arch. Expt. Pathol. Pharmacol.* , Vol. 24, 247-260.
- Kang, D. M. (2006). Development of Non-Gel-Based Two Dimensional Separation of Intact Proteins by an On-Line Hyphenation of Capillary Isoelectric Focusing and Hollow Fiber Flow Field-Flow Fractionation. *Analytical Chemistry Vol. 78, No. 16* , 78, 57895798.
- Kim, Y. R. (2003). Congo Red Populates Partially Unfolded States of an Amyloidogenic Protein to Enhance Aggregation and Amyloid Fibril Formation. *Journal of Biological Chemistry* , Vol. 278, No. 2, 10842-10850.
- Krimm, S. B. (1986). Vibrational Spectroscopy and Conformation of Peptides, Polypeptides and Proteins . *Adv. Protein Chem.* , 38: 181-364.

- Laue. (1992). *Short Column Sedimentation Equilibrium Analysis for Rapid Characterization of Macromolecules in Solution*. Palo Alto, CA: Beckman Instruments Inc.
- Laue T.M. (1999). Modern Applications of Analytical Ultracentrifugation. *Annu. Rev. Biophys. Biomol. Struct.* , Vol 28: 75-100.
- Laue, T. (2001). Biophysical studies by ultracentrifugation. *Current Opinions in Structural Biology* , Vol. 11, 579-583.
- Liu, J. N. (2005). Reversible Self-Association Increases the Viscosity of a Concentrated Monoclonal Antibody in Aqueous Solution. *Journal of Pharmaceutical Sciences* , Vol. 94, No. 9, 1928-1940.
- Lobo, E. H. (2004). Antibody Pharmacokinetics and Pharmacodynamics. *Journal of Pharmaceutical Sciences* , Vol 93, 2645-2668.
- Loertscher, R. (2002). The Utility of Monoclonal Antibody Therapy in Renal Transplantation. *Transplantation Proceedings* , 797-800.
- M. Sukumar, B. D. (2004). Opalescent Appearance of an IgG1 Antibody at High Concentrations and Its Relationship to Noncovalent Associations. *Pharmaceutical Research* , Vol. 21, No. 7, 1087-1093.
- M.Deszczynski, S. H. (2006). Negative second virial coefficients as predictors of protein crystal growth: Evidence from sedimentation equilibrium studies that refutes the designation of those light scattering parameters as osmotic virial coefficients. *Biophysical Chemistry* , Vol. 120, 106-113.
- M.N. Stoner, N. F. (2004). Protein-Solute Interactions Affect the Outcome of Ultrafiltration/Diafiltration Outcomes. *Journal of Pharmaceutical Sciences* , Vol. 93, No. 9, 2332-2342.
- MacKay. (1927). The Concentration of Urea in the Blood of Normal Individuals. *The Journal of Clinical Investigation* , 295-306.
- MacKay, E. M. (1927). The Concentration of Urea In the Blood of Normal Individuals. *J. Clin. Invest.* , 295-306.
- Mathews and van Holde. (1996). *Biochemistry 2nd Ed*. Menolo Park, CA: The Benjamin/Cummings Publishing Company, Inc.
- Moody, T. K. (2005). Valence and anion binding of bovine ribonuclease A between pH 6 and 8. *Analytical Biochemistry* , 336: 243-252.

- Muschol, M. R. (1997). Liquid-Liquid phase separation in supersaturated lysozyme solutions and associated precipitate formation/crystallization. *J. Chem. Phys.* , Vol. 107 (6) 1953-1962.
- Nassau, K. (1983). *The Physics and Chemistry of Color*. New York: John Wiley and Sons.
- Neal, B. A. (1998). Molecular Origins of Osmotic Second Virial Coefficients of Proteins. *Biophysical Journal* , Vol 75, 2469-2477.
- Oro, J. D. (2001). Role of Co-Solute in Biomolecular Stability: Glucose, Urea and the Water Structure. *Journal of Biological Physics* , Vol. 27, 73-79.
- P.M. Tessier, A. L. (2002). Rapid Measurement of Protein Osmotic Second Virial Coefficients by Self-Interaction Chromatography. *Biophysical Journal* , Vol. 82, 1620-1631.
- P.R. Davis-Searles, A. S. (2001). Interpreting the Effects of Small Uncharged Solutes on Protein-Folding Equilibria. *Annu. Rev. Biophys. Biomol. Struct.* , Vol. 30, 271-306.
- Paliwal, A. A. (2005). Light Scattering Studies of Protein Solutions: Role of Hydration in Weak Protein-Protein Interactions. *Biophysical Journal* , Vol. 89, 1564-1573.
- Prausnitz, J. M. (1997). Interactions of Lysozyme in Concentrated Electrolyte Solutions from Dynamic Light Scattering Measurements. *Biophysical Journal* , Vol. 73, 3211-3224.
- R. Daniel Camerini-Otero, L. A. (1978). The Wavelength Dependence of the Turbidity of Solutions of Macromolecules. *Biopolymers* , Vol. 17, 2241-2249.
- Roessner, D. (1995). Characterization of Proteins by Means of Multi-Angle Laser Light Scattering Coupled with Field-Flow Fractionation. *Polymer Science* .
- Rosenberg, A. S. (2006). Effects of Protein Aggregates: An immunological Perspective. *AAPS Journal* , 8 (3) Article 59, E501-E507.
- Saluja, A. B. (2006). Application of High Frequency Rheology Measurements for Analyzing Protein-Protein Interactions in High Protein Concentration Solutions Using a Model Monoclonal Antibody. *Journal of Pharmaceutical Sciences* , Vol. 95, No. 9, 1967-1983.
- Scatchard, G. S. (1950). Physical chemistry of protein solutions. *J. Amer. Chem. Soc.* , 72: 540-546.

- Schuck, P. (2000). Size-distribution analysis of macromolecules by sedimentation velocity ultracentrifugation and Lamm equation modelling. *Biophys. J.* , 78: 1606-1619.
- Shire, S. S. (2004). Challenges in the development of high protein concentration formulations. *J. Pharm. Sci.* , Vol 93: 1390-1402.
- Shultz, C. P. (2000). Illuminating Folding Intermediates. *Nature Structural Biology* , Vol. 7, No. 1, 7-10.
- Stigter, D. D. (1990). Charge Effects on Folded and Unfolded Proteins. *Biochemistry* , Vol. 29, 1262-1271.
- Stockmayer, W. H. (1950). Light-Scattering in multicomponent systems. *J. Chem. Phys.* , Vol. 18, 58-61.
- Sukumar, M. D. (2004). Opalescent Appearance of an IgG 1 Antibody at High Concentrations and its Relationship to Noncovalent Association. *Pharmaceutical Research* , Vol. 21, No. 7: 1087-1093.
- Svedberg, T. P. (1940). The Ultracentrifuge. *Johnson Reprint Corporation* .
- T.M. Laue, A. H. (1989). Direct Determination of Macromolecular Charge by Equilibrium Electrophoresis. *Analytical Biochemistry* , Vol. 182, 377-382.
- T.M. Laue, S. C. (n.d.). The determination of protein valence by capillary electrophoresis.
- T.M. Ridgeway, T. M. (1998). An Apparatus for Membrane-Confined Analytical Electrophoresis. *Electrophoresis* , Vol. 19, 1611-1619.
- T.P. Moody, H. S. (2004). Nonequilibrium thermodynamics of membrane confined electrophoresis. *Biophysical Chemistry* , Vol. 108, 51-76.
- T.P. Moody, J. D. (2003). The experimental determination of protein valence. *Nature* .
- T.P. Moody, J. K. (2005). Valence and anion binding of bovine ribonuclease A between pH 6 and 8. *Analytical Chemistry* , Vol. 336, 243-252.
- Tanford. (1961). *Physical Chemistry of Macromolecules*. New York: John Wiley and Sons, INC.
- Tanford, C. (1955). The Electrostatic Free Energy of Globular Protein Ions In Aqueous Salt Solutions. *J. Am. Chem. Soc.* , Vol. 59, 788-793.
- Timasheff. (1992). Water as Ligand: Preferential Binding and Exclusion of Denaturants in Protein Unfolding. *Biochemistry* , Vol. 31, No. 41 9857-9864.

- Timasheff, S. (1986). The Measurement of Cooperative Protein Self-Assembly by Turbidity and Other Techniques. *Methods in Enzymology* , Vol. 130, 47-59.
- Vermeer, A. W. (2000). The Thermal Stability of Immunoglobulins: Unfolding and Aggregation of a Multi-Domain Protein. *Biophysical Journal* , Vol 78, 394-404.
- von Hippel, P. S. (1969). The effects of neutral salts on the structure and conformational stability of macromolecules in solution. *Biological Macromolecules* , Vol. 2, 417-574.
- Wen, J. J. (2007). *Using Differential Scanning Calorimetry in Understanding the Correlation Between Thermal Stability and Protein Stability*. MicroCal Application Note.
- White, R. J. (1997). FFF-MALS A New Tool for the Characterization of Polymers and Particles. *Polymer International* , 373-379.
- Whitesides, G. M. (2006). Why are Proteins Charged? Networks of Charge-Charge Interactions in Proteins Measured by Charge Ladders and Capillary Electrophoresis. *Angewandte Chemie* , 3022-3060.
- Wright, A. M. (1997). Effect of Glycosylation on Antibody Function: implications for genetic engineering. *TIBTECH* , 26-32 (Vol 15).
- Wyatt, P. J. (1993). Light Scattering and the Absolute Characterization of Macromolecules. 272 (1-40).
- Zimm, B. (1945). *J. Chem. Phys.* , 13: 141.